In compliance with the
Canadian Privacy Legislation
some supporting forms
may have been removed from
this dissertation.

While these forms may be included
in the document page count,
their removal does not represent
any loss of content from the dissertation.

University of Alberta

Ozone mass transfer analyses of two new ozone reactor designs

By:

Allison R. Bale

A thesis submitted to the Faculty of Graduate Studies and Research in partial fulfillment of the requirements of the degree of Master of Science in Environmental Engineering

Department of Civil and Environmental Engineering

Edmonton, Alberta

Fall 2003

National Library
of Canada

Acquisitions and
Bibliographic Services

395 Wellington Street
Ottawa ON K1A 0N4
Canada

Bibliothèque nationale
du Canada

Acquisisitons et
services bibliographiques

395, rue Wellington
Ottawa ON K1A 0N4
Canada

Your file Votre référence
ISBN: 0-612-87717-5
Our file Notre référence
ISBN: 0-612-87717-5

The author has granted a non-exclusive licence allowing the National Library of Canada to reproduce, loan, distribute or sell copies of this thesis in microform, paper or electronic formats.

The author retains ownership of the copyright in this thesis. Neither the thesis nor substantial extracts from it may be printed or otherwise reproduced without the author's permission.

L'auteur a accordé une licence non exclusive permettant à la Bibliothèque nationale du Canada de reproduire, prêter, distribuer ou vendre des copies de cette thèse sous la forme de microfiche/film, de reproduction sur papier ou sur format électronique.

L'auteur conserve la propriété du droit d'auteur qui protège cette thèse. Ni la thèse ni des extraits substantiels de celle-ci ne doivent être imprimés ou aturement reproduits sans son autorisation.

Canada

University of Alberta

Library Release Form

Name of Author: Allison R. Bale

Title of Thesis: Ozone mass transfer analyses of two new ozone reactor designs

Degree: Master of Science

Year this Degree Granted: 2003

Permission is hereby granted to the University of Alberta Library to reproduce single copies of this thesis and to lend or sell such copies for private, scholarly or scientific research purposes only.

The author reserves all other publication and other rights in association with the copyright in the thesis, and except as herein before provided, neither the thesis nor any substantial portion thereof may be printed or otherwise reproduced in any material form whatever without the author's prior written permission.

Date submitted: 15/08/03.

University of Alberta

Faculty of Graduate Studies and Research

The undersigned certify that they have read, and recommend to the Faculty of Graduate Studies and Research for acceptance, a thesis entitled *Ozone mass transfer analyses of two new ozone reactor designs* submitted by Allison R. Bale in partial fulfillment of the requirements for the degree of Master of Science in Environmental Engineering.

Date approved: August 15, 2003

ABSTRACT

Mazzei Injector Corporation and GDT Corporation designed two reactors for the dissolution of ozone gas into the liquid being treated – the flash mix reactor and the opposing jets reactor. The objectives of this research were to determine the mixing characteristics inside the individual components of the systems; the auto-decomposition kinetics of the test liquid (tap water); and the ozone mass transfer characteristics of the systems at low to high ozone feed gas concentrations. The mass transfer of ozone was characterized while varying the applied ozone dose, ratio of gas to motive flow, system back pressure, and liquid flow rate. The ozone transfer efficiency (OTE) and the volumetric liquid mass transfer coefficient ($k_L a$) were obtained as measures of the ozone mass transfer. Mechanistic models were developed and tested for predicting the performance of the ozone mass transfer process in the injector and in the flash mix and opposing jets reactors.

This manuscript is dedicated to my mom and dad, Patricia and Tom Bale, for always supporting me in my academic and life pursuits.

To my brother Ian: here is the secret to the Caramilk bar!

To Alfredo Mendoza Ahuatzin, for continuously encouraging and inspiring me.

ACKNOWLEDGEMENTS

Many people were involved with all aspects of this project that I would like to acknowledge: Nick Chernuka and Garry Solonynko helped with the setup of the ozonation system. Ahmed Moawad was with me for the fun stages of debugging the system and washing the floors a few times. Debra Long helped with the mass transfer experiments. Special thanks to Maria Demeter for working overtime with me in some of the last days of experiments in the old Newton Research building! Without the help of Kevin McCullum I might still be copying and pasting data.

Thanks to Dr. Daniel Smith for his input into this project. Many thanks to Dr. Mohamed Gamal El-Din for spending the time necessary to answer all of my questions and for providing me with so much guidance and support along the way. I am grateful for his dedication to this project.

I would also like to thank the Department of Civil and Environmental Engineering at the University of Alberta for providing the facilities for this research. Thank you to Mazzei Injector Corporation for providing the ozone reactor system. I am grateful for the financial assistance provided to me by the Natural Sciences and Engineering Research Council of Canada (NSERC) Post Graduate Scholarship, the Alberta Ingenuity Studentship, and the Government of Alberta's Alberta Learning Graduate Student Scholarship.

TABLE OF CONTENTS

1. INTRODUCTION 1
   1.1 Problem Statement 1
   1.2 Research Objectives 1

2. LITERATURE REVIEW 4
   2.1 Uses of Ozone 4
   2.2 Ozonation 6
   2.3 Chemical Properties of Ozone 10
      2.3.1 Solubility 11
      2.3.2 Reactivity 11
   2.4 Ozone Measurement 12
   2.5 Ozone Contactor Hydrodynamics 12
      2.5.1 Mixing Regimes 17
      2.5.2 Hydrodynamic Modeling 21
   2.6 Ozone Mass Transfer Process 27
      2.6.1 Volumetric Liquid Mass Transfer Coefficient 36
      2.6.2 Types of Ozone Injectors 40
      2.6.3 Recent Technologies in Gas-Liquid Contacting 42
   2.7 Kinetics 46

3. MATERIALS AND METHODS 52
   3.1 Kinetics of Ozone Auto-decomposition in Sample Water 52
   3.2 Hydraulic Performance Study 55
   3.3 Characteristics of Sample Water 56
      3.3.1 Alkalinity 56
      3.3.2 Total Carbon 57
      3.3.3 Temperature and pH 58
   3.4 Tracer Study 58
   3.5 Ozone Mass Transfer Experiments 64

4. RESULTS AND DISCUSSION 71
   4.1 Kinetics of Ozone Auto-decomposition in Sample Water 71
   4.2 Hydraulic Performance Study 74
   4.3 Characteristics of Sample Water 75
   4.4 General Observations from Ozone Mass Transfer Experiments 76
   4.5 Mixing Regime of Degas Separator 78
   4.6 Injector 80
      4.6.1 Mixing Regime 80
      4.6.2 Theoretical Analysis 82
      4.6.3 Mass Transfer of Ozone 90

4.6.4 Analysis of Volumetric Liquid Mass Transfer Coefficients 94
4.6.5 Ozone Transfer Efficiency 98
4.7 Flash Mix Reactor 101
4.7.1 Mixing Regime 101
4.7.2 Theoretical Analysis 103
4.7.3 Mass Transfer of Ozone 107
4.7.4 Ozone Transfer Efficiency 109
4.8 Opposing Jets Reactor 112
4.8.1 Mixing Regime 112
4.8.2 Theoretical Analysis 114
4.8.3 Mass Transfer of Ozone 115
4.8.4 Ozone Transfer Efficiency 117
4.9 Comparison of Ozonation Systems 119
4.9.1 Ozone Transfer Efficiency 121
4.9.2 Comparison with Static Inline Mixer 125
4.9.3 Overall System Performance 127

5. CONCLUSIONS AND RECOMMENDATIONS 130

6. REFERENCES 132

APPENDIX A – Summary Table of Kinetics Experiments 144

APPENDIX B – Tables from Hydraulic Performance Study 145

APPENDIX C – Tracer Study Data 148

APPENDIX D – Raw Data Sheets 154

APPENDIX E – Data Analyses Sheets 158

APPENDIX F – Summary of Mass Transfer Experiments 164

LIST OF TABLES

Table 4-1 Average values of the main characteristics of the sample tap water. 76

Table 4-2 Ranges of hydraulic parameters for the flash mix and opposing jets systems. 119

Table 4-3 Ranges and averages of ozone mass transfer results from flash mix system runs and opposing jets system runs. 120

LIST OF FIGURES

Figure 3-1 Reactor apparatus for kinetics of tap water experiments. 53
Figure 3-2 Experimental setup of flash mix system indicating important points for tracer study and for ozone mass transfer experiments. 61
Figure 3-3 Experimental setup of opposing jets system indicating important points for tracer study and for ozone mass transfer experiments.. 62
Figure 3-4 Critical dimensions and geometry of the injector. 64
Figure 3-5 Critical dimensions and geometry of the flash mix reactor..... 65
Figure 3-6 Critical dimensions and geometry of the opposing jets reactor. ... 66
Figure 4-1 Natural logarithm of concentration of ozone versus time at an average temperature of 5.9 °C. 72
Figure 4-2 Natural logarithm of concentration of ozone versus time at an average temperature of 32.4 °C. 72
Figure 4-3 Effect of water temperature on the auto-decomposition rate constant of ozone in tap water. 73
Figure 4-4 Exit age distribution curve of degas separator by injection of nonreactive tracer potassium chloride (KCl)..... 79
Figure 4-5 Hydrodynamic modeling of injector by injection of nonreactive tracer potassium chloride (KCl) as a plug flow reactor..... 81
Figure 4-6 Volumetric liquid mass transfer coefficient of injector versus ratio of gas to motive flow. 91
Figure 4-7 Residual concentration of ozone in the liquid phase sampled after the injector versus the applied ozone dose. 93
Figure 4-8 Volumetric liquid mass transfer coefficient of injector from nonlinear regression versus volumetric liquid mass transfer coefficient of injector from modeled experimental data. 95
Figure 4-9 Volumetric liquid mass transfer coefficients modeled by several researchers including the model of the injector versus the superficial velocity of gas, at standard temperature and pressure. 98
Figure 4-10 Ratio of ozone transfer efficiency to gas flow rate of injector versus ratio of gas to motive flow. 99
Figure 4-11 Hydrodynamic modeling of flash mix reactor by injection of nonreactive tracer potassium chloride (KCl) as a continuous flow stirred tank reactor. 102
Figure 4-12 Volumetric liquid mass transfer coefficient of flash mix reactor at four ratios of gas to motive flow. 107
Figure 4-13 Residual concentration of ozone in the liquid phase sampled after the flash mix reactor versus the applied ozone dose. 109
Figure 4-14 Ratio of ozone transfer efficiency to gas flow rate of flash mix reactor versus ratio of gas to motive flow. 111

Figure 4-15 Hydrodynamic modeling of opposing jets by injection of nonreactive tracer potassium chloride (KCl) as a continuous flow stirred tank reactor. 113
Figure 4-16 Volumetric liquid mass transfer coefficient of opposing jets reactor at five ratios of gas to motive flow. 116
Figure 4-17 Residual concentration of ozone in the liquid phase sampled after the opposing jets reactor versus the applied ozone dose. 117
Figure 4-18 Ratio of ozone transfer efficiency to gas flow rate of opposing jets reactor versus ratio of gas to motive flow. 118
Figure 4-19 Ozone transfer efficiency of system in liquid phase versus ozone transfer efficiency of system in gas phase for flash mix and opposing jets systems. 122
Figure 4-20 Ratio of zone transfer efficiency to gas flow rate of flash mix system versus ratio of gas to motive flow. 123
Figure 4-21 Ratio of ozone transfer efficiency to gas flow rate of opposing jets system versus ratio of gas to motive flow. 124
Figure 4-22 Natural logarithm of ratio of ozone transfer efficiency to gas flow rate versus ratio of gas to motive flow for injector, flash mix reactor, opposing jets reactor, flash mix system, and opposing jets system. 125
Figure 4-23 Ozone transfer efficiency of injector only, flash mix, opposing jets, and static mixer systems versus ratio of gas to motive flow. 127
Figure 4-24 Ozone transfer efficiency of the injector versus ozone transfer efficiency of the flash mix reactor at various ranges of ozone transfer efficiency of the flash mix system. 128
Figure 4-25 Ozone transfer efficiency of the injector versus ozone transfer efficiency of the opposing jets reactor at various ranges of ozone transfer efficiency of the opposing jets system. 129

1. INTRODUCTION

1.1 Problem Statement

Ozone has become an advanced process for both water and wastewater treatment systems. The process is optimized when the ozone gas is efficiently dissolved into the liquid being treated. It is therefore important to study the physical devices or reactors used to create a contact area for the ozone gas and the liquid. Mazzei Injector Corporation (MIC) has recently designed two such reactors – the flash mix reactor and the opposing jets reactor. It was desired to determine which of the two new ozone reactors is most efficient at dissolving ozone from the gas phase into the liquid phase and also to compare them to previously designed ozone dissolution systems.

1.2 Research Objectives

The objectives of this research are to determine:

a) the mixing characteristics inside the injector, the flash mix reactor, and the opposing jets reactor;

b) the auto-decomposition kinetics of the test liquid (tap water); and

c) the ozone mass transfer characteristics of the injector, the flash mix reactor, and the opposing jets reactor at low to high ozone feed gas concentrations and over a wide range of ratios of gas to motive flow (i.e., the ratio of gas to liquid flow).

The ozone mass transfer efficiency of the reactors was characterized over a wide range of operating parameters. The ranges of operation were as follows:

a) applied ozone dose = 1 to 20 $mg \cdot L^{-1}$;

b) ozone applied dose concentration = 1 to 12 % w/w;

c) ratio of gas to motive flow, G/L = 0.005 to 0.200;

d) system back pressure, P_B = from baseline rounded to next 34 kPa (5 psig) value to maximum allowable pressure; and

e) liquid flow rate, Q_L = 1.9 to 37.9 $L \cdot min^{-1}$ (0.5 to 10 $gal \cdot min^{-1}$).

The injector and either the flash mix reactor or the opposing jets reactor was used to transfer ozone gas into the liquid phase. For maximum transfer to occur, the gas-liquid contactor system should produce an intense mixing environment that can lead to a large amount of interfacial area and increase the speed of the mass transfer process. The experiments were performed in accordance with the prescribed range of parameters with the feed gas flow under positive pressure (injection) or negative (i.e. vacuum) pressure (ejection). The ozone mass transfer performances of the flash mix and opposing jets systems were measured by experimentally determining the volumetric liquid mass transfer coefficients of the reactors, $k_L a_{FM}$ and $k_L a_{OJ}$ (s^{-1}), the ozone transfer efficiency of the two reactors, OTE_{FM} and OTE_{OJ} (%), and the ozone transfer efficiency of the entire systems,

$OTE_{sys,liq}$ (%). Information on mass transfer performance of the injector was also obtained in the form of $k_L a_{inj}$ and OTE_{inj} (%).

2. LITERATURE REVIEW

2.1 Uses of Ozone

With increasing concerns regarding byproducts from the chlorination process, treatment with ozone has become the alternative treatment of choice (Oke *et al.* 1998). The use of ozone in water and wastewater treatment for achieving microbial reduction has accelerated over recent years due to increasing demands and regulations for high quality drinking water and due to the carcinogenic nature of byproducts of chlorination. Ozone has been used as a disinfectant because of its high oxidation potential (Kuo 1982). This high oxidation potential has made ozone a very attractive alternative to chlorine. Ozone has an excellent capacity to inactivate viruses and bacteria in water and is also capable of reducing dissolved organic substances, destroying cyanides and pesticides, and precipitating iron and manganese (Sheffer and Esterson 1982). Ozone is very efficient for the inactivation of bacteria, including gram-negative bacteria such as *Escherichia coli*, coliforms, and Salmonella spp. The reactivity of ozone with lipids and proteins causes degradation of the bacterial membrane and consequently cellular lysis. For viruses ozone attacks the coat, the virion capsid, and the nucleic acids. Ozone also attacks parasites like amoebae to cause inactivation by damaging the plasma membrane (Martin *et al.* 1992).

Further to its potential to kill bacteria and viruses, ozone has the strongest ability to inactivate protozoans such as Giardia spp. cysts and Cryptosporidium spp. oocysts (Smith and Zhou 1994). The traditional chemicals used for microbial reduction such as free or combined chlorine are practically ineffective against such protozoans (Kim *et al.* 2002).

Ozonation can have several purposes in water treatment apart from microbial reduction. According to von Gunten (2003), the main reasons for the use of ozone are microbial reduction and oxidation. Applications of oxidation with ozone include control of taste and odour, decolouration, control of algal growth, elimination of inorganic pollutants, organic micropollutants, and organic macropollutants, as well as improvement of coagulation (Langlais *et al.* 1991; von Gunten 2003). Also, ozone is used in drinking water as an aid to improve other unit operations such as coagulation-flocculation or biological filtration with activated carbon (Beltrán *et al.* 2001).

With regards to wastewater treatment, ozonation is being studied for use in industries whose wastewaters contain compounds that are difficult to treat using conventional methods. For example, wastewater from the textile industry may contain large amounts of dye, mordant, sizing agents, and dyeing aids. Wastewater from the petrochemical industry may contain refractory phenolic compounds. Hsu *et al.* (2002) proposed the use of ozonation for the treatment of

dye and textile wastewater and phenolic wastewater. These researchers developed a gas-liquid reactor with an improved ozone utilization rate to alleviate the limitations caused by the high production cost of ozone and low ozone solubility in water.

Although ozone is being used to control the formation of disinfection byproducts (DBPs) from chlorination, it can also produce harmful byproducts. The reaction of ozone with bromide ions that exist naturally in source waters results in the formation of a variety of brominated organics and inorganic byproducts, including potentially carcinogenic bromate (BrO_3^-) ions (Zhou and Smith 2000*b*).

2.2 Ozonation

Ozonation refers to the dissolution of ozone gas in a liquid to be treated. A feed gas of either air (dried and filtered) or high purity oxygen generates ozone. Up to a certain volume of gas, the high purity oxygen is more cost effective than air. However air remains the most popular choice as a feed gas despite producing an ozone yield two to four times smaller than with the high purity oxygen for the same volume of gas. During microbial reduction, sufficient dissolved ozone concentration for a sufficient time must be achieved and therefore the optimum ozone dose must be determined experimentally. It is necessary for the feed gas to have a very low dewpoint temperature to ensure a dry environment within the ozone generator. Moisture can be removed from the feed gas by compression,

cooling, or desiccant drying. Particulates and contaminants should also be minimized as much as possible. Ozone is typically generated by silent electric discharge, or corona discharge, by applying a high voltage across two electrodes (Langlais *et al.* 1991). Recently designed ozone generators produce as high as 16 % (on a weight-weight basis) of ozone in the gas phase. The mixture of air or oxygen with ozone gas is transferred to the liquid by bubbling it through the bulk solution (Chen *et al.* 2002).

Ozone transfers from the gas bubbles into the liquid where it begins to decompose and reacts with other components present in water (Mariñas *et al.* 1993). The unique feature of ozone is its decomposition into hydroxyl (OH) radicals ($^{\bullet}$OH), which are the strongest oxidants in water. In the process of ozonation, both ozone and $^{\bullet}$OH are involved in reactions. While microbial reduction or disinfection occurs mainly through ozone, the process of oxidation can involve both ozone and $^{\bullet}$OH. Undesired byproducts can be formed from the reaction of ozone and $^{\bullet}$OH with components present in the water being treated, including numerous organic and some inorganic species. The only undesirable byproduct regulated in drinking waters is bromate, which is formed during ozonation of waters that contain bromide. Although ozonation may be followed by biological filtration, bromate is not degraded or removed in the process of biological filtration (von Gunten 2003).

The mass transfer process from gas phase to liquid phase limits ozonation (Gamal El-Din and Smith 2002). Therefore the performance of the ozonation system is a direct function of the rate of the mass transfer of ozone. The efficiency of the ozonation system is influenced by the rate of transport of each phase, the rate of chemical transformation, the contactor configuration, the operating conditions, and the water quality. Non-ideal flow of the phases is also responsible for lowering the efficiency of a reactor (Shetty *et al.* 1992).

During the process of ozonation, several other processes occur including convection and backmixing of the gas and liquid phases, ozone gas mass transfer, ozone auto-decomposition, and competitive reactive processes of constituents present in the liquid with dissolved ozone. The rate of auto-decomposition of ozone is dependent on the temperature of the water, the pH level, the organic and inorganic constituents in the water, and the organic and inorganic initiators and inhibitors in the water (Gamal El-Din 2001). Sotelo *et al.* (1989) studied an ozone-water system and determined that high values of pH induce the auto-decomposition of ozone; however the concentration of dissolved ozone decreased as the pH increased. High values of temperature also caused a decrease in the concentration of dissolved ozone.

Ozone is applied directly into contactors for disinfection or oxidation due to its insolubility and instability (Huang *et al.* 1998; Mariñas *et al.* 1993). The

dissolution of ozone in the liquid phase can be achieved by several techniques including: 1) conventional fine bubble diffusion; 2) turbine mixers; 3) injectors; 4) packed columns; 5) spray chambers; and 6) porous plate diffusers (Langlais *et al.* 1991). The three main types of gas-liquid reactors are: 1) film reactors (e.g. wetted wall, trickling filter); 2) bubble bed (sparged) reactors (e.g. multistage bubble reactor); and 3) spray reactors (e.g. spray columns, venturi scrubbers) (Kaštánek *et al.* 1993). Cocurrent devices such as venturi injectors, jet reactors, and tubular loop reactors have higher energy efficiency in terms of gas dispersion because the kinetic energy from the high velocity liquid jet is used to achieve fine dispersion and intense mixing between the phases (Radhakrishnan and Mitra 1984). According to Martin and Galey (1994), different types of reactors are used for different ozonation functions with respect to water treatment plants in Europe: turbine reactors for preozonation and bubble reactors with porous plates for interozonation or postozonation.

In the field of water treatment, contactors have been designed for applications of microbial reduction with ozone; however many times the unit operation of ozonation is used specifically for the removal of organic matter (Xu and Liu 1990). In any unit operation consideration, it is critical to establish a model for ozone mass transfer in order to determine the optimal operating conditions for the specific ozone contactor.

The bubble bed, bubble column, and deep pool are three interchangeable names for a reactor where gas is distributed at the base by a suitable distributor and moves as a dispersed phase of bubbles relative to a continuous liquid phase (Shetty *et al.* 1992). There are no mechanical moving parts in the bubble column and it is best suited for reactions involving aggressive gases and for high pressure and high temperature processes (Deckwer and Schumpe 1987). The flow arrangement of phases of a bubble column is semibatch, countercurrent, or cocurrent. According to Valentin (1967), the minimum depth of a bubble column reactor is 0.30 m. The maximum allowable depth may be limited by bubble coalescence because as coalescence increases, so does the height of the bed, causing a smaller bubble size distribution. Advantages of the bubble column reactor include low maintenance, high liquid phase content for treatment, good mass transfer rates at low energy input, low space requirement, and relatively low cost (Deckwer and Schumpe 1993).

2.3 Chemical Properties of Ozone

Ozone is the allotropic form of oxygen. The endothermic reaction (Equation 2-1) has an enthalpy of ΔH^{o} = + 284.5 $kJ \cdot mol^{-1}$ at one atm. With a large negative value for entropy of ΔS^{o} = - 69.9 $J \cdot mol^{-1} \cdot K^{-1}$ at one atm, the reaction easily tends in the reverse direction. It is crucial to control the temperature of the system to ensure efficient ozone generation (Langlais *et al.* 1991).

$$3O_2 \Leftrightarrow 2O_3$$ Equation 2-1

2.3.1 Solubility

Ozone is an insoluble and unstable gas in water (Mariñas *et al.* 1993). When the temperature of the system is increased ozone becomes less stable and less soluble in water. Langlais *et al.* (1991) presented a rule of thumb stating that by increasing the temperature by 10 °C, the rate of the ozone auto-decomposition reaction will increase by a factor of two or three.

2.3.2 Reactivity

The stability of dissolved ozone is dependent on the water matrix, especially its pH, content of UV light, concentration of ozone, concentration of radical scavengers, type and content of natural organic matter, and its alkalinity (Langlais *et al.* 1991; von Gunten 2003). Ozone is unstable in water and will decay or auto-decompose. Depending on the water quality, the half-life of ozone is in the range of seconds to hours (von Gunten 2003). Due to the high reactivity of ozone, it is very important to maximize ozone mass transfer. Gamal El-Din (2001) suggests that additional ozone applied should be added at a lower dose in subsequent chambers to maintain a proper concentration of the ozone residual in water distribution systems.

2.4 Ozone Measurement

It is possible to determine the applied ozone dose by analyzing the amount of ozone in the gas being fed into the contactor and by knowing the gas and liquid flow rates (Langlais *et al.* 1991). The efficiency of mass transfer, or specifically the transfer of ozone from the gas phase to the liquid phase, depends on the diffusion system, the immediate liquid demand for ozone, the temperature, and the pH of the liquid. The net amount of ozone absorbed into the liquid phase is known as the absorbed ozone dose or the utilized ozone dose and is determined by the difference between the concentration of ozone in the contactor feed gas and the concentration of ozone in the contactor exhaust gas. While measuring the concentration of dissolved ozone, it is important to ensure that the sampling is done without agitation, that the sample is prepared following a set standard, and that the sample is handled properly to avoid imprecision. Several methods are available to measure ozone in the aqueous phase including indigo method, iodometric method, colourimetric method, UV absorption, and electrochemical devices. In the gas phase, ozone is measured by iodometric method, KI method, direct (amperometric) method, direct UV absorption measurements, calorimetry, or isothermal pressure range (Langlais *et al.* 1991).

2.5 Ozone Contactor Hydrodynamics

The hydrodynamics of an ozone contacting system are very important to achieve a proper design of such reactors (Gamal El-Din 2001). Laboratory scale

investigations are a very important step in the design of ozone contactors because of the complex hydrodynamic conditions occurring in multiphase reactors (Deckwer and Schumpe 1987). In chemical reactors, mixing characteristics of the individual phases depend on reactor type, geometry of the reactor, operational conditions, and the properties of the reaction system. The flow of phases can vary between ideal plug flow and perfect complete mixing (Kaštánek *et al.* 1993). For example, in bubble column reactors the bubbles usually produce complete mixing at certain gas flow rates by agitating the liquid. A multistage bubble column is a reactor comprising several short bubble columns in an array one over another (Voigt and Schügerl 1979). The probability of coalescence of bubbles is lower in a multistage bubble column because of the shorter residence time of the bubbles in the short columns, resulting in higher specific interfacial areas than in a single stage column.

As the average bubble size increases, the gas holdup decreases. Gas holdup (ε_G) is the ratio of the volume of gas phase to the total volume (of both gas and liquid phases) of the reactor, as shown in Equation 2-2. Gas holdup is an important concept in the hydrodynamics of a gas-liquid reactor system. It provides information such as the fractional volume of the gas phase or the residence time inside the reactor and the specific interfacial area (Gamal El-Din 2001). When gas holdup information is combined with information on the distribution of bubble size in the reactor, the rate of interfacial mass transfer can be determined

(Kaštánek *et al.* 1993). In a conventional bubble column design, Shetty *et al.* (1992) observed that gas holdup was not dependent on superficial liquid velocity and diameter of the bubble column, but was dependent on the superficial gas velocity. In an impinging jet bubble column, Gamal El-Din (2001) observed that gas holdup was dependent on superficial gas and liquid velocities. Bin *et al.* (2001) investigated the hydrodynamics and ozone mass transfer in a tall bubble column (2 m) with a porous gas sparger. It was determined that the gas holdup depended slightly on the vertical location as higher values were observed at the bottom of the column. An almost linear dependence between ε_G and u_G was observed for a homogeneous bubbling flow regime.

$$\varepsilon_G = \frac{V_G}{(V_G + V_L)} \qquad \text{Equation 2-2}$$

where: ε_G = gas holdup [dimensionless]

V_G = volume of gas [m^3]

V_L = volume of liquid [m^3]

The residence time distribution (RTD) of phases in a reactor is also referred to in the literature as the extent of mixing. Elements of fluid take different routes through a reactor and therefore take a different amount of time to exit the reactor. The distribution of these times is called the RTD, or exit age distribution, E, of the fluid (Levenspiel 1999). The RTD of a reactor depends on the reactor

configuration, the flow arrangement of phases, the two phase flow regime, and the flow rates of the phases and their corresponding ratio (Kaštánek *et al.* 1993). The factors affecting the mixing depend on the type of reactor used. For bubble column reactors or bubble bed reactors, coalescence and breakup of bubbles contribute to a high residence time in the gas phase due to their lower buoyancy. As the gas velocity increases or as the column diameter increases, the peak of the RTD curve decreases while its width increases. It is also suggested that if there is a hump in the RTD curve, then multiple bubble groups exist and therefore a dispersion model is too simple as a model (Kawagoe *et al.* 1989).

Axial mixing in the liquid phase can be influenced by the gas flow rate, the diameter of the reactor, and by the properties of the liquid phase (Kaštánek *et al.* 1993). The coefficient of axial dispersion in the liquid phase (D_L) is not constant over the entire height of the column. Liquid phase backmixing was not affected by the arrangement of flow (i.e. cocurrent or countercurrent) for reactors with typical ratios of height to diameter of reactor. Backmixing in the liquid phase depends on the flow rates of gas and liquid phases and on the configuration and geometry of the ozone contactor being studied (Roustan *et al.* 1993). Performing dynamic tracer studies can closely approximate both the coefficient of axial dispersion in the liquid phase and the RTD. The gas and liquid phase tracers are introduced either as pulse or step inputs. Whether the input signal is ideal depends on the speed and reproducibility of the introduction of the tracer. From

the tracer studies, two other important parameters can be determined: 1) the time for 10 % of the total mass of tracer to exit the contactor, t_{10}; and 2) the time for 50 % of the total mass of tracer to exit the contactor, t_{50} (Mariñas *et al.* 1993).

For the gas phase of the system, generally there is less information available than for the liquid phase because the ideal plug flow model can approximate gas flow in bubble beds or columns and because there are technology limitations with respect to the RTD data (Kaštánek *et al.* 1993). Since it is difficult to determine the characteristics of gas mixing, fewer studies have been done to develop relations for gas phase mixing parameters (Zahradník and Fialová 1996). Other factors contributing to the lack of gas phase mixing studies include the difficulty in measuring the RTD of the bubbles because of the time delay in the detector that measures the tracer concentration, and the large end effect in the gas-liquid disengagement section at the top of the bubble column (Kawagoe *et al.* 1989).

At low gas flow rates, the plug flow model can describe the gas phase. For fast reactions with a low intensity of interfacial contact and with low gas flow rates, the reaction will take place in the liquid film. With the absorption time being greater than the reaction time, the liquid film at the interface becomes rate limiting (Kaštánek *et al.* 1993). Roustan *et al.* (1993) observed that backmixing in the gas phase can be assumed to be negligible due to the large buoyancy of the gas bubbles, allowing the perfect plug flow model to be applied. However Shetty

et al. (1992) explained that the differences between predicted and experimental values from different researchers with regards to backmixing in the gas phase are due to the assumption of negligible mass transfer between gas and liquid phases. Most of the data on backmixing in the gas phase are for the homogeneous mixing regime. Different flow mixing regimes must be approached separately in the gas phase of a multiphase flow system. Dominant factors for gas phase mixing were determined to be the mean rising velocity of bubbles and the diameter of the bubble column (Kawagoe *et al.* 1989).

It is important to understand the axial mixing in both the gas and liquid phases for modeling, design, and optimization of the ozonation reactor (Zahradník and Fialová 1996). The mass transfer characteristics of gas-liquid reactors are influenced by the mode of primary gas dispersion. Primary gas dispersion is also referred to as the bubbling regime of the system. Bubbling regimes within a bubble bed reactor can affect the bubble size distribution, the gas holdup, and the extent of backmixing in each of the phases.

2.5.1 Mixing Regimes

Bubbly flow regime is flow with almost uniform distribution of bubble sizes and uniform radial distribution of bubbles in the reactor. This regime is limited to low superficial gas velocities (≤ 0.05 m·s^{-1}). Bubbles do not interfere with each other and have a rising velocity equal to the velocity of free bubbles ascending in an

infinite liquid range (e.g. 0.2 to 0.3 $m \cdot s^{-1}$ for an air-water system). *Turbulent or heterogeneous flow regime* consists of a mixture of large and small bubble sizes that undergo simultaneous coalescence and breakup at higher gas velocities, where flow becomes chaotic. The large gas bubbles in this regime have an increased rising velocity (≤ 1 $m \cdot s^{-1}$). *Slugging regime* is flow that occurs in low diameter columns (≤ 0.15 m) where the diameters of large bubbles are close in size to the diameter of the column. *Homogeneous bubbling regime* is fully developed turbulent flow with bubbles whose population density is large and that are in close contact in the reactor. Homogeneous bubbles have a uniform size distribution, resulting in a constant bubble rising velocity, negligible interference between bubbles, and uniform distribution of gas holdup in the column (Kaštánek *et al.* 1993). In general, the flow regime is bubbly flow at low gas velocities and turbulent flow at high gas velocities (Kawagoe *et al.* 1989).

In all systems it is important to consider the transition stage between the turbulent and homogeneous bubbling regimes because it affects the efficiency of the mass transfer process. As the mixing regime changes from homogeneous to turbulent, gas velocities increase, causing an increase in the number of bubbles with high rising velocities and coincidentally there is a large decrease in the absorption rate due to insufficient time of residence. This transition is also characterized by the development of a non-uniform distribution of bubble sizes.

Zahradník and Fialová (1996) investigated the links between the mixing of phases and the bubbling regime using a semibatch (zero liquid flow) air-water system in a cocurrent flow arrangement. Two distributing plates were used alternatively to create homogeneous and heterogeneous bubbling regimes in the reactor. The RTD in both the liquid and gas phases were characterized by their respective Peclet numbers (Pe_L and Pe_G), calculated from tracer studies:

$$Pe = \frac{uL}{D} \qquad \text{Equation 2-3}$$

where: u = real velocity of phase [$m \cdot s^{-1}$]

L = reactor length [m]

D = axial dispersion coefficient of phase [$m^2 \cdot s^{-1}$]

The Peclet number represents a dimensionless form of the dispersion coefficients of the gas and liquid phases and denotes the degree of backmixing (Shetty *et al.* 1992). A Pe value of zero represents complete backmixing and an ideal completely stirred tank reactor. An infinite Pe value represents an ideal plug flow behaviour and an ideal plug flow reactor. Zahradník and Fialová (1996) observed that as the Pe_G value increased in the homogeneous regime, uniform radial and axial distribution was observed and therefore flow in the gas phase was approximated by a plug flow regime. The data of gas mixing in the transition zone were highly sensitive. After the gas velocity surpassed a u_G of 0.12 $m \cdot s^{-1}$,

Pe_G reached a constant value. The characteristics of mixing in the fully developed turbulent bubbling regime were determined primarily by the circulation of bulk liquid with a decreasing effect of the primary gas dispersion and a negligible effect of the geometry of the distributing plate. These results allow the gas mixing in the heterogeneous regime to be described by a convective gas flow model.

Zahradník and Fialová (1996) also determined that with respect to the liquid phase, Pe_L was directly proportional to the liquid flow rate and that the transport of the liquid by means of the wakes of bubbles was a dominant mode of liquid mixing in bubble columns. Liquid mixing and gas mixing in the heterogeneous bubbling regime were both described by perfectly mixed tanks in series with backflow between adjacent stages. It was concluded that the gas dispersion mode or bubbling regime had an effect on the extent of axial mixing in the gas phase and in the liquid phase.

The flow pattern in a bubble column is most often referred to as a "two bubble class model" which begins at superficial gas velocities greater than the transition velocity. Large bubbles travel upwards in plug flow due to high rising velocity. Small bubbles tend to completely backmix due to the recirculation of liquid. It was also observed that the mean residence time for large bubbles is much less than the mean residence time for small bubbles (Shetty *et al.* 1992). Kawagoe *et*

al. (1989) indicated that the circulation of liquid occurs in the upflow direction in the core of the reactor, while it flows downward near and adjacent to the walls. This is explained by the fact that as bubbles rise in the liquid, liquid will be entrained upwards and due to continuity an equal amount of liquid must flow downwards. This circulation pattern is known as macroscopic and has a scale that depends on the regime of bubble flow. The rate of macroscopic circulation is high in heterogeneous (turbulent) flow regime systems (Deckwer and Schumpe 1987). With reference to the two bubble class model, the larger upward flowing bubbles with higher velocities and lower RTD values are referred to as Group 1, while the smaller, downward flowing bubbles are part of Group 2. It is assumed that no exchange of bubbles occurs between Groups 1 and 2. Shetty *et al.* (1992) assumed that the dispersion coefficients for the gas phase and the liquid phase (D_G and D_L, respectively) are equal in the Group 2 bubble class.

2.5.2 Hydrodynamic Modeling

The tanks-in-series model is primarily used for small deviations from plug flow and is often applied to turbulent flow in pipes, laminar flow in very long tubes, flow in packed beds, shaft kilns, long channels, and screw conveyors (Levenspiel 1999). The tanks-in-series (also known as CFSTR-in-series) model can be used for the same applications as the axial dispersion model. It is a simple model that works with any kinetics and can easily be extended to describe any number of compartments with recycle or without recycle of flow. Each CFSTR in the series

has the same volume and the outputs of tank number n are equal to the inputs of tank number n+1.

Tracer and ozonation tests using countercurrent and unpacked columns with fine and coarse diffusers were performed to calibrate a CFSTR-in-series model and predict ozone residual concentrations (Mariñas *et al.* 1993). Ozone profile tests were also performed to compare with the results of the computer model. The performance of the countercurrent ozone contactor ranged from well mixed conditions when the gas flow rate was high and the liquid flow rate was low to plug flow conditions when the gas flow rate was low and the liquid flow rate was high. The number of continuous flow stirred tank reactors (N_{CFSTR}) varied from 2 (well mixed) to 21 (plug flow). For the packed cocurrent contactor, the dispersion number followed a trend similar to that of the countercurrent contactor; however the values were much lower. The N_{CFSTR} values ranged from 37 to 90. At constant temperature, the concentration of ozone residual decreased as the liquid flow rate decreased and as the gas flow rate increased. As the number of CFSTRs deviates from one, the flow goes from being perfectly mixed to a plug flow behaviour.

According to Deckwer and Schumpe (1987), the mathematical character of the hydrodynamic model can be determined by the knowledge of the flow regime, the RTD of phases, the kinetics of the reactions taking place, the number of reactants

present, and the absorption-reaction theory for the process. To determine these parameters it might be necessary to make crude simplifications, however this may lead to significant uncertainties. The axial dispersion model (ADM) is considered by Deckwer and Schumpe (1987) to be the best approximation of the physics and the hydrodynamics of a bubble column reactor. The parameters not accurately known include the volume fraction of the phases, the properties of mass transfer, dispersion, and kinetics. The ADM visualizes the flow of fluids in tubular bubble columns as a plug flow on top of which is superimposed an axial dispersion of the fluid under investigation (Smith and Zhou 1994). Dispersion is assumed to occur in the liquid phase only with the large buoyancy of the gas bubbles causing the dispersion in the gas phase to be negligible.

Dispersion modeling requires the following assumptions: 1) dispersion can be represented by diffusion laws; 2) the concentration profile is uniform in the radial direction, i.e. infinite radial dispersion; and 3) axial dispersion is uniform throughout the water column, i.e. constant axial dispersion coefficient (Mariñas *et al.* 1993). The analysis of mass transfer can be made using these three assumptions in addition to the following assumptions: 1) the ozone contactor operates under steady state flow conditions; 2) dispersion occurs in the liquid phase only; 3) the two-film model is valid; 4) ozone is stable in the gas phase; and 5) the apparent rate of combined ozone auto-decomposition and reaction in the liquid phase, referred to as the utilization rate, follows the equation:

$$\frac{dC}{dt} = -k_d C^n$$ Equation 2-4

where: C = concentration of the ozone residual at time = t $[mg \cdot L^{-1}]$

k_d = utilization rate constant $[s^{-1}]$

n = reaction rate order coefficient

The parameters n and k_d vary for each type of water. It was observed that the utilization rate constant increased with increasing pH and decreased in the presence of hydroxyl radical scavengers. It was further affected by reactions with suspended solids and solutions containing dissolved inorganic and organic matter.

In the study of a pilot scale ozone bubble diffuser column, Kim et al. (2002) represented the reactor hydrodynamics with the axial dispersion model. This mathematical model was used to optimize the process design of an ozone bubble diffuser contactor by simulating the effects of contactor configuration, operating conditions, and water quality parameters on the efficiency of microbial reduction. The ozone utilization kinetics was approximated by either a first order term or a second order term and the disinfection kinetics by a second order expression. The ADM simultaneously represented the ozone concentration profiles and the inactivation data. ADM expressions were developed for both cases of ozone utilization kinetics and then integrated by analytical or numerical methods. The

model was then validated with experimental data obtained for the inactivation of Cryptosporidium spp. oocysts in a pilot scale ozone bubble diffuser column.

Chen *et al.* (2002) investigated a dynamic ADM that considered the dynamic state, the mass transfer of oxygen, the effect of ozone auto-decomposition, and the change in superficial velocity of the gas. Their dynamic ADM was validated using experimental data from ozone contacting in a countercurrent bubble column and found the model to accurately predict the dynamic variations in the concentrations of oxygen during the dissolution of ozone in the bubble column.

Gamal El-Din and Smith (2001) deviated from the complete ADM, which is also known as the two phase axial dispersion model because it is represented by two nonlinear partial differential equations. They proposed a one phase axial dispersion model that comprises a single non-homogeneous linear second order differential equation representing the liquid phase. A simple spreadsheet was used to analytically solve the differential equation. The model was tested for water treatment conditions and provided excellent predictions of the concentration profiles of dissolved ozone obtained in a diffuser bubble column for the cocurrent and countercurrent flow modes.

Deckwer and Schumpe (1987) introduced two-dimensional models that were developed on the basis of dispersed plug flow models with axial and radial

dispersion for single phase flows. The backflow cell model (BFCM) visualizes bubble columns as cells where backmixing occurs between two neighbouring cells of the liquid phase and where convection exists. The BFCM is used to characterize the behaviour of flow mixing within gas-liquid contactors. The BFCM offers a great deal of flexibility for a model that does not assume backflow in the gas phase. The BFCM assumes flow in different directions; in turbulent regime the liquid is assumed to be entrained upward by the large bubbles in plug flow, known as exchange flow. It represents back flow in the downward direction (not unmixed), also referred to as circulation cells. Flow backmixing occurs due to the presence of shear dispersion, molecular diffusion, and eddy diffusion and can range from plug flow to completely mixed flow (Zhou and Smith 2000*b*). The BFCM model is simple in formulation, can be applied to a wide range of backmixing conditions, and is generally easy to solve mathematically (Smith and Zhou 1994).

In the BFCM the contactor is represented by a number of continuous flow stirred tank reactors (CFSTRs) of equal size, with exchange flow between the adjacent CFSTRs to characterize axial dispersion. The extent of backmixing is characterized by N (the number of CFSTRs in series) and γ (the ratio of exchange flow to convective flow). A high N and low γ represent plug flow; a low N and a high γ represent a CFSTR. The BFCM is reduced to the axial dispersion model as

N approaches infinity. Further, a value of zero for γ allows the BFCM to be represented by the CFSTRs-in-series model (Zhou and Smith 2000*b*).

Zhou and Smith (2000*b*) used an integrated BFCM approach to model the main process components of ozonation: mass transfer, ozone utilization in water, inactivation of microorganisms, contactor flow backmixing, and the formation of DBPs. The validity of using this approach to model the concentration of dissolved ozone and to predict the disinfection and formation of DBPs was proven by experimental ozonation tests.

Smith and Gamal El-Din (2002) modeled the performance of ozone bubble columns for water and wastewater treatment using both the ADM and the BFCM. Using pilot scale experimental data, both models were shown to reliably predict the concentration profiles of dissolved ozone in the bubble column for cocurrent and countercurrent modes. The researchers concluded that the BFCM was easier to formulate and to solve than was the ADM.

2.6 Ozone Mass Transfer Process

The most important goal in a gas-liquid reactor is to achieve mass transfer from the gas phase to the liquid phase (Bouaifi *et al.* 2001). Kuo (1982) suggested that the mechanisms at work in a gas-liquid reaction system are: 1) the diffusion of ozone through the gas phase into the gas-liquid interface; 2) the transport across

the interface to the liquid phase boundary; and 3) the transfer into the bulk liquid. Absorption of ozone by the liquid is controlled mainly by molecular diffusion of the dissolved ozone and chemical reactions in the region between the interface and the liquid phase boundary. The molecular diffusivity of ozone in dilute solutions is equal to 2 x 10^{-5} cm·s^{-1} at room temperature (Kuo 1982). The main mass transfer theories (film, penetration, and surface renewal) maintain that mass transfer is predominantly by molecular diffusion and that convective transport is unimportant. Equation 2-5 and Equation 2-6 show the relationship between diffusivity, D, and the volumetric liquid mass transfer coefficient, $k_L a$, for the film theory and the penetration theory, respectively (Beltrán *et al.* 1998):

$$k_L a_{O_3} = k_L a_{O_2} \frac{D_{O_3}}{D_{O_2}} \qquad \text{Equation 2-5}$$

$$k_L a_{O_3} = k_L a_{O_2} \sqrt{\frac{D_{O_3}}{D_{O_2}}} \qquad \text{Equation 2-6}$$

The film theory states that the liquid film is assumed to be very thin without any accumulation of diffusing mass. Steady state diffusion prevails and the distribution of the concentration is a linear function of the distance in the liquid film. In the penetration theory it is assumed that turbulent eddies travel from the bulk phase to the interface and remain there for a short period of time. If the time

of exposure in the bulk phase is short no steady state concentration gradient is achieved. Therefore the thickness of the liquid film is assumed infinite because the transporting species may never approach the outer edge of the liquid film, resulting in constant time of exposure. The surface renewal theory asserts that the liquid phase is assumed to be continuously disturbed by infinitesimally small eddies, resulting in turbulence at the boundary of the interface and the continuous transport of microscopic masses of fresh phase from the bulk to the surface of the interface (Kuo 1982). As the mixing intensity increases the liquid film at the gas-liquid interface will be renewed at a higher rate, causing the mass transfer coefficient, k_L, to increase (Danckwerts 1970).

Kaštánek *et al.* (1993) presented a rule of thumb stating that the phase in which the resistance against mass transfer is concentrated should always be kept as the continuous phase, making it easier to use hydrodynamics to enhance the mass transfer. In experiments with a bubble column operating under a recirculation flow regime, Nakao *et al.* (1983) made the following four assumptions: 1) that liquid phase resistance controlled the rate of mass transfer; 2) that the gas and liquid flowed under steady state conditions; 3) that mass transfer through the free liquid surface was negligible; and 4) that Henry's law held. The assumption that the mass transfer of ozone gas is controlled by the resistance of the liquid phase is very important. The gas flow rate and the agitation influence the resistance against mass transfer in the liquid and film phases (Sotelo *et al.* 1989). The extent

of mass transfer effects depends on several factors such as reaction kinetics, concentrations of reactants, values of molecular diffusion coefficients of the components in each phase, and on a hydrodynamic parameter describing the interfacial mass transfer rate. Interfacial mass transfer is the amount of gas transferred from the gas bubbles into the liquid phase and it is determined by the magnitude of the volumetric liquid mass transfer coefficient, $k_L a$. The mass transfer coefficient is represented by k_L while the specific interfacial area is represented by a (Kaštánek *et al.* 1993). The volumetric liquid mass transfer coefficient is essential for determining the overall rate of the reaction which allows the effect of mass transfer on the overall reaction rate to be evaluated. Equation 2-7 indicates that the value of $k_L a$ is dependent on the size of bubbles. Therefore for tiny bubbles ($d_s \leq 0.002$ m), k_L rapidly increases as d_s increases. For larger bubbles ($d_s \geq 0.002$ m) k_L will slightly decrease as d_s increases (Kaštánek *et al.* 1993).

$$k_L a = \frac{6\varepsilon_G k_L}{d_s} \qquad \text{Equation 2-7}$$

where k_L = mass transfer coefficient [$m \cdot s^{-1}$]

ε_G = gas holdup

d_s = mean Sauter diameter [m]

As turbulent shear stress increases in the reactor due to higher liquid velocity, a thinner liquid film causes k_L to increase. The high turbulent shear stress also creates smaller gas bubbles, which correspond to an increased specific interfacial surface area, *a*, and therefore an increase in the volumetric mass transfer coefficient, $k_L a$. Higher gas velocities also increase the $k_L a$ value of the system by increasing the gas bubble specific interfacial area (Gamal El-Din 2001). Although increasing superficial gas velocity increases the $k_L a$ value, the superficial liquid velocity has no effect on the performance of the column (Voigt and Schügerl 1979). Increasing the superficial gas velocity causes an increase in power input and a subsequent increase in the fraction of microturbulence. Voigt and Schügerl (1979) concluded that this microturbulence dissipates energy and disperses gas with greater efficiency than large scale turbulence.

Diffusion of ozone in water obeys Fick's law for molecular diffusion. The diffusion constant, D_{O3} is equal to 1.74×10^{-9} $m^2 \cdot s^{-1}$ at 20 °C (Langlais *et al.* 1991). For the transfer of ozone to water with no chemical reactions between the gas constituents, the mass transfer occurs according to the two-film model with a driving force equal to $(C_L^* - C_L)$:

$$\Psi = \frac{dC}{dt} = k_L a (C_L^* - C_L) \qquad \text{Equation 2-8}$$

where: Ψ = gas absorption rate [$mg \cdot L^{-1} \cdot s^{-1}$]

k_L = local liquid mass transfer coefficient [$m \cdot s^{-1}$]

a = specific interfacial area of gas bubbles [m^{-1}]

C_L^* = concentration of the dissolved ozone in equilibrium with the bulk ozone gas [$mg \cdot L^{-1}$]

C_L = concentration of the dissolved ozone in the bulk liquid [$mg \cdot L^{-1}$]

From this equation it is shown that the gas absorption rate is proportional to the chemical mass transfer coefficient, the concentration driving force, and the specific interfacial area per unit volume of the solution. This concentration driving force for mass transfer between the gas phase and the liquid phase is derived from the displacement of the system from equilibrium (AWWA 1999). In other words the difference between the actual concentration of dissolved gas in the liquid phase and the concentration of dissolved gas at equilibrium is proportional to the rate of dissolution or absorption of the gas. This proportionality is represented by Henry's law, which describes the equilibrium partitioning of a gas between air and water. It states that at constant temperature, the amount of gas dissolved into a liquid at equilibrium is directly proportional to the partial pressure of the gas above the liquid (Sawyer *et al.* 1994).

Since ozone is quicker to diffuse in the gas phase than in the liquid phase, the liquid phase is the limiting rate reaction and therefore the overall volumetric mass

transfer coefficient is approximated by the local mass transfer coefficient in the liquid phase (Gamal El-Din 2001). According to the film theory and assuming there is no resistance to mass transfer in the gas phase, the only resistance to mass transfer exists in the liquid film near the interface because ozone is a sparingly soluble gas in water (Sotelo *et al.* 1989). This hypothesis allows the concentration of ozone in the aqueous phase at the gas-liquid interface at equilibrium, C_L^*, to be defined in Equation 2-9 (AWWA 1999). Diffusion of the gas in the contactor varies depending on the gas and liquid flow rates, the gas bubble diameter, the contactor geometry, and the location and distribution of diffusers (Mariñas *et al.* 1993).

$$y = HC_L^* \qquad \text{Equation 2-9}$$

where: y = concentration of ozone in the bulk gas

H = Henry's law constant

The units of Henry's law constant vary and the units of the concentration of ozone in the bulk gas reflect this.

In their study of gas phase backmixing in bubble columns, Shetty *et al.* (1992) determined that the assumption of negligible interphase mass transfer was only good for insoluble tracers with a Henry's law constant greater than 1,000

$m^3_{liq} \cdot m^{-3}_{gas}$. Furthermore, due to the solubility of the tracer, the actual residence time of the gas phase tracer is greater than that calculated based on the superficial gas velocity because the gas phase is backmixed and some of the tracer disappeared into the liquid phase.

Salazar *et al.* (1993) performed mass transfer experiments involving a jet bubble column with air at steady state. The $k_L a$ in a jet bubble column can be evaluated by assuming perfect mixing in the liquid phase if the liquid phase is stagnant. It was determined that the $k_L a$ values for jet bubble columns were approximately 1.5 times greater than the $k_L a$ values for typical bubble columns at the same conditions. With zero liquid velocity, $k_L a$ was independent of the axial position in the reactor due to the liquid velocity having negligible effect on the overall $k_L a$ of the bubble column and due to the $k_L a$ being larger near the cone inlet when liquid flow exists. The concentration of oxygen at the entrance of the column was greater due to higher mass transfer rates and due to partial backmixing in the liquid phase.

Xu and Cunli (1990) calculated the mass balance for a conventional bubble column, its ozone utilization efficiency, ozone consumption, and ozone transfer efficiency. The ozone mass transfer coefficients were determined from the mass balance analysis of ozone in the gas and liquid phases and were then regressed into a model of ozone transfer. This model allowed the prediction of mass

transfer efficiency in the bubble column at different operating conditions. The volumetric liquid mass transfer coefficient was determined to be a function of gas flow rate. The kinetics appeared to have a considerable effect on the ozone mass transfer efficiency.

Shulman and Molstad (1950) investigated the characteristics of mass transfer in bubble columns using CO_2 desorption and absorption and H_2 desorption studies. Factors affecting mass transfer were gas flow rate (for streamline regime only), liquid flow rate, water temperature, column height, and liquid diffusivity. Factors that had no effect on mass transfer rate were gas flow rate (for turbulent regime only), column diameter, plate porosity, and desorption versus absorption. The study used plates with coarse pores and with fine pores and the size of the bubbles produced by both plates appeared the same, except at very low gas rates. When gas was passed rapidly through a bubble column with countercurrent flow there was very little recirculation within the reactor. The investigators found it difficult to compare the results of the absorption study with the results of other investigators because of the large variation of specialized apparatus. At high gas rates the gas holdup was constant, the bubble size was constant, and the interfacial area decreased due to an increase in bubble coalescence. At low liquid rates, the gas holdup decreased because the bubbles were widely spaced and the interfacial area per unit volume decreased. The bubbles were formed in the liquid and not at

the surface of the plate and therefore the bubble size was dependent on the properties of the liquid.

Sotelo *et al.* (1989) determined that the rate of the ozonation process in a water that contains several salts depended on the diffusion of ozone in water, the auto-decomposition of ozone, and the chemical reaction with the dissolved pollutant. Henry's law constants obtained for the system deviated by approximately 10 % from the average values and deviated by 15 % when fitted as a function of pH, temperature, and ionic strength.

2.6.1 Volumetric Liquid Mass Transfer Coefficient

Many researchers have calculated the volumetric liquid mass transfer coefficients of a variety of different systems and setups in an attempt to describe the mass transfer of ozone from the gaseous to the aqueous phase. According to Kaštánek *et al.* (1993), typical values of $k_L a$ for different types of reactors are 0.01 s^{-1} for bubble columns, 0.5 to 1 s^{-1} for stirred tank reactors, and 0.05 to 0.1 s^{-1} for wetted plate reactors. Experiments involving an ozone/tap water system with perpendicular jets (Sheffer and Esterson 1982) obtained $k_L a$ values between 0.01 and 0.02 s^{-1} for lower water flow rates and between 0.02 and 0.03 s^{-1} for higher water flow rates. A new gas-inducing reactor for use in wastewater treatment introduced by Hsu *et al.* (2002) provided $k_L a$ values that ranged from 0.01 to 0.02 s^{-1}.

In the many mass transfer experiments performed with ozone there have been as many variations on the methods used to predict the volumetric liquid mass transfer coefficient, $k_L a$. Roustan *et al.* (1996) developed a computer model based on mass balance equations and on the stirred tanks-in-series flow model to calculate the $k_L a$ value and the kinetic constant, k_c, of ozone consumption by water. The hydrodynamic parameters measured experimentally in a bubble column with a porous distributor were the gas holdup, the bubble size, and the residence time distribution. The rate of ozone decomposition kinetics was assumed to be first order. It was also assumed that the gas phase had plug flow behaviour and that the liquid phase had a behaviour described by a series of equally sized well mixed reactors. The mass balance equations were formulated for the gas and liquid phases using these assumptions and the mass transfer parameters were solved using numerical methods that compared the measured and simulated values of ozone concentrations. It was determined that the hydrodynamic parameters must be solved to properly develop an overall mathematical model.

Wright *et al.* (1998) developed a model for a cocurrent gas-liquid downflow contactor by taking the walls of the unit and one inlet and one outlet stream as the boundary conditions. The ozone-water and ozone-contaminant reactions and kinetics were reduced to a first order relationship. For plug flow behaviour, the

steady state mass balances for cocurrent downflow were solved using a numerical solution technique for ordinary differential equations. The experimentally determined gas and liquid holdups, ratio of gas to liquid flow rate, ozone concentrations, and hydraulic residence times for the jet-pump contactor were substituted into the cocurrent mathematical model equations to solve for k_La. Firstly an initial guess for k_La was provided and then the model equations were iteratively solved until the output parameters of the simulation converged with the experimental data. The variable chosen to test this convergence was the gas phase ozone concentration in the outlet. The k_La values obtained were high; however they were not a strong function of physical parameters such as flow and flow ratios for the range of parameters studied.

The approach taken by Huang *et al.* (1998) to analyze the mass transfer of ozone absorption and decomposition in a bubble column gas-liquid contactor by deriving equations from the mass balance, absorption equilibrium, and the effect of hydrostatic pressure. Dimensionless differential equations were obtained for the liquid phase and the gas phase ozone. Further differential equations from the film model were solved by applying boundary conditions and by numerical integration. The kinetic expression used was of three-halves order. Among other parameters the liquid phase mass transfer coefficient, k_L, was solved. By considering the concentrations of ozone in the bulk liquid and the holdup gas, the

rate of ozone decomposition and variable enhancement factor and gas velocity, this refined mathematical model adequately described the bubble column system.

Bouaifi *et al.* (2001) compared the interfacial area and volumetric liquid mass transfer coefficient of two types of gas-liquid contactors – a ring sparger with dual impeller and two bubble columns with three types of spargers. The interfacial area, *a*, was found to be dependent on the geometrical size of the unit, operating parameters, and physical and chemical properties of the liquid. The volumetric liquid mass transfer coefficient was calculated using Equation 2-8, assuming perfect mixing for the liquid phase. The $k_L a$ of the bubble column was greater than the $k_L a$ of the stirred gas-liquid reactor because of the larger interfacial area in bubble columns. The value of k_L was dependent on the diffusivity coefficient and on the turbulence in the liquid phase. As the bubble size increased, so did the k_L value.

Using mass balances along the height of a bubble column, Laplanche *et al.* (1991) established a computer simulation to obtain the profiles of dissolved ozone residual in the liquid phase and of the residual ozone concentration in the gas. The volumetric liquid mass transfer coefficient, $k_L a$ was solved by knowing the rest of the variables in the mass balance of the liquid phase from the pilot scale experiments. The driving concentration gradient, $(C_L^* - C_L)$ was approximated by calculating the logarithmic average of the differences between the concentrations

of ozone at the entrance and the exit. The simulated value of k_La was calculated using a relationship given by Roustan *et al.* (1987) and based on commercial contact columns: $k_La = 0.0139 \cdot u_G^{0.82}$; with k_La in min^{-1} and u_G in $m \cdot h^{-1}$. The k_La values obtained from this formula were lower than the values found in the pilot scale unit.

Salazar *et al.* (1993) indicated that correlations for the volumetric liquid mass transfer coefficient in bubble columns, such as the one proposed by Deckwer *et al.* (1974), cannot be applied to analyze experimental mass transfer measurements. Instead, this equation was integrated over the entire bubble column and k_La became a function of the volume, cross-sectional area, and liquid flow rate of the entire column.

The determination of k_La for a new gas-inducing reactor involved the two-film theory and the mass balance of ozone (Hsu *et al.* 2002). Knowing the ozone auto-decomposition rate constants at two values of pH, the equilibrium concentration of ozone in the water, and the concentration of ozone in the water at different times, the volumetric liquid mass transfer coefficient was obtained.

2.6.2 Types of Ozone Injectors

Although diffusers are the most common method of injecting the gas into the liquid, new and different technologies have emerged in an attempt to increase the

efficiency of ozone mass transfer. Jets in different configurations are used in ozone mass transfer experiments. Inline injection of ozone can be achieved using either sidestream or direct injection. In sidestream injection, a small flow is diverted and ozone is pulled into this sidestream using a gas-liquid injector. Prior to blending into the main flow of water, the ozonated sidestream passes through static mixing elements to enhance mass transfer. New alternatives such as injectors designed by Mazzei Injector Corporation are replacing the static mixing elements. These venturi injectors are high efficiency, can draw ozone into the liquid by suction (ejection mode), and can create a stream of fine bubbles that enhances the mass transfer (Schulz and Prendiville 1993).

Radhakrishnan and Mitra (1984) measured pressure drop, holdup, and interfacial area in a vertical column that used a multi-liquid jet ejector for the dispersion of gas. The multi-liquid jet ejector consisted of primary and secondary inlets followed by a nozzle, throat, and diffuser. From the results it was assumed that the high turbulence and shear stress in the ejector throat produced very small bubbles with very high interfacial area, and these primary bubbles coalesced during their flow through the diffuser to form stable secondary bubbles.

Gamal El-Din and Smith (2003) performed ozone mass transfer experiments with an impinging-jet bubble column. Two Mazzei venturi injectors were placed at the bottom of a 1520 mm tall bubble column with an elliptical base at an intersecting

angle of 125 ° with the two nozzles separated by 60 mm. With this arrangement, the intensities of turbulence in the ambient fluid increased significantly, resulting in an increase in mass transfer rates compared to conventional bubble column systems. Another advantage over conventional bubble column designs is the unit's compact size, which can handle high liquid and gas flow rates without compromising the mass transfer efficiency.

2.6.3 Recent Technologies in Gas-Liquid Contacting

Bubble columns with some type of diffuser tend to be the most commonly studied gas-liquid contactor found in the literature. Brodard *et al.* (1986) observed the disadvantages associated with mass transfer of ozone via contact chambers with diffusers as being the large volume involved, the dead zones and preferential pathways in the reactors, and the limited transfer efficiency. In their desire to study a newer technique, the researchers investigated a deep U tube. Operating as a plug flow reactor in the liquid phase allowed the deep U tube to be efficient at mass transfer with contact times shorter than those of conventional columns. High turbulence in the tube caused bubbles to break, which results in a higher interfacial area, *a*. An increase in static pressure at the lowest point in the deep U tube caused an increase in the equilibrium saturation concentration of ozone, C_L^*. An increase in *a* and in C_L^* will cause an increase in $k_L a$ and therefore increase the transfer efficiency.

According to Heyouni *et al.* (2002), static mixers are becoming integral and basic equipment in the industries involving chemical processing for applications such as laminar and turbulent mixing of miscible liquids, laminar flow heat exchangers, laminar and turbulent homogenization, tubular reactors, dispersion of immiscible phases, and interphase mass transfer between immiscible phases. The static mixer comprises rigidly structured stationary mixing elements that are inserted in series in a pipe. Each element divides and recombines the flow. Contacting between the phases occurs as the fluids are sheared and directed radially across the pipe. The main characteristics of static mixers are plug flow behaviour, intensive radial mixing, located inline in a pipe, continuous operation, compact design, easy scaleup, and no mobile parts (Martin and Galey 1994). Advantages of static mixers include high mixing between the gas and liquid phases, bubbles with small diameters, high interfacial area, high mass transfer coefficient, and plug flow behaviour. Heyouni *et al.* (2002) characterized the hydrodynamic behaviour of two-phase flow and the mass transfer in a static mixer. In terms of mass transfer, much higher values of the volumetric liquid mass transfer coefficient were obtained than with other gas-liquid reactors because of the ability of the static mixer to develop large interfacial areas and therefore high mass transfer in the system.

Research by Thalasso *et al.* (1995) studied the combination of a venturi injector and a static mixer in a bubble column. Compared to mass transfer of oxygen with

the injector only, the addition of a static mixer in the bottom of the reactor did not improve the mass transfer of oxygen already provided by the venturi injector.

Craik *et al.* (2002) studied the effect on microorganism reduction of ozone gas-liquid contacting conditions in a static mixer. The static mixer provided high turbulence and high interfacial area and consequently high mass transfer rates and rapid gas dissolution within a compact device. The static mixer, the connecting tubing, and a bubble column were used to calculate the ozone transfer efficiency (OTE) of the reactor. Trials showed that, at the same superficial liquid velocity and ratio of gas to liquid flow, the OTE was independent of the applied ozone dose and of the concentration of ozone in the gas. It was concluded that both the superficial liquid velocity and the ratio of gas to liquid flow significantly affected the OTE in the experimental static mixer system. Values for OTE for the static mixer system ranged from 66.3 to 93.8 %.

A confined plunging liquid jet contactor (CPLJC) was used to transfer ozone into a stream of pure water by Jakubowski *et al.* (2003). The CPLJC is comprised of a vertical column (downcomer) that performs the gas-liquid mixing and a riser at the base of the downcomer where the gas disengages from the liquid. The advantages of the CPLJC over other contacting reactors are its compact size and the suction that is maintained inside the downcomer and in the gas feed line that improves safety with respect to potential ozone leaks. The $k_L a$ values ranged

from 0.301 to 0.474 s^{-1} which compared well to other commonly used contactors. The k_La increased with increasing gas flow rate due to greater gas holdup inside the downcomer which caused a higher interfacial area, *a*. Conversely, an increase in liquid flow rate caused a decrease in gas holdup and consequently lower interfacial areas and lower k_La values.

Briens *et al.* (1992) studied the hydrodynamics and the gas-liquid mass transfer in a venturi combined with a bubble column, with the liquid flowing downward. It was theorized that, since high liquid velocities had been shown to enhance gas-liquid mass transfer, the venturi nozzles would provide this high liquid velocity in its converging section in high intensity gas-liquid reactions with short contact time. The coefficient of volumetric liquid mass transfer in the annular zone of the venturi was calculated based on the mixing being approximated as liquid phase plug flow. The volumetric mass transfer coefficient in the bubbling zone of the venturi was obtained by assuming perfect liquid backmixing. The downflow configuration of the venturi in the bubble column produced much higher gas-liquid mass transfer rates than the upflow venturi (studied by Huynh *et al.* 1991), providing that the annular zone did not occupy the entire venturi.

Schulz *et al.* (1995) evaluated an ozone contactor referred to as the sidestream venturi injector with downflow tube (SVI-DT). The sidestream venturi injectors were contained in an internal downflow tube and they controlled the size and

uniformity of the gas bubbles inside the tube. The contactor comprised one or more diffusion chambers that contained at least one of the internal downflow tubes. This high efficiency ozone injection contactor was studied at pilot scale with gas to liquid flow ratio, G/L, ranging from 0.01 to 0.07 and was found to facilitate the dissolution of ozone into the water, resulting in high mass transfer rates. The superficial velocity of the water had an effect on the gas bubble flow patterns maintained in the downflow tube and on the gas holdup effects. The SVI-DT was found to remove more colour and yield higher dissolved ozone residuals than the traditional countercurrent flow, fine-bubble diffusion contactor. It was able to operate effectively at gas flows with high ozone doses and low volumes. Mass transfer efficiency rates at the pilot plant ranged from 88 to 98 %.

2.7 Kinetics

The instability of ozone gas causes it to auto-decompose within an aqueous solution. To know what amount of ozone leaving the gas phase is caused by mass transfer processes and what amount is caused by auto-decomposition, researchers must first determine the reaction order of ozone auto-decomposition kinetics. Two methods exist to determine the ozone demand of the water, the Solution Ozone Test (S.O.T.) and the Gas Ozone Test (G.O.T.). In the S.O.T. a solution of maximal concentration of ozone dissolved in water is injected into the water to be treated; while in the G.O.T. a predetermined volume of ozone-containing gas is mixed with a certain volume of water to be treated. The initial ozone

consumption or demand can be determined within a short period of time. Following this initial ozone demand, there is a period of auto-decomposition where the concentration of dissolved ozone in the water decreases. This reduction in concentration of dissolved ozone depends on characteristics of water such as pH, alkalinity, temperature, Fe, Mn and Br^- ion, nature, and concentration of organic matter (Richard 1994).

The overall consumption of dissolved ozone occurs in two distinct pathways: 1) direct oxidation of all available organic and inorganic solutes; and 2) a self-decomposition cycle which can be initiated by hydroxide ions, $(OH)^-$, as well as other initiating compounds, and then accelerated by the subsequent attacks of various free radicals on ozone (Yurteri and Gurol 1988). The oxidation of organic and inorganic compounds during ozonation occurs via ozone, OH radicals, or a combination thereof. The pathway is determined by the ratio of ozone and OH radical concentrations and the corresponding kinetics of the water (von Gunten 2003). Various impurities found in natural water sources may directly consume ozone and thereby affect the apparent rate of ozone consumption by interacting with the hydroxyl free radicals. Yurteri and Gurol (1988) found that the measured ozone consumption rates conformed to first order kinetics with respect to the concentration of dissolved ozone. The overall rate constant, here called the specific ozone utilization rate, was found to be a function of the pH and chemical composition of the raw water.

The ozone demand tests as described by Richard (1994) allow the kinetic reaction order of the test liquid to be determined. Mariñas *et al.* (1993) and Sotelo *et al.* (1989) remarked that there was no agreement between authors with respect to the order of the ozone decomposition reaction in water. According to Huang *et al.* (1998) the overall kinetic reaction order varies from 0 to 2 for ozone. Some researchers have considered the decomposition reaction to be first order with respect to ozone, while others have chosen three-halves order with respect to ozone concentration for the decomposition of ozone. However many kinetic models do not consider the effects of pH and temperature even though the kinetic expressions tend to be dependent on pH, temperature, type of salt, ionic strength, and concentration of hydroxyl radical scavenger in the test liquid (Huang *et al.* 1998).

Sheffer and Esterson (1982) measured the mass transfer coefficient and kinetic parameters of a well-mixed, perpendicular-jet contacting system with continuous tap water treatment using ozone. Analysis of results revealed a linear relationship between the ozone feed and ozone residual, suggesting that a zero kinetic order for linearity best described the results.

Research by Oke *et al.* (1998) indicated that the commonly used first order kinetics rate constant was not sufficient to describe the behaviour of ozone decay.

Various natural waters were studied to determine the effects of raw water quality on the ozone decay kinetics in a bubble column. Results showed that first order kinetics were not valid for waters containing natural organic material due to a decreasing rate constant. During the course of ozonation the quality of the water changes and therefore an exponentially decreasing function was identified as a more suitable description of the ozone decay kinetics over the first order kinetics equation. The pH, total organic carbon, concentration of carbonate ion, UV absorbance at 254 nm, total solids, concentration of bicarbonate ion, magnesium hardness, and calcium hardness of the natural waters were all determined to be significant in the determination of ozone decay kinetics.

It was assumed that the auto-decomposition of ozone could be represented by a pseudo-first order kinetics reaction. Gamal El-Din (2001) noted that a first order reaction rate constant was assumed to be inadequate for high initial ozone demand because of changing water characteristics. The specific ozone utilization rate constant, k_w, is introduced to describe the exponential decrease in dissolved ozone concentration, C_L.

$$\frac{dC_L}{dt} = -k_w C_L = -(k_1 + k_2 e^{-k_3 \Delta O_3}) C_L \qquad \text{Equation 2-10}$$

where: C_L = instantaneous concentration of dissolved ozone [$mg \cdot L^{-1}$]

k_w = specific ozone utilization rate constant [s^{-1}]

k_1, k_2, k_3 = empirical non-linear regression constants [s^{-1}]

t = reaction time [s]

ΔO_3 = amount of utilized ozone [$mg \cdot L^{-1}$]

Hermanowicz *et al.* (1999) also concluded that the order of ozone reaction could vary with the extent of reaction. As the organic matter reacts with the ozone, intermediate products are formed and the reaction rate changes. These intermediates can be either less or more reactive than the original compounds, thereby slowing down or speeding up the reaction rate with respect to the concentration of ozone. Therefore although first order kinetics were adequate in describing the initial stages of ozone reaction in the batch experiments with surface water, the results showed that other types of kinetics may have better represented the whole extent of the reaction. In these batch experiments the ozone reaction rates were better described by the n^{th} order kinetics. The change in reaction order suggested that the original water components were transformed into intermediates that were more reactive with ozone. It was also found that the rate coefficient and the order of reaction decreased with increasing dose of ozone transferred to the water before each of the batch tests.

In a study on oxidation kinetics and product formation for the ozonation of drinking water, von Gunten (2003) observed that the rate constants for the oxidation of selected natural and anthropogenic micropollutants with ozone and

OH radicals were second order. These rate constants covered a range of more than nine orders of magnitude. The main mechanism for the oxidation of inorganic compounds was the transfer of an oxygen atom from ozone to the inorganic compound. In other words, electron-donating groups enhanced the oxidation by ozone and the electron-withdrawing groups reduced the rates of reaction.

Richard (1994) made an important point when he noted that the quality of the water to be treated varies throughout the year, causing the ozone demand of the water to fluctuate. The amount of ozone lost in an ozone-water contacting system depends on the ozone transfer efficiency of the system and on the ozone demand of the water being treated. This fact should be considered by the designers and the operators of a water treatment plant to ensure the loss of ozone does not get too high.

3. MATERIALS AND METHODS

3.1 Kinetics of Ozone Auto-decomposition in Sample Water

The sample water used was building tap water supplied by EPCOR Water Services Rossdale Water Treatment Plant in Edmonton, Alberta, Canada. To determine the reaction rate and order of reaction between ozone and tap water, a series of experiments at temperatures ranging from approximately 6 to 32 °C was performed. The glassware used for all experiments involving ozone was made ozone-demand-free (ODF) to rid the surfaces of any impurities that would consume ozone. Ozone solution was prepared by ozonating a 20 L bottle of deionized water using the PCI Ozone Corporation ozone generator (model C2P-9C-4). The source of deionized water was a Maxima Ultra Pure Water tank from ELGA. The ODF glassware was prepared by filling the required glassware with a solution of ozone and allowing the solution to sit for 30 min while any impurities were consumed. The glassware was then emptied of the solution, covered with aluminum foil to ensure no contaminants would make contact, and allowed to dry in the oven overnight.

The day of the kinetics experiments the tap water from the cold faucet was allowed to run for a minimum of 10 min. For all temperatures, a 600 mL volume of ozone solution was added to a 600 mL volume of sample water in a reactor

with a tight fitting and height adjustable lid (Figure 3-1). The reactor was placed on a magnetic stir plate and the solution was well mixed. The sample of tap water was preheated on a heating plate for temperatures above ambient conditions. For temperatures below ambient, a cold water bath and sometimes an ice pack were used to maintain the desired temperature in the reactor.

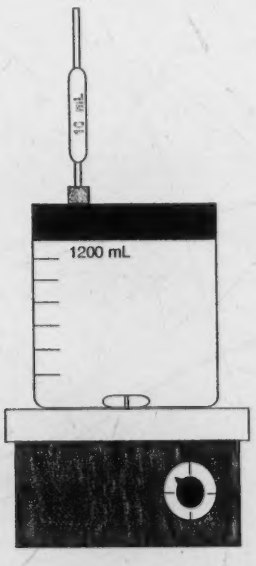

Figure 3-1 Reactor apparatus for kinetics of tap water experiments.

Once the ozone solution was added to the tap water sample, the stopwatch was started and 10 mL samples were taken using a volumetric pipette every 1 to 2 min for a period of 15 min. Immediately after sampling through the lid of the reactor, a temperature probe was inserted and the temperature was measured. After the samples were taken, the pH and temperature of the solution in the reactor were measured using the Accumet pH meter (model 25).

Ozone residual was measured using the Indigo Colourimetric Method (American Public Health Association 1995). Ten 100 mL volumetric flasks were filled with 10 mL of indigo reagent II, 10 mL of sample from the reactor, and filled to volume with deionized water. One flask was used as a blank (control) that contained 10 mL indigo reagent II and filled to volume with ODF water. The flasks were gently mixed and then the absorbance was measured at 600 nm. The Ultrospec 3000 spectrophotometer (Pharmacia Biotech, model 80-2106-20) was used to read the absorbance in quartz cuvettes. If all of the ozone had decayed in a sample, there would be no reaction with the reagent, the solution would remain dark indigo, and the absorbance would equal that of the blank. Therefore since most of the ozone had decayed after 15 min of mixing, the flask containing the tenth sample was a darker indigo colour than the flask containing the initial sample.

To calculate the amount of residual ozone in the sample, the following equation was used:

$$mgO_3 / L = \frac{100 \times \Delta A}{f \times b \times V} \qquad \text{Equation 3-1}$$

where: ΔA = difference in absorbance between sample and blank

$f = 0.42$

b = path length of cell [cm]

V = volume of sample [mL]

According to *Standard Methods for the Examination of Water and Wastewater* (1995), the factor *f* is based on a sensitivity factor of 20,000/cm for the change of absorbance (600 nm) per mole of added ozone per liter. Alternatively, with respect to the UV absorbance of ozone in pure water, the factor *f* corresponds to an absorption coefficient for aqueous ozone, ε = 2950/Mcm at 258 nm.

The order of the auto-decomposition reaction was then modeled and the reaction rate constant, k_1, determined for each temperature. The Arrhenius equation was used to correlate the k_1 values to their respective temperatures by plotting the natural logarithm of the k_1 values against the respective temperature less 20 °C.

3.2 Hydraulic Performance Study

Studies of hydraulic performance for both systems were completed to determine the maximum allowable system back pressure, the range of feed gas flow rates achievable at various liquid flow rates, and under what combination of conditions would the gas flow be ejected or injected into the liquid. Following the given ranges of liquid flow rate and of gas to motive flow ratio, various combinations of liquid and gas flows were tested and recorded. The PCI–WEDECO ozone generator (model GLS-7) was set to *purge* mode, which meant that extra-dry oxygen was used as the feed gas instead of ozone. The inlet gas pressure at the throat of the injector, the liquid pressures before and after the injector, and the

system back pressure were recorded. The pressure gauges used were previously calibrated using a Druck calibrator (type DPI 603) rated from –15 to 100 psig. The liquid flowmeter was calibrated using tap water, a 20 L bucket, and a timer. The rotameters were calibrated using a cylinder of extra-dry oxygen, a pressure gauge, the wet test meter (GCA Corp./Precision Scientific Group, Cat. No. 63115), and a timer.

3.3 Characteristics of Sample Water

The characteristics of water discussed in this section were determined for each day of mass transfer experiments.

3.3.1 Alkalinity

The alkalinity of the tap water was tested using the Titration Method (American Public Health Association 1995). The 0.1 *N* sulfuric acid (H_2SO_4) solution was standardized using an approximately 0.05 *N* sodium carbonate (Na_2CO_3) solution. The normality of the sulfuric acid was calculated by:

$$Normality, N = \frac{A \times B}{53.00 \times C} \qquad \text{Equation 3-2}$$

where: A = mass of Na_2CO_3 weighed into a 1 L flask = 2.6498 g

B = volume of Na_2CO_3 solution taken for titration = 50 mL

C = volume of acid used [mL]

A 100 mL sample of tap water was then titrated with the sulfuric acid to a preselected endpoint pH of 4.3. The alkalinity as calcium carbonate was determined by the following equation:

$$Alkalinity, mgCaCO_3 / L = \frac{A \times N \times 50000}{mL.sample} \qquad \text{Equation 3-3}$$

where: A = volume of standard acid used [mL]

N = normality of standard acid

The alkalinity of the tap water was determined for each day that a kinetics experiment or a mass transfer experiment was performed.

3.3.2 Total Carbon

The total carbon (TC) and total inorganic carbon (TIC) of the tap water were directly measured using the Persulfate-Ultraviolet Oxidation Method (American Public Health Association 1995). From these two values, the total organic carbon (TOC) of the tap water was calculated. In this method, organic carbon is oxidized to carbon dioxide (CO_2) by persulfate in the presence of ultraviolet light and measured directly by a nondispersive infrared analyzer. For these experiments, the Dohrmann Carbon Analyzer (Folio Instruments, model DC80) was used along

with a 0 to 1 mL syringe, and the reagents potassium acid phthalate (KHP) and sodium carbonate (Na_2CO_3). For the TC tests, the carbon analyzer was calibrated by injecting (in triplicate) 1 mL of 10 ppm KHP standard. After calibration, 1 mL of sample was injected into the carbon analyzer. A calibrated total carbon value in ppm ($mg \cdot L^{-1}$) was printed out after the detector calculated the area of the peaks produced by the analyzer and compared them to the peak area of the calibration standard. The same procedure was followed for the TIC tests, however calibration was performed by injecting 1 mL of 10 ppm Na_2CO_3 standard. The value for TOC was calculated by subtracting TIC from TC.

3.3.3 Temperature and pH

The temperature and pH values of the tap water were also determined on each day that tap water was used. Approximately 200 mL of sample tap water was poured into a beaker and the pH and temperature probes were immersed. Gentle mixing was maintained by stirring the probes in the beaker until a constant pH was reached. The pH and temperature values of the tap water were read from the Accumet meter (model 25).

3.4 Tracer Study

Elements of fluid take different routes through a reactor and therefore take a different amount of time to exit the reactor. The distribution of these times is

called the exit age distribution, E, or the residence time distribution, RTD, of the fluid (Levenspiel 1999). The value E has the units of time^{-1} and is commonly represented by a curve whose area is unity:

$$\int_0^\infty E dt = 1 \qquad \text{Equation 3-4}$$

The exit age distribution curve can be found by using a nonreactive tracer, by pulse input or by step input. Tracer studies for the injector, the flash mix reactor, and the opposing jets reactor were performed to determine the mixing characteristics of these components. For the tracer studies, a nonreactive tracer – potassium chloride (KCl) – and conductivity probes were used to determine the conductivity of the water. Conductivity is a measure of the ability of an aqueous solution to carry an electric current, which depends on the presence of ions in the solution (American Public Health Association 1998). The E curve for the individual components to be modeled could be created by reading the conductivities at three locations: following the injector, following the flash mix or opposing jets reactor, and following the gas-liquid separator. The location of the KCl injection points were upstream of the components and are indicated in Figure 3-2 and Figure 3-3 by the numbers 1, 3, and 4. The corresponding locations for the conductivity probes were numbered 2, 4, and 5.

Three YSI conductance meters were used (models 34 and 35) alongside the Ultra Logger data logger (model UL-16D) and a laptop computer running Lakewood

software to record the conductivity. The conductance meters and their probes were calibrated in KCl solutions of concentrations ranging from 0 to 160 $mg \cdot L^{-1}$ to produce a calibration curve linking the recorded measurements in volts to the concentration of KCl. A solution of 70 $g \cdot L^{-1}$ KCl was prepared and one 5 mL syringe was filled for injection into the system. Once the system had reached the condition of steady state, the data logger was initiated and the KCl solution was injected into the center of the liquid flow using a long needle at the end of the syringe (at time zero). In the case of the opposing jets, two syringes of 5 mL were simultaneously injected into each liquid line entering the opposing jets. The conductivity values were recorded by the data logger every one second. The two gas wash bottles were each filled with 400 mL of tap water to simulate the back pressure produced during the mass transfer experiments. The tracer studies were performed at the same gas and liquid flow rates and system back pressures as selected for the mass transfer experiments. The ozone generator was again set to *purge* mode, using extra-dry oxygen as the feed gas.

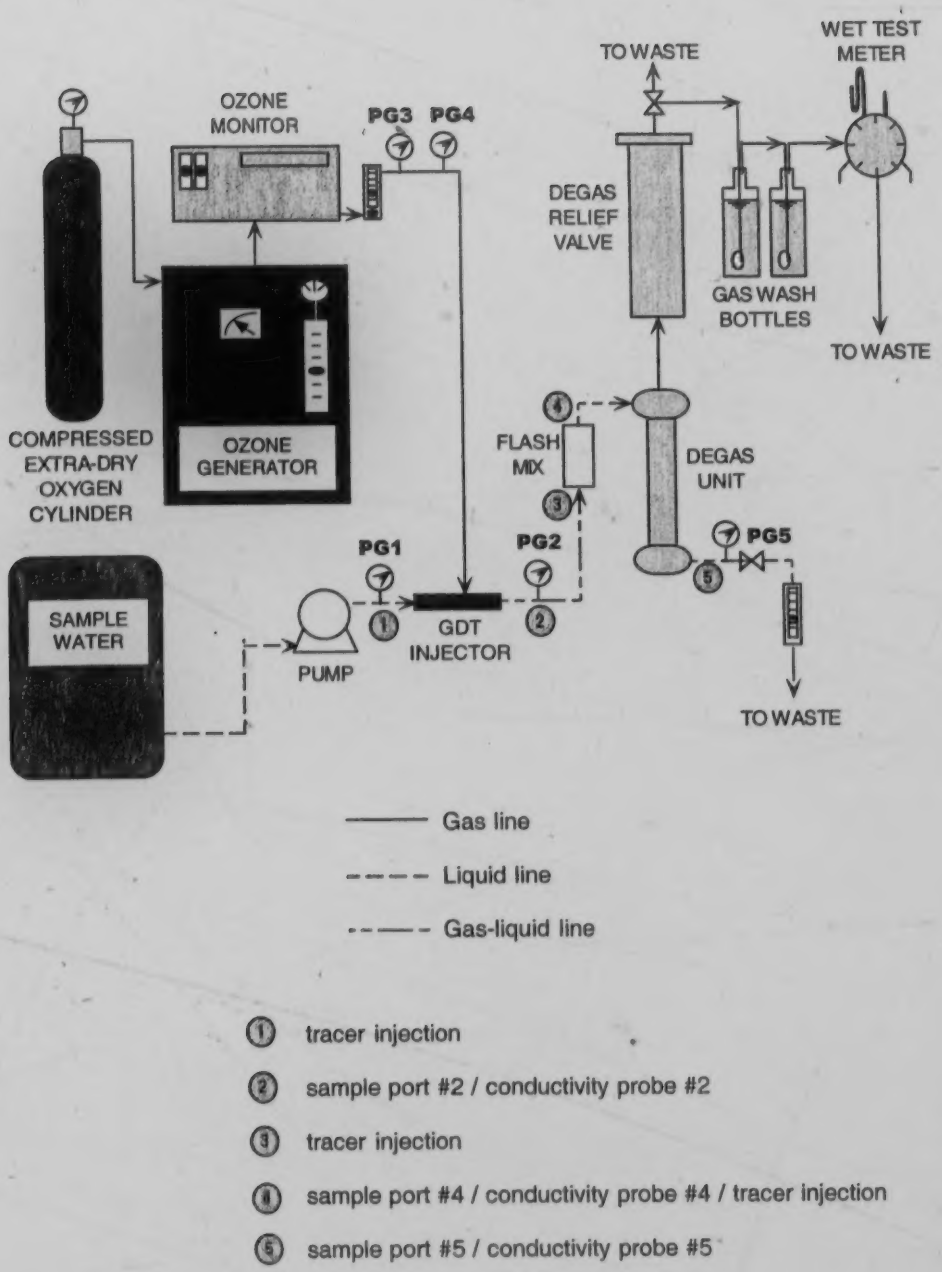

Figure 3-2 Experimental setup of flash mix system indicating important points for tracer study and for ozone mass transfer experiments.

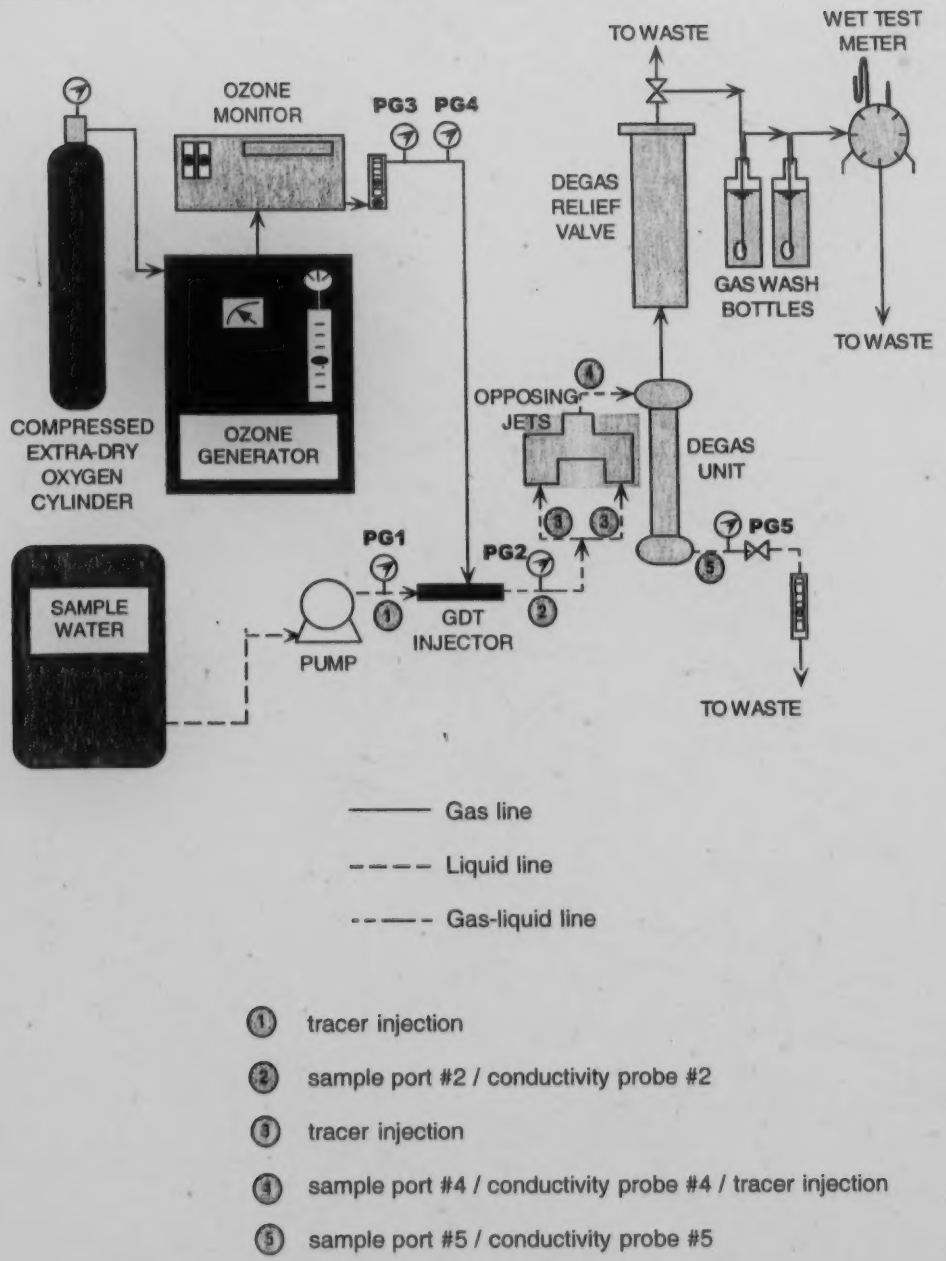

Figure 3-3 Experimental setup of opposing jets system indicating important points for tracer study and for ozone mass transfer experiments.

By applying the calibration equation, the concentration, C, of the tracer leaving the component at different time, t, could be determined. Plotting C versus t would result in a curve whose area was equal to M/Q (mass of tracer per flow rate). The following equation gives a curve with area equal to unity:

$$E = \frac{C}{M/Q} \qquad \text{Equation 3-5}$$

where: E = exit age distribution [T^{-1}]

C = concentration of KCl leaving reactor component [$M \cdot L^{-3}$]

M = mass of tracer introduced [M]

Q = flow rate of liquid through reactor component [$L^3 \cdot T^{-1}$]

From this equation, E curves were created from the data logged during the tracer studies of the injector, the flash mixer, the opposing jets, and the degas separator. The E curves could then be interpreted to determine whether the gas-liquid reaction followed the plug flow reactor (PFR) model or the continuous flow stirred tank reactor (CFSTR) model. The PFR is characterized by an orderly flow of fluid through the reactor with no element of fluid mixing with an element behind or ahead. Lateral mixing is present in a PFR, ideally with no mixing or diffusion along the path of flow. The CFSTR is a reactor whose contents are ideally fully mixed and uniform throughout. The fluid exiting the reactor

therefore has the same composition as the fluid within the reactor (Levenspiel 1999).

3.5 Ozone Mass Transfer Experiments

The setup for the flash mix system was shown in Figure 3-2. The setup for the opposing jets is almost identical and is illustrated in Figure 3-3. Extra-dry oxygen was the feed gas used to produce the ozone. Ozone gas was formed in the PCI–WEDECO ozone generator (model GLS-7) and monitored by the PCI-WEDECO ozone monitor (model HC-400). The flow rate of the ozone gas entering the reactor was controlled by a rotameter upstream of the injector. The Mazzei injector (model 978) was 0.23 m in length, with an internal diameter of 0.02 m at the inlet and outlet of liquid flow, and a volume of 0.09 L, as shown in Figure 3-4.

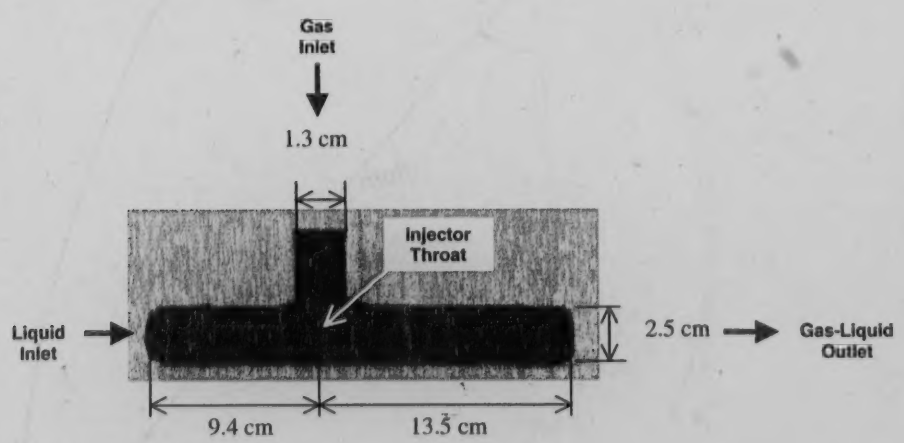

Figure 3-4 Critical dimensions and geometry of the injector.

Tap water was continuously collected in a large barrel and was drawn by a centrifugal pump through a 19 mm (¾ inch) line. The tap water and the ozone gas were combined initially in the Mazzei injector. The gas was subsequently further dissolved into the liquid by either the flash mix reactor or the opposing jets reactor. The flash mix reactor was 0.10 m in the direction of flow, with an internal diameter of 45 mm, and a volume of 0.08 L, illustrated in Figure 3-5.

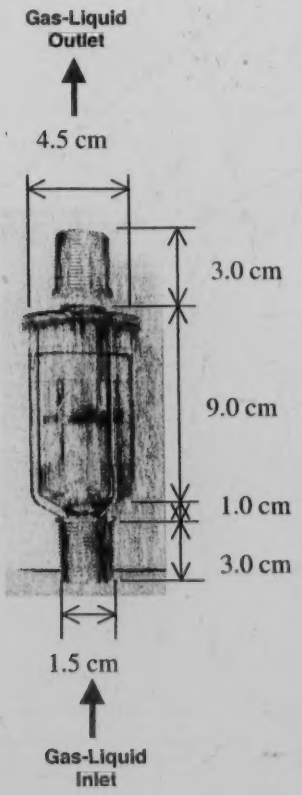

Figure 3-5 Critical dimensions and geometry of the flash mix reactor.

The opposing jets reactor was shaped like a "T" and the critical length was taken as the distance between the intersection of the jets and the gas-liquid outlet: 70 mm, as shown in Figure 3-6. The internal diameter of the opposing jets reactor was 40 mm and the volume was 0.21 L.

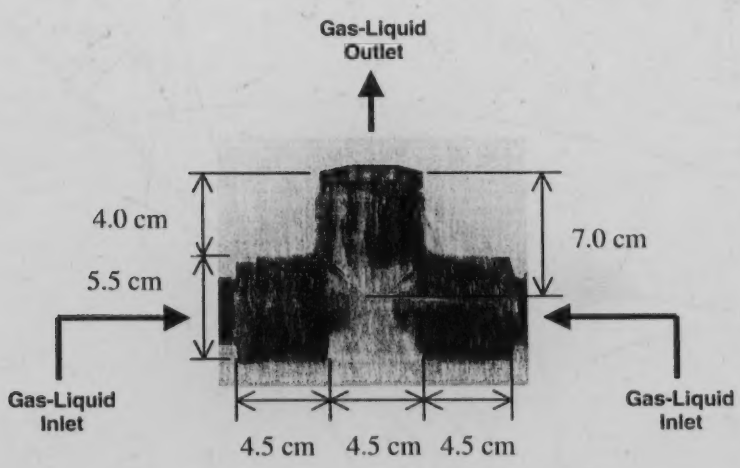

Figure 3-6 Critical dimensions and geometry of the opposing jets reactor.

A MIC degas separator (model DS100-WM) allowed the liquid to flow out through the bottom and the gas to exit through the top and into the degas relief valve (model DRV48-S). The degas separator had a volume of 4.54 L. A pressure gauge and ball valve were downstream of the degas separator unit to control the back pressure acting on the system. A liquid flowmeter was downstream of the degas separator to ensure the flow of water was within the target range of 2 to 38 $L \cdot min^{-1}$. The parameters varied were the liquid flow rate,

the feed gas flow rate, the system back pressure, and the concentration of ozone feed gas.

Downstream of the degas relief valve were two gas wash bottles for the determination of ozone residual in the off-gas in conjunction with the wet test meter. From the outlet of the wet test meter, the gas was sent to the waste stream. While the reactor was reaching the condition of steady state, the off-gas was not run through the wash bottles or wet test meter; instead the gas was run to waste. A needle valve on this waste line was used to ensure that the back pressure provided by the meter and by the bottles was maintained throughout the course of the mass transfer experiments.

There were three sampling ports for the determination of residual concentration of ozone in the reactor. Figure 3-2 and similarly Figure 3-3 indicate that the three ports (operated by ball valves) were found at locations numbered 2, 4, and 5. Once the desired flow rates, back pressure, and concentration of ozone feed gas (in % w/w basis as indicated on ozone monitor) were reached and a steady state was achieved (by allowing at least five volumes of water to pass through the system), the needle valve on the off-gas line was switched from the waste to the wash bottles and wet test meter. A timer was started and the ozone was collected in the wash bottles until at least 4 L of gas had passed through the wet test meter.

To analyze the amount of ozone concentrated in the off-gas, the Ozone Demand/Requirement Semi-Batch Method (American Public Health Association 1998) was used. With this method, gas wash bottles were used as the batch reactors. A solution of 2 % potassium iodide (KI) was made by dissolving 80 g of KI in 4 L of ODF water. Standard sodium thiosulfate titrants ($Na_2S_2O_3$) of 0.1*N* and 0.5*N* were prepared and standardized using a 0.100*N* solution of potassium bi-iodate ($KH(IO_3)_2$). Each wash bottle contained 400 mL of KI solution to trap the ozone gas in solution. After at least 4 L of gas had passed through the wet test meter, the needle valve on the off-gas line was switched from the wash bottles back to the waste and the tubing was disconnected between the system, the bottles, and the wet test meter. The contents of each bottle were transferred into one Erlenmeyer flask containing a magnetic stir bar and 0.5 to 1 mL of sulfuric acid (H_2SO_4) was added. The normality of the $Na_2S_2O_3$ titrant selected was dependent on the amount of ozone trapped in the KI solution; a darker orange solution contained a high amount of ozone while a paler yellow solution contained a low amount of ozone. A titrant of 0.500 N was selected for the darker solutions and a titrant of 0.100 N was selected for the lighter solutions. The flask contents were mixed with the magnetic stirrer and titrated with the standardized $Na_2S_2O_3$ until the yellow iodine colour almost disappeared. Then 1 mL of starch indicator solution was added causing the solution to turn dark gray. Titrating continued until the pale blue-gray colour of the solution disappeared. The following equation was used to calculate the ozone dose:

$$[O_3], mg/L_g = \frac{C \times N \times 24}{V}$$ Equation 3-6

where: C = volume of $Na_2S_2O_3$ titrant [mL]

N = normality of $Na_2S_2O_3$

V = volume of gas recorded through wet test meter [L_g]

While the off-gas was being passed through the wash bottles and wet test meter, sampling of the water at the three locations took place. The Indigo Colourimetric Method was used to determine the concentration of ozone in the liquid phase; therefore 100 mL volumetric flasks were prepared containing 10 mL of the indigo reagent II. One port at a time was flushed and then enough sample to change the indigo to a lighter shade of blue was added to the flask. Duplicates were sampled at each of the three ports. The volume of sample water added to the flasks was calculated using a balance (Mettler PC 2200) to determine the volume of ODF water required to fill the flask to the 100 mL volume. Excess water on the flask was wiped off, then the flask was placed on the balance, the balance tared, the flask filled to volume with ODF water, and the mass of this water recorded. Knowing the density of water, 1 g = 1 mL, the volume of ODF water and the volume of indigo reagent II (10 mL) were subtracted from 100 mL to determine the volume of the sample water.

For all experiments involving ozone, the glassware used was made ODF. ODF water was used to wash the glassware, to fill to volume in the Indigo Colourimetric Method, and to rinse glassware during titration for the Ozone Demand/Requirement Semi-Batch Method.

4. RESULTS AND DISCUSSION

4.1 Kinetics of Ozone Auto-decomposition in Sample Water

The data were analyzed to determine the order of the reaction between ozone and tap water while considering the effect of temperature on the auto-decomposition of ozone. A nonlinear approach was used initially; however the values of one of the reaction rate constants yielded negative values for each of the runs. It was determined that a first order reaction rate provided a better fit to the data. Graphically, for first order reactions, the natural logarithm of the concentration of ozone plotted against time produces a linear relationship with a negative slope whose value is equal to the reaction rate constant, k_1. Figure 4-1 and Figure 4-2 illustrate the first order relationship at average temperatures of 5.9 and 32.4 °C.

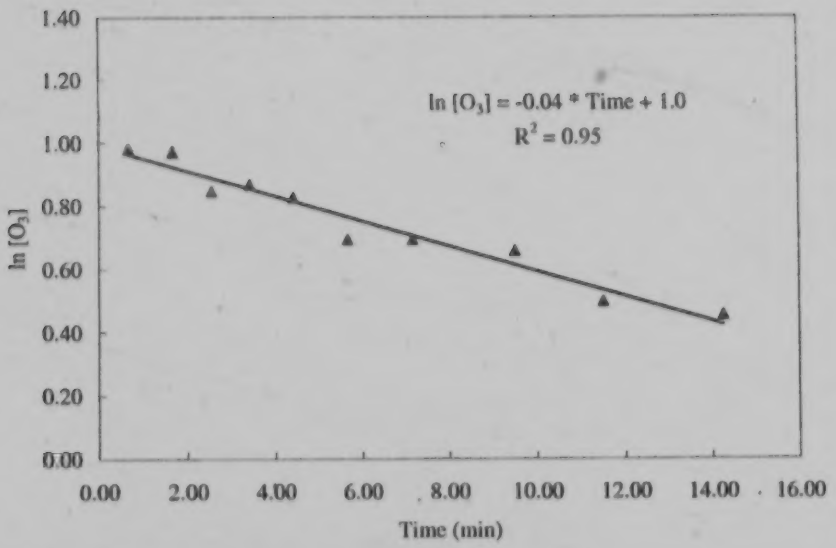

Figure 4-1 Natural logarithm of concentration of ozone versus time at an average temperature of 5.9 ℃.

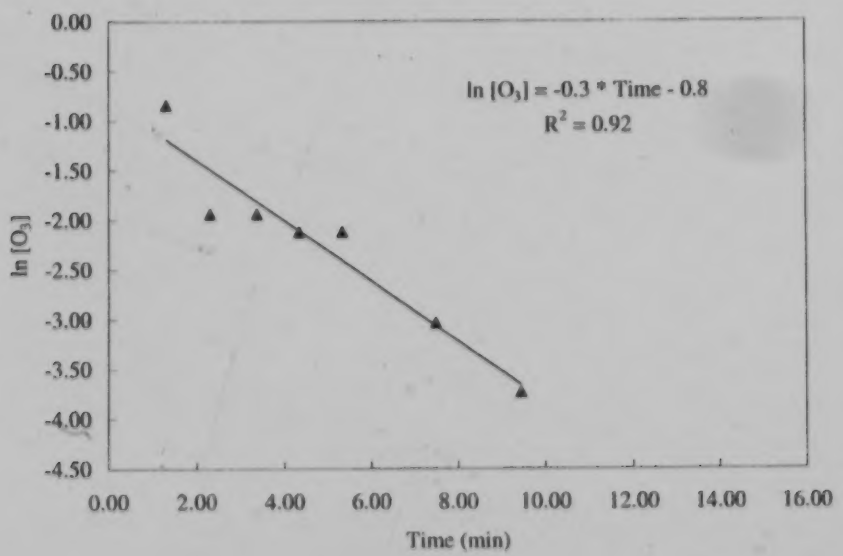

Figure 4-2 Natural logarithm of concentration of ozone versus time at an average temperature of 32.4 ℃.

The first order reaction rate constant, k_1, was determined graphically for each temperature as the slope of the best fit line of the $\ln[O_3]$ versus time graph. The kinetics data from the 17 runs appear in Appendix A. Since the time was plotted in minutes, the k_1 value from these figures was represented in min^{-1}. The Arrhenius equation was used to correlate the k_1 values to their respective temperatures by plotting the natural logarithm of the k_1 values against the respective temperature less 20 °C (Figure 4-3).

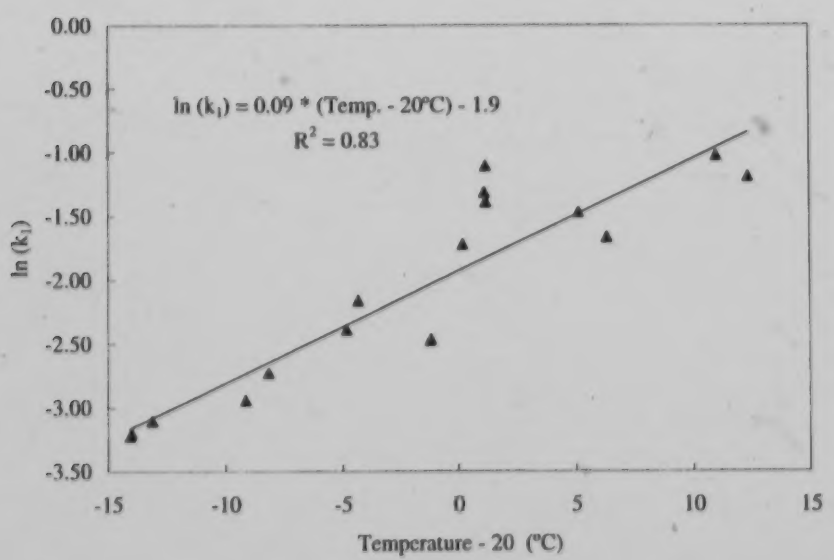

Figure 4-3 Effect of water temperature on the auto-decomposition rate constant of ozone in tap water.

The resulting Arrhenius equation was:

$$k_1 = 0.145 * 1.09^{(T-20°C)} \qquad \text{Equation 4-1}$$

Equation 4-1 indicates that the reaction rate constant, k_1, increases with the temperature of the water. At high liquid temperatures – such as in a hot tub or swimming pool – ozone will auto-decompose very rapidly. Conversely at very low liquid temperatures, ozone will auto-decompose very slowly. The average temperature of the sample tap water was 2.57 °C, meaning that the rate of auto-decomposition of ozone would be relatively slow, resulting in a higher amount of ozone available for the mass transfer reaction since only a small amount will be lost to auto-decomposition. From Equation 4-1 and at a water temperature of 2.6 °C, the reaction rate constant k_1 is equal to 0.03 min^{-1} (0.0005 s^{-1}).

4.2 Hydraulic Performance Study

Detailed experimental information on each of the preliminary runs performed with the flash mix system and with the opposing jets system was provided in Appendix B. It was determined that the maximum back pressure of the system was 116 kPa (16.8 psig). The baseline back pressure (i.e. with the ball valve fully open) varied depending on the liquid flow rate applied, but at a maximum it was 18 kPa (2.6 psig). With the pressure gauge having only tick marks at 1 psig increments, it was impossible to read values that would result in a rounded number (i.e. 5.0, 10.0, 15.0 psig) after the calibration equation was applied. It was therefore decided to operate at four back pressures: 25, 46, 74, and 102 kPa (3.6, 6.7, 10.7, and 14.8 psig). From the results of the hydraulic performance test,

runs were selected at each of the four back pressures. Runs were not selected if the G/L ratio was too high or too low during the hydraulic performance study.

It was observed that as the liquid flow rate increased, the maximum feed gas flow rate increased. As the system back pressure increased, the range of gas flow rates decreased. Statistical selection of runs was not possible for this research because the range of gas flow rates was not consistent under different system back pressures. A fractional factorial design would therefore not have worked analytically because not all gas flow rates could have been achieved. Furthermore, at the same gas and liquid flow rate but at different system back pressures, the gas flowed under both ejection and injection conditions.

4.3 Characteristics of Sample Water

The average values of the main characteristics of the test water are summarized in Table 4-1. The temperature of the water was read from a thermometer before each ozone mass transfer run. The pH, TOC, and alkalinity were sampled each day that ozone mass transfer runs were performed. While the pH meter was stabilizing at a constant pH value, the temperature of the sample water increased due to the stirring action, causing the daily pH values to be recorded at a variety of temperatures. An Arrhenius equation was determined by plotting the logarithm of the pH values versus the temperature minus 20 °C. The average pH value was

then calculated using the average temperature of the sample water used during the experiments and the equation derived from the graphical method described:

$$\log(pH) = -0.0004 \times (T - 20) + 0.872 \qquad \text{Equation 4-2}$$

An abnormally high value of TOC was calculated on one day, which accounts for the high standard deviation for TOC in Table 4-1.

Table 4-1 Average values of the main characteristics of the sample tap water.

Parameters	Alkalinity (mgL^{-1})	TOC (mgL^{-1})	Temperature (°C)	pH (pH units)
Mean	119.48	1.133	2.57	7.57
Standard deviation	4.50	1.291	1.25	-

4.4 General Observations from Ozone Mass Transfer Experiments

Upon sampling water from the port directly following the flash mix unit or the opposing jets, it was evident that gas bubbles were trapped in the liquid because ozone could be smelled while sampling. This means that a higher concentration of dissolved ozone was reported due to the entrained gas bubbles, resulting with the experimental residual concentration of ozone exceeding the applied ozone dose for certain runs. For many runs the dissolved ozone concentrations sampled at the exit of the flash mix or opposing jets reactor were very close or equal to the

applied ozone dose. This means that there was almost no consumption of ozone due to auto-decomposition. Other errors emerged from sampling and weighing during the Indigo Colourimetric Method, from the transferring of liquids and titrations during the Ozone Demand/Requirement Semi-Batch Method, from instrumental errors, and from calibration equations.

Throughout the mass transfer experiments at lower ratios of gas to motive flow, it was commonly observed that flow through the wash bottles and wet test meter was intermittent. Often there would be little to no flow with intermittent bursts of bubbles appearing in the wash bottles. During these runs, it was not possible to collect the desired 4 L of gas and therefore the flow to the bottles was stopped after approximately 12 minutes. Considerable error in the flow rate of the off-gas was introduced because the flow rate was so close to zero and the time recorded was not accurate because the flow of gas from the degas relief valve was not continuous. The intermittency of these bubbles could have been caused by the back pressure on the off-gas line produced by the wet test meter, the gas wash bottles, and the degas relief valve. It is possible that the gas was accumulating in the degas relief valve and the spurts of bubbles through the wash bottles occurred once the accumulation reached a certain maximum level. Since the degas separator is essentially a "black box" in that it was not possible to see how it operated, it can be hypothesized that not all of the gas was separated from the liquid as it should have been. If gas left the system through the liquid instead of

through the off-gas line, the low to no flow of gas through the wash bottles could be explained. Certain runs had gas accumulating for up to 6 min before a spurt of gas was visible in the wash bottles.

When operating with the opposing jets reactor, the first big burst of bubbles for these runs with low gas flow rate often occurred when port #4 (following the opposing jets reactor) was opened for sampling. This phenomenon was also observed a few times when operating with the flash mix reactor, but the abruptness of the burst of bubbles was much more dramatic and frequent with the opposing jets. By opening the valve at port #4, gas bubbles that could not be broken due to system back pressure would escape with the liquid being sampled. This sudden decrease in back pressure may have allowed some of the ozone gas to dissolve into the liquid phase and therefore be passed through the system and into the wash bottles on the off-gas line.

4.5 Mixing Regime of Degas Separator

As the degas separator unit was essentially a "black box" in that it was not possible to view its internal geometry or physical process, it was desired to determine its mixing regime. The volume of the degas separator was 4.54 L. The liquid flow rates passing through the system ranged from 18.5 to 38.8 $L \cdot min^{-1}$. The corresponding range of liquid retention times for the degas separator was 7.0 to 14.7 s. With the data logger recording the conductivity at intervals of 1.0 s for

the tracer study, the peak conductivity through the degas separator should have been captured with these retention times. The exit age distribution curve for the degas separator is shown in Figure 4-4.

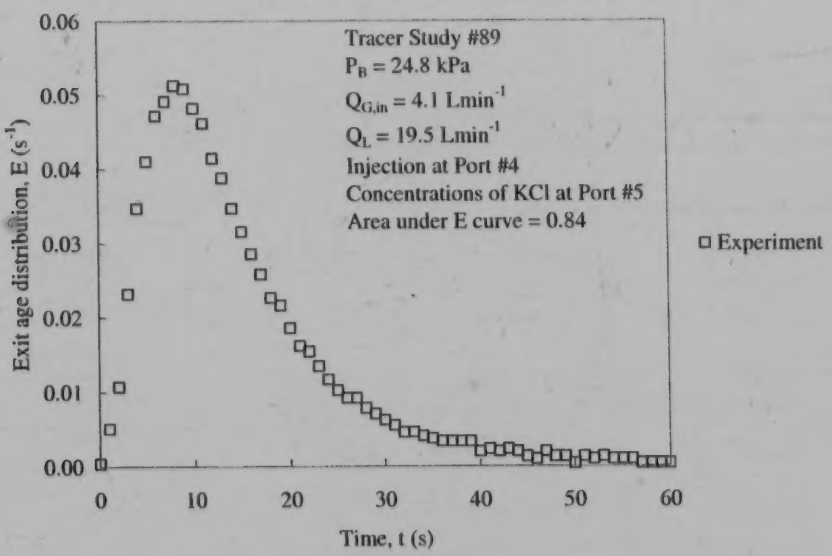

Figure 4-4 Exit age distribution curve of degas separator by injection of nonreactive tracer potassium chloride (KCl).

The area under the exit age distribution curve in Figure 4-4 is equal to 0.84. This indicates that only 84% of the mass of the tracer was recovered and that the peak concentration of the KCl was not recorded by the data logger. A possible error contributing to this could be that the two-way valve attaching to the syringe to the needle used to inject the KCl tracer solution leaked slightly and therefore mass of the tracer could have been lost. Another possibility, though unlikely, is that there was short-circuiting occurring due to dead zones inside the degas separator

causing the tracer to not be fully recovered at the exit. Another unlikely source of error was that the tracer was absorbing and desorbing within the system. Likely, the peak concentration was simply missed by the data logger. The degas separator served to separate the gas phase from the liquid phase and no mass transfer of ozone would occur at this point in the system. Therefore there was no attempt to calculate the volumetric liquid mass transfer coefficient or ozone transfer efficiency values by modeling the experimental data from the mass transfer experiments for the degas separator. However, Figure 4-4 illustrates that the shape of the curve of the experimental exit age distribution behaves like an axial dispersion model.

4.6 Injector

The total number of mass transfer runs used to model and analyze the Mazzei injector was 144 (60 from the flash mix system runs and 84 from the opposing jets system runs).

4.6.1 Mixing Regime

The volume of the injector was determined to be 0.09 L. The liquid flow rates passing through the system ranged from 18.5 to 38.8 $L \cdot min^{-1}$. Therefore the range of liquid retention times for the injector was 0.1 to 0.3 s. Since the data logger recorded conductivity values at intervals of 1.0 s for the tracer study, it is highly

probable that the actual peak conductivity or concentration was missed. The exit age distribution curve for the injector is shown in Figure 4-5.

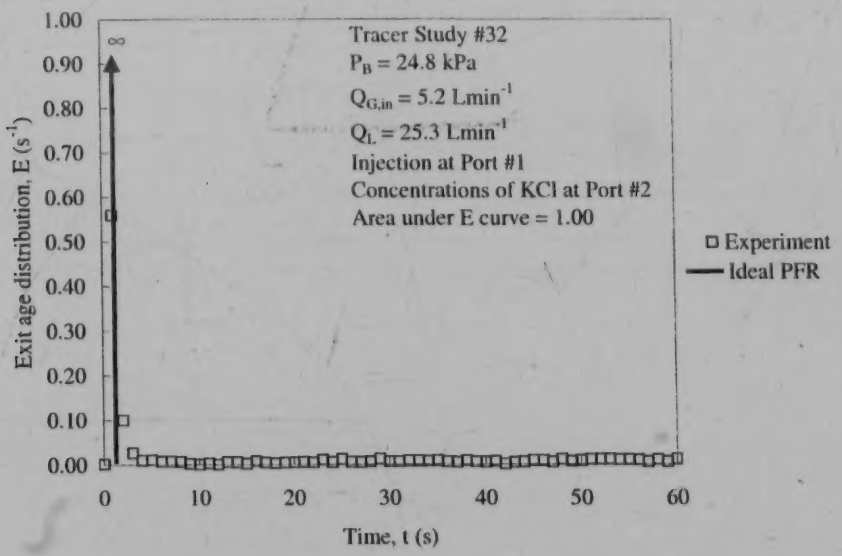

Figure 4-5 Hydrodynamic modeling of injector by injection of nonreactive tracer potassium chloride (KCl) as a plug flow reactor.

The area under the experimental curve in Figure 4-5 is equal to 1, meaning the data logger recorded the peak concentration of KCl and thus the mass of tracer was fully recovered for this run. The curve for an ideal plug flow reactor is a spike with an area equal to 1 and a width of 0. From the figure it was concluded that the injector can be modeled as a plug flow reactor (PFR). With respect to the liquid flow, the injector's geometry is a venturi, which validates the assumption of plug flow because the flow is annular and there are no internal physical devices such as baffles to create a fully mixed reactor. Huynh *et al.* (1991) assumed that

ideal plug flow conditions existed in a venturi injector based on flow visualization performed with methylene blue dye.

4.6.2 Theoretical Analysis

Data analysis for the ozone mass transfer experiments is explained here. The method used resembles that used by Wright *et al.* (1998) to model their cocurrent downflow jet-pump contactor. The following iterative method of analysis was applied to each mass transfer run performed. To apply a plug flow model to the analysis of the injector, the following assumptions were made:

1. liquid and gas phases are in plug flow regime;
2. steady state isothermal operation;
3. constant water and gas flow rates during operation of the ozonation system;
4. Henry's law applies;
5. resistance to the mass transfer of ozone occurs in the liquid side only;
6. the enhancement factor of the mass transfer due to the occurrence of chemical reactions is equal to 1.0 because the absorption of ozone in water treatment can be considered a slow chemical reaction;
7. air and/or O_2 are assumed to be inert;
8. gas holdup and interfacial area are constant along the length of the injector;
9. total pressure varies linearly with the length of the injector;

10. local mass transfer coefficient, k_L, is constant along the length of the injector;
11. superficial velocity of the gas is variable due to the absorption and depletion of ozone and the changes in pressure;
12. superficial velocities of the liquid and of the gas change due to the change in cross-sectional area, but the velocity used in the model equations will be based on the average cross-sectional area; and
13. ozone decay is first order in the liquid phase and is negligible in the gas phase.

The first step was to create a mass balance equation for the liquid phase. A plug flow reactor can be analyzed using a CFSTR-in-series model with the number of CFSTRs (N_{CFSTR}) equal to or greater than 10. Sensitivity analysis was performed by varying N_{CFSTR} from 5 to 21. It was found that when N_{CFSTR} exceeded 10, the difference in $k_L a_{inj}$ values varied by only 4 %. A value of 11 was chosen for N_{CFSTR} so that the midpoint in the injector could be modeled using the sixth CFSTR. Equation 4-3 is the mass balance of the liquid phase:

$$Q_L C_{L,i-1} - Q_L C_{L,i} - k_1 C_{L,i} V + k_L a (C_L^* - C_{L,i}) V = 0 \qquad \text{Equation 4-3}$$

where: i = number of the CFSTR ($1 \le i \le N_{CFSTR}$)

Q_L = flow rate of liquid [$L \cdot min^{-1}$]

C_L = concentration of dissolved ozone in the liquid phase [$mg \cdot L^{-1}$]

C_L^* = equilibrium saturation concentration of ozone [$mg \cdot L^{-1}$]

k_1 = kinetics reaction rate constant [min^{-1}]

V = volume of the CFSTR unit [L]

$k_L a$ = volumetric liquid mass transfer coefficient of the injector [min^{-1}]

For the analysis of the injector, the section containing both liquid and gas was considered and therefore the volume of the injector used for this calculation was the volume of the venturi between the throat and the exit of the injector. The volume was calculated using the equation for the volume of a cone. Since the total length of this section of the injector was only 0.135 m, the volumetric liquid mass transfer coefficient, $k_L a$, and the equilibrium saturation concentration, C_L^*, were assumed to be constant throughout.

There was no dissolved ozone in the liquid phase at the entrance of the injector and therefore $C_{L,0}$ was equal to zero and the mass balance for the first CFSTR (i = 1) was reduced to:

$$C_{L,1} = \frac{k_L a C_L^* V}{(Q_L + k_1 V + k_L a V)} \qquad \text{Equation 4-4}$$

Equation 4-3 was applicable to each of the CFSTRs in series. When i = 2, the substitution of Equation 4-4 for the $C_{L,1}$ term in Equation 4-3 resulted in:

$$C_{L,2} = \frac{k_L a C_L^* V + {k_L a C_L^* V Q_L}/{(Q_L + k_1 V + k_L a V)}}{(Q_L + k_1 V + k_L a V)} \qquad \text{Equation 4-5}$$

To simplify the above equation, the following constants were created by lumping some of the grouped terms together:

$$K_1 = (Q_L + k_1 V + k_L a V) \qquad \text{Equation 4-6}$$

$$K_2 = k_L a C_L^* V \qquad \text{Equation 4-7}$$

$$K_3 = k_L a V \qquad \text{Equation 4-8}$$

Using these constants, Equation 4-5 was simplified to:

$$C_{L,2} = \frac{K_2 + {K_2 Q_L}/{K_1}}{K_1} \qquad \text{Equation 4-9}$$

By using these steps for i = 3 to i = N_{CFSTR}, a pattern became obvious and the following general solution for the residual concentrations of ozone in the liquid phase was determined,

for i = 1:

$$C_{L,i} = \frac{K_2}{K_1} \qquad \text{Equation 4-10}$$

for $2 \leq i \leq N_{CFSTR}$:

$$C_{L,i} = \frac{K_2 + K_2 \sum_{j=1}^{j=i-1} \left(\frac{Q_L}{K_1} \right)^j}{K_1} \qquad \text{Equation 4-11}$$

For the first iteration the value of C_L^* was taken as the equilibrium saturation concentration of ozone at the inlet of the injector, or $C_{L,0}^*$, and was calculated by applying Henry's law:

$$C_{L,i}^* = \frac{P_i y_i}{H} \qquad \text{Equation 4-12}$$

where: P = pressure at CFSTR i [kPa]

y = ratio of moles of ozone to moles of feed gas [ ]

H = Henry's law constant [kPa·L·mg^{-1}]

The value for Henry's law constant of 0.22 kPa·L·mg^{-1} was obtained from Sotelo *et al.* (1989). The molar ratio of ozone in the feed gas, y_i, for $0 \leq i \leq N_{CFSTR}$ was calculated from the following equation derived from the ideal gas law:

$$C_{G,i} = \frac{P_i y_i}{RT_i} \qquad \text{Equation 4-13}$$

where: C_G = concentration of ozone in the gas phase [mg·L^{-1}]

R = universal gas law constant = 8.31 $kPa \cdot L \cdot K^{-1} \cdot mol^{-1}$

T = temperature of CFSTR i [K]

The concentration of ozone in the gas phase at the inlet of the injector, $C_{G,0}$, was determined using the calibration equation obtained from the ozone monitor and converting it to the experimental pressure and temperature (Equation 4-14). Therefore when applying the previous equation to determine y_0, the required pressure was the experimental atmospheric pressure.

$$C_{G.0} = (\%w/w) \times 12.185 \times \frac{T_{calib}}{T_{air}} \times \frac{P_{air}}{P_{calib}} \qquad \text{Equation 4-14}$$

where: % w/w = weight of ozone per weight of feed gas from ozone monitor [%]

T_{calib} = temperature of ambient air during calibration of ozone monitor [K]

T_{air} = temperature of ambient air during experiment [K]

P_{calib} = pressure of atmosphere during calibration of ozone monitor [kPa]

P_{air} = pressure of atmosphere during experiment [kPa]

Using a spreadsheet approach, the value of the concentration of residual ozone of the 11th CFSTR, $C_{L,11}$, was calculated using the previous steps by providing an

initial guess for $k_L a$. By setting this theoretical concentration equal to the experimentally determined concentration of residual ozone at the outlet of the injector, a new value of $k_L a$ was obtained. The C_L^* value used for this first iteration was at the inlet of the injector, which was not ideal to represent the length of the injector. It was preferable to use $C_{L,6}^*$, which was at the midpoint of the injector. Recalling that the pressure varied linearly along the length of the injector, the pressure at the midpoint, P_6, was obtained by taking the average of the pressures measured at the throat and exit of the injector. In order to use Equation 4-12 to determine the new C_L^* from the midpoint, y_6 had to be calculated first. The mass balance of the gas phase allowed y_i and therefore y_6 to be solved along with the parameters in the gas phase at the exit of the injector to be used as inputs for the analysis of the flash mix and opposing jets reactors. Following is the mass balance of the gas phase performed for $1 \leq i \leq N_{CFSTR}$:

$$Q_{G,i-1}C_{G,i-1} - Q_{G,i}C_{G,i} - k_L a(C_L^* - C_{L,i})V = 0 \qquad \text{Equation 4-15}$$

where: Q_G = flow rate of gas [$L \cdot min^{-1}$]

C_G = concentration of ozone in gas phase [$mg \cdot L^{-1}$]

Similarly to the steps followed to evaluate the mass balance of the liquid phase, the mass balance of the gas phase was simplified into a general expression using the same constants K_1, K_2, and K_3.

$$C_{G,i} = \frac{Q_{G,0}C_{G,0} - iK_2 + \sum_{j=1}^{j=i} K_3 C_{L,j}}{Q_{G,i}}$$ Equation 4-16

The values of C_L were determined for each CFSTR using Equation 4-11. A mass balance of the inert gases between the throat of the injector and the midpoint provided an equation for the determination of $Q_{G,6}$:

$$Q_{G,i} = Q_{G,0}\frac{(1-y_0)P_0T_i}{(1-y_i)P_iT_0}$$ Equation 4-17

By substituting Equation 4-17 and the $C_{L,i}$ values for $1 \leq i \leq 6$ into Equation 4-16, the molar ratio of ozone in the feed gas at the midpoint, y_6, was determined and used to solve $C_{L,6}^*$. This C_L^* was then used in the next iteration. Iterations continued until the value of k_La converged. Typically this took five iterations. Similarly, by substituting Equation 4-17 and the $C_{L,i}$ values for $1 \leq i \leq 11$ into Equation 4-16, the molar ratio of ozone in the feed gas at the exit of the injector, y_{11} or y_{exit}, was solved. The flow rate of the gas at the exit, $Q_{G,exit}$, and the concentration of ozone in the gas phase at the exit, $C_{G,exit}$, were then solved using y_{exit} and Equation 4-17 and Equation 4-16, respectively.

A mass check was performed on the injector using a mass balance of the inert gases since no mass of the inerts was transferred:

$$Q_{inerts,0}C_{inerts,0} = Q_{inerts,exit}C_{inerts,exit}$$ Equation 4-18

Using Equation 4-13 and recalling that the molar ratio of the inert gases in the feed gas is equal to (1 – y), Equation 4-18 became:

$$Q_{G,0}(1-y_0)\frac{P_0}{RT_0} = Q_{G,exit}(1-y_{exit})\frac{P_{exit}}{RT_{exit}} \qquad \text{Equation 4-19}$$

In all runs, the mass balance terms from the inlet and outlet were equal.

4.6.3 Mass Transfer of Ozone

It was desired to determine which factors had an influence on the volumetric liquid mass transfer coefficient of the injector. Figure 4-6 shows the relationship between $k_L a_{inj}$ and the ratio of gas to motive flow at both injection and ejection conditions. From Figure 4-6 it can be seen that runs under injection conditions did not produce higher $k_L a$ values than the runs under ejection conditions. Therefore the gas inlet pressure, P_{in}, had no effect on the volumetric liquid mass transfer coefficients of the injector.

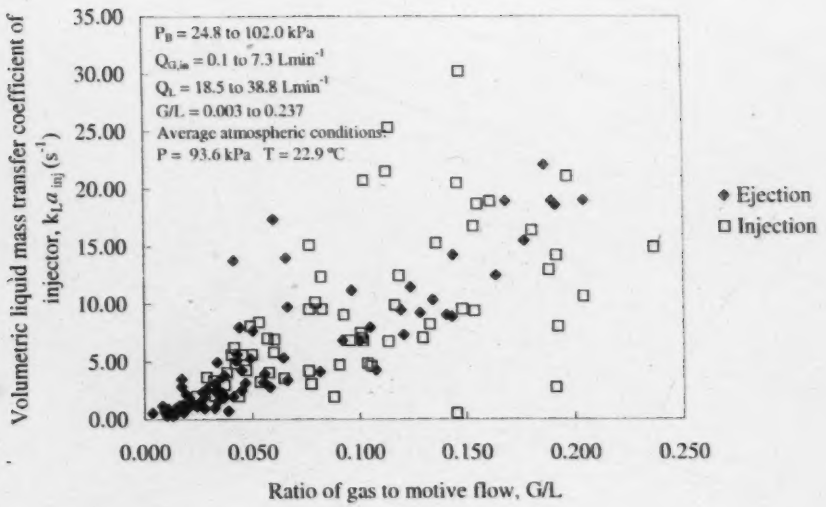

Figure 4-6 Volumetric liquid mass transfer coefficient of injector versus ratio of gas to motive flow.

The values of $k_L a_{inj}$ ranged from 0.28 to 30.17 s^{-1} with an average of 6.97 s^{-1}. Neither the concentration of feed gas ozone nor the system back pressure had an effect on $k_L a_{inj}$. The $k_L a$ of the injector was seen to be directly proportional to the G/L ratio. Further inspection showed that $k_L a_{inj}$ increased with an increasing superficial velocity of gas, u_G. No clear relationship between $k_L a_{inj}$ and the superficial velocity of liquid, u_L, was visually evident from these data. The superficial velocities of the injector were determined by dividing the flow rate by the average cross-sectional area between the throat and the exit of the injector.

An increase in u_G was shown to result in an increase in $k_L a$ by previous researchers (Deckwer *et al.* 1974, Roustan *et al.* 1987, Laplanche *et al.* 1991,

Huynh *et al.* 1991, Zhou 1995, Zhou and Smith 2000, Chen *et al.* 2002, Gamal El-Din and Smith 2003). As the u_G increases, the volume-to-surface area mean bubble diameter causes an increase in the gas bubble mean specific interfacial area, *a* (Gamal El-Din and Smith 2003). An increase in *a* equals an increase in $k_L a$. Further, higher values of u_G increase the equilibrium saturation concentration of the dissolved ozone and therefore result in higher mass transfer coefficients (Chen *et al.* 2002). An increase in u_L was also shown to cause an increase in $k_L a$ by Wang and Fan (1978), Huynh *et al.* (1991), and Gamal El-Din and Smith (2003). As the u_L increases, the turbulence increases, causing higher shear stresses that create smaller gas bubbles with higher bubble mean specific interfacial area. Again, this increase in *a* equals an increase in $k_L a$.

Based on the directly proportional relationship between $k_L a_{inj}$ and the G/L ratio shown in Figure 4-6, it was concluded that either an increase in Q_G or a decrease in Q_L caused the increase in $k_L a_{inj}$. However the previous discussion showed that an increase in both u_G and u_L (equivalently Q_G and Q_L) can cause an increase in $k_L a$. One of these phenomena outweighed the other and clearly the effect of the velocity of the gas flow was greatest.

The applied ozone dose, $C_{L,a}$, was calculated for each run using Equation 4-20. In Figure 4-7, the residual ozone concentration sampled at the exit of the injector was plotted against the applied ozone dose with a 45 ° line indicating complete

mass transfer from the gas phase to the liquid phase over the length of the injector. It was observed that as the applied ozone dose increased, the difference between the residual ozone concentration and the applied ozone dose also increased.

$$C_{L,a} = \frac{Q_{G,0} C_{G,0}}{Q_L}$$ Equation 4-20

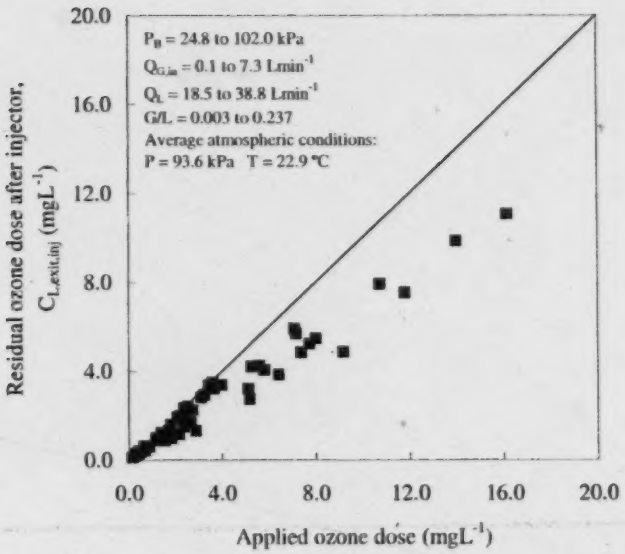

Figure 4-7 Residual concentration of ozone in the liquid phase sampled after the injector versus the applied ozone dose.

4.6.4 Analysis of Volumetric Liquid Mass Transfer Coefficients

It was desired to model the $k_L a_{inj}$ values obtained from the mass transfer experiments with the flash mix and opposing jets systems to determine its dependence on the superficial velocity of the liquid and of the gas. The empirical correlation for modeling $k_L a_{inj}$ data in terms of u_G and u_L was introduced by Huynh *et al.* (1991):

$$k_L a = \alpha \times u_G^{\beta} \times u_L^{\gamma} \qquad \text{Equation 4-21}$$

where: α, β, γ = empirical coefficients [ ]

u_G = superficial velocity of the gas [$m \cdot s^{-1}$]

u_L = superficial velocity of the liquid [$m \cdot s^{-1}$]

This equation was normalized by taking the logarithm. A nonlinear regression was performed on the normalized data to determine the values of the coefficients. Modeled $k_L a_{inj}$ values were obtained using the equation from the nonlinear regression and were plotted against the $k_L a_{inj}$ values modeled from the experimental data (Figure 4-8). The line of ideal correlation was inserted with a slope of 1 and it is seen that the data points are hugging the line at the lower $k_L a_{inj}$ values and spreading a bit as $k_L a_{inj}$ increased. Although there may appear to be outliers in Figure 4-8, the values on both axes were modeled and therefore

statistical analysis alone was not deemed sufficient enough cause to reject data points from experimental runs that did not show any signs of unusual behaviour.

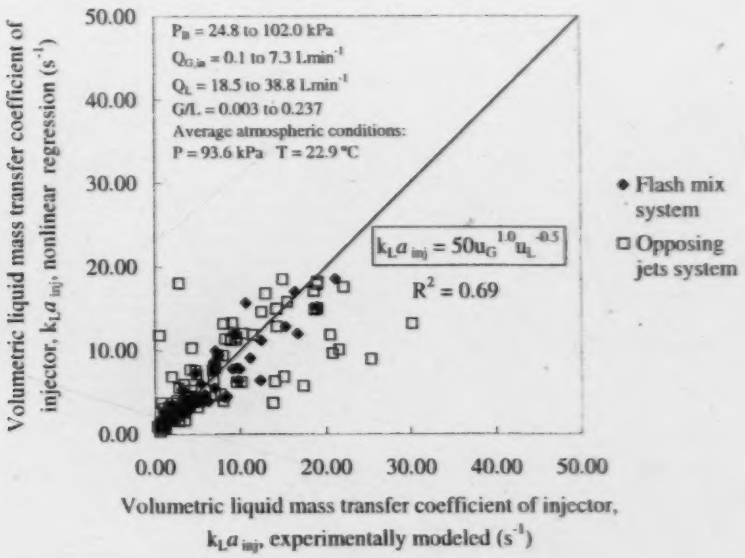
P_{in} = 24.8 to 102.0 kPa
$Q_{G,in}$ = 0.1 to 7.3 L.min^{-1}
Q_L = 18.5 to 38.8 L.min^{-1}
G/L = 0.003 to 0.237
Average atmospheric conditions:
P = 93.6 kPa T = 22.9 °C
$k_L a_{inj} = 50 u_G^{1.0} u_L^{-0.5}$
$R^2 = 0.69$
Flash mix system
Opposing jets system
Volumetric liquid mass transfer coefficient of injector, $k_L a_{inj}$, nonlinear regression (s^{-1})
Volumetric liquid mass transfer coefficient of injector, $k_L a_{inj}$, experimentally modeled (s^{-1})
0.00
10.00
20.00
30.00
40.00
50.00

Figure 4-8 Volumetric liquid mass transfer coefficient of injector from nonlinear regression versus volumetric liquid mass transfer coefficient of injector from modeled experimental data.

The mixing in the injector occurred mainly at the throat of the venturi when the jet of gas hit the flowing liquid at a 90 ° intersection. As the velocity of the gas increased, consequently the impact of the gas with the liquid increased. This increase in impact resulted in higher turbulence, which caused more gas bubbles to break and be dissolved into the liquid phase, resulting in an increase in the mass transfer of ozone. The α coefficient was determined to be 50. The β coefficient was positive (1.0), which indicated that the volumetric liquid mass transfer coefficient increased with increasing gas velocity. A negative γ

coefficient (-0.5) implied that the volumetric liquid mass transfer coefficient of the injector decreased with increasing liquid velocity.

Farines *et al.* (2003) discovered that at each operating condition, the dissolved ozone concentration increased with the superficial gas velocity and decreased with an increase in liquid velocity. Jakubowski *et al.* (2003) performed ozone mass transfer experiments with a confined plunging liquid jet contactor which showed that $k_L a$ increased with increasing gas flow rate and decreased with increasing liquid flow rate. An increase in gas flow rate resulted in a greater gas holdup which enhanced the interfacial area, a, and thus $k_L a$. Conversely, the increase in liquid flow rate caused a decrease in gas holdup that lowered the interfacial area and also the $k_L a$. Researchers also found that an increase of the superficial gas velocity resulted in a nearly proportional increase of the $k_L a$ value while the liquid velocity had little effect, suggesting that the overall mass transfer variation is mainly controlled by the specific interfacial area variation, a, linked to the gas holdup change. It was found that the change in gas holdup is strongly dependent on the superficial gas velocity (Alexander and Shah 1976; Larachi *et al.* 1991; Roustan *et al.* 1996). Furthermore, Shetty *et al.* (1992) observed that gas holdup was not dependent on superficial liquid velocity and diameter of the bubble column, but was dependent on the superficial gas velocity. In a study involving ozone gas mass transfer into water using a new gas-inducing reactor for the treatment of wastewater from the dye and textile and petrochemical industries

by Hsu *et al.* (2002), experimental results showed that the ozone volumetric mass transfer coefficient increased with increasing agitation speed, temperature, and superficial gas velocity. Applied to the present research, these findings conclude that the velocity of the gas affected the volumetric liquid mass transfer coefficient to such an extent that it resulted in a positive variation in $k_L a$ despite the lowering effect of the liquid velocity.

Volumetric liquid mass transfer coefficients have been similarly modeled by Huynh *et al.* (1991) and Gamal El-Din and Smith (2003). The volumetric liquid mass transfer coefficient was modeled without the u_L^{γ} term in Equation 4-21 by Deckwer *et al.* (1974), Deckwer *et al.* (1982), Roustan *et al.* (1987), and Zhou (1995). The $k_L a$ models from these previous studies were compared with the model of the injector in Figure 4-9. At superficial velocities of the liquid of 1.8 and 3.5 $m \cdot s^{-1}$, the volumetric liquid mass transfer coefficient varying with respect to the superficial velocity of the gas of the injector was higher than the previous research.

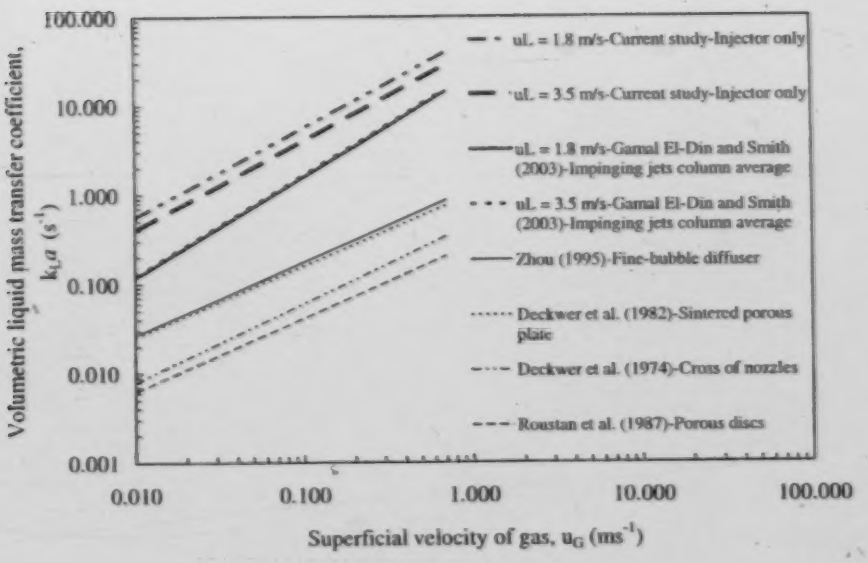

Figure 4-9 Volumetric liquid mass transfer coefficients modeled by several researchers including the model of the injector versus the superficial velocity of gas, at standard temperature and pressure.

4.6.5 Ozone Transfer Efficiency

The ozone transfer efficiency is another method of analyzing the data from the mass transfer experiments. The ozone transfer efficiency (OTE) of the injector was calculated using the following equation:

$$OTE_{sys} = \frac{(C_{G,in} \times Q_{G,in}) - (C_{G,out} \times Q_{G,out})}{(C_{G,in} \times Q_{G,in})} \times 100\% \qquad \text{Equation 4-22}$$

This equation represents the percent decrease of mass of ozone in the gas phase through the injector. The ozone transfer efficiency of the injector for the mass

transfer experiments using the flash mix system and the opposing jets system ranged from 43.3 to 92.3 % with an average of 69.7 %. The ozone transfer efficiency of the injector decreased with an increasing ratio of gas to motive flow. Further analysis showed that the gas flow rate component of the G/L ratio had a greater influence on the ozone transfer efficiency and therefore the OTE_{inj} values were normalized by dividing through by the feed gas flow rate, $Q_{G,in}$. Figure 4-10 illustrates the relationship between the normalized OTE_{inj} and the ratio of gas to motive flow, G/L.

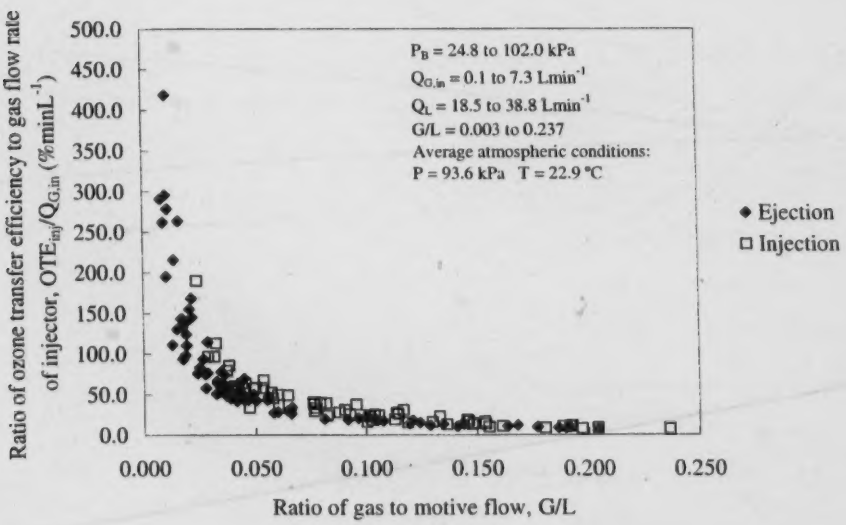

Figure 4-10 Ratio of ozone transfer efficiency to gas flow rate of injector versus ratio of gas to motive flow.

This normalized plot indicates that as the G/L ratio and the flow rate of gas increased, the ozone transfer efficiency of the injector decreased. Figure 4-10

shows a relationship that is exponential in shape. As the $Q_{G,in}$ increased (consequently causing an increase in the G/L ratio), there was a decrease in the gas retention time in the injector. Therefore there was less time for the ozone to react, causing a decrease in ozone transfer efficiency. Further, at higher gas flow rates, interfering bubble patterns and the coalescence of bubbles caused the mass transfer efficiency to be reduced (Schulz and Prendiville 1993).

Jakubowski *et al.* (2003) observed that with regards to their confined plunging liquid jet contactor, the OTE was found to increase marginally with increasing Q_L and constant Q_G. Similarly, it was found that an increasing Q_G and constant Q_L caused the value of k_La to increase and the OTE to decrease. In their investigation of a dynamic ozone dissolution process in a bubble column, Chen *et al.* (2002) found that increasing u_G resulted in an increase in k_La and a decrease in OTE. In pilot scale experiments with a static mixer, Martin and Galey (1994) found that the ozone transfer efficiency decreased by 10 to 20 % when the flow rate of gas was increased from 0.2 to 1.5 $N \cdot m^3 \cdot h^{-1}$. They also found that the transfer efficiency increased with the flow rate of liquid due to the increase of mixing associated with head loss.

The OTE was also affected by the concentration of ozone in the feed gas. Laplanche *et al.* (1991) observed that the transfer efficiency and the quantity of ozone dissolved in the water increases with increasing initial ozone concentration

in the air. In terms of the efficiency of ozone transfer in a reactor, Laplanche *et al.* (1991) concluded that although it is an important economical factor, it does not give any information about the efficiency of ozone with respect to water treatment. The values of OTE_{inj} showed no relationship with the concentration of ozone in the feed gas or with the back pressure of the system.

4.7 Flash Mix Reactor

The total number of ozone mass transfer runs used to model the flash mix reactor was 60.

4.7.1 Mixing Regime

The volume of the flash mix reactor was determined to be approximately 0.08 L. The liquid flow rates passing through the reactor ranged from 18.5 to 38.8 $L \cdot min^{-1}$. Therefore the range of liquid retention times for the flash mixer was 0.1 to 0.3 s. With a maximum retention time so much lower than the interval of recording of the data logger (1 s), it was likely that the actual peak conductivity or concentration was missed. The exit age distribution curve for the flash mixer is illustrated in Figure 4-11.

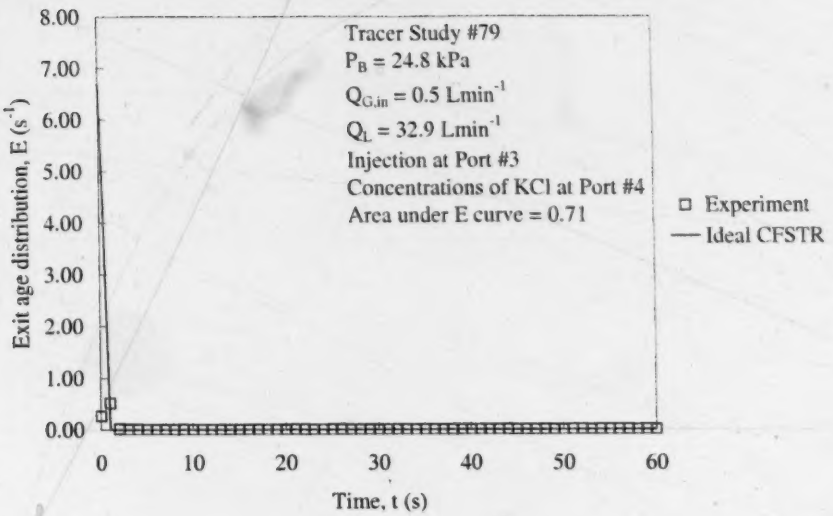

Figure 4-11 Hydrodynamic modeling of flash mix reactor by injection of nonreactive tracer potassium chloride (KCl) as a continuous flow stirred tank reactor.

The area under the exit age distribution curve in Figure 4-11 is equal to 0.71. This indicates that only 71 % of the mass of the tracer was recovered and that the peak concentration of KCl was not recorded by the data logger. As is shown on the exit age distribution curves, the areas of the curves were calculated for the first 60 s following the injection of the tracer. In an attempt to determine whether the peak was truly missed or whether some dead pockets existed in the system, a run was performed where the logging of data was allowed to continue for 300 s. This attempt did not succeed in recovering more mass of KCl and therefore it was concluded that the peak was simply not recorded.

Considering that the peak concentration of tracer was not indicated in Figure 4-11, the shape of the experimental exit age distribution through the flash mixer was very similar to that of the CFSTR. It was therefore concluded that the flash mixer could be modeled as a CFSTR. The geometry of the flash mix reactor consisted of two identical chambers separated at mid-height by a horizontal disc with a hole in the center. This hole mixed the fluids further by decreasing the cross-sectional area of the flow and thus increasing the rate of flow and the turbulence. The fluids were mixed initially in the bottom chamber, flow through the hole and then were mixed further in the second chamber. Each chamber had baffled slots through which the fluids could mix. Flow visualization was performed using an injection of dye upstream of the flash mix reactor. The mixing occurred instantaneously – further justifying the decision to model the flash mixer as a CFSTR.

4.7.2 Theoretical Analysis

Data analysis for the ozone mass transfer experiments involving the flash mix reactor is explained here. To apply a CFSTR model to the analysis of the flash mixer, the following assumptions were made:

1. both liquid and gas phases are assumed to be perfectly mixed, therefore the concentration of dissolved ozone and the concentration of gaseous ozone are constant everywhere in the reactor and are equal to the exit concentrations;

2. steady state isothermal operation;
3. flow rates of gas and liquid are constant during operation of ozone contactor;
4. Henry's law applies;
5. resistance to mass transfer of ozone for the absorption of ozone is confined to the liquid side only;
6. enhancement factor of the mass transfer due to the occurrence of chemical reactions is assumed to be 1.0 because the absorption of ozone in water treatment could be considered a slow chemical reaction;
7. air and/or O_2 are assumed to be inert gases;
8. gas holdup and interfacial area are constant along the height of the reactor;
9. local mass transfer coefficient, k_L, is constant along the height of the reactor;
10. total pressure varies linearly along the height of the reactor;
11. ozone auto-decomposition is first order in the liquid phase and is negligible in the gas phase; and
12. superficial velocity of the gas varies along the height of the reactor due to the absorption and depletion of ozone gas.

The height, in the direction of upward flow, of the flash mixer was 0.10 m. The value of $C_{L,0}$ was equal to the concentration of dissolved ozone in the liquid sampled upstream of the flash mix reactor at the exit of the injector (port #2). It was assumed that no mass transfer of ozone occurred in the steady state tubing between the exit of the injector and the inlet of the flash mixer and therefore the concentration and flow rate of the gas modeled at the exit of the injector were used as the inlet conditions for the flash mix reactor.

Modeled as one CFSTR, the mass balance of the liquid phase (Equation 4-23) and of the gas phase (Equation 4-24) for the flash mix reactor were performed:

$$Q_L C_{L,0} - Q_L C_{L,exit} - k_1 C_{L,exit} V + k_L a(C_L^* - C_{L,exit})V = 0 \qquad \text{Equation 4-23}$$

$$Q_{G,0} C_{G,0} - Q_{G,exit} C_{G,exit} - k_L a(C_L^* - C_{L,exit})V = 0 \qquad \text{Equation 4-24}$$

By adding Equation 4-23 to Equation 4-24, a value for the term $\{Q_{G,exit}C_{G,exit}\}$ was derived:

$$\{Q_{G,exit} C_{G,exit}\} = Q_L C_{L,0} - Q_L C_{L,exit} - k_1 C_{L,exit} V + Q_{G,0} C_{G,0} \qquad \text{Equation 4-25}$$

Equation 4-13 was multiplied by $Q_{G,exit}$ and rearranged to get:

$$\{Q_{G,exit}\, y_{exit}\} = \{Q_{G,exit} C_{G,exit}\} \frac{RT_{exit}}{P_{exit}} \qquad \text{Equation 4-26}$$

The mass balance of the inerts, Equation 4-19, was rearranged and added to Equation 4-26 to solve for $Q_{G,exit}$:

$$Q_{G,exit} = \{Q_{G,exit} C_{G,exit}\} \frac{RT_{exit}}{P_{exit}} + Q_{G,0}(1 - y_0) \frac{P_0}{RT_0} \frac{RT_{exit}}{P_{exit}} \qquad \text{Equation 4-27}$$

The molar ratio of ozone to feed gas at the exit of the flash mix reactor was determined by using the value of $Q_{G,exit}$ and then dividing into the $\{Q_{G,exit} \cdot y_{exit}\}$ term from Equation 4-26. Similarly, the concentration of gaseous ozone in the exit of the flash mixer was obtained by dividing the $\{Q_{G,exit} \cdot C_{G,exit}\}$ term (from Equation 4-25) by $Q_{G,exit}$. Using Henry's law the value of $C_L^*{}_{exit}$ was calculated. From the definition of a CFSTR, the conditions at the exit of a CFSTR are equal to the conditions at any point inside the completely mixed vessel. Therefore the C_L^* value used for the calculation of $k_L a$ was equal to $C_L^*{}_{exit}$. These terms were then all inserted into Equation 4-24 to solve for the volumetric liquid mass transfer coefficient of the flash mix reactor, $k_L a_{FM}$.

4.7.3 Mass Transfer of Ozone

The average $k_L a_{FM}$ value under ejection was 0.14 s^{-1} and under injection was 0.54 s^{-1}, indicating that the gas inlet pressure, P_{in}, had an effect on the volumetric liquid mass transfer coefficient of the flash mixer. Neither $C_{G,0}$ nor P_B had an effect on $k_L a_{FM}$. The range of $k_L a_{FM}$ was from 0.01 to 1.46 s^{-1} with an average of 0.33 s^{-1}. It appeared that $k_L a_{FM}$ tended to increase as the G/L ratio increase but the correlation was not as strong as the relationship apparent with the injector. Figure 4-12 illustrates the general increasing trend between the volumetric liquid mass transfer coefficient of the flash mix reactor and the G/L ratio.

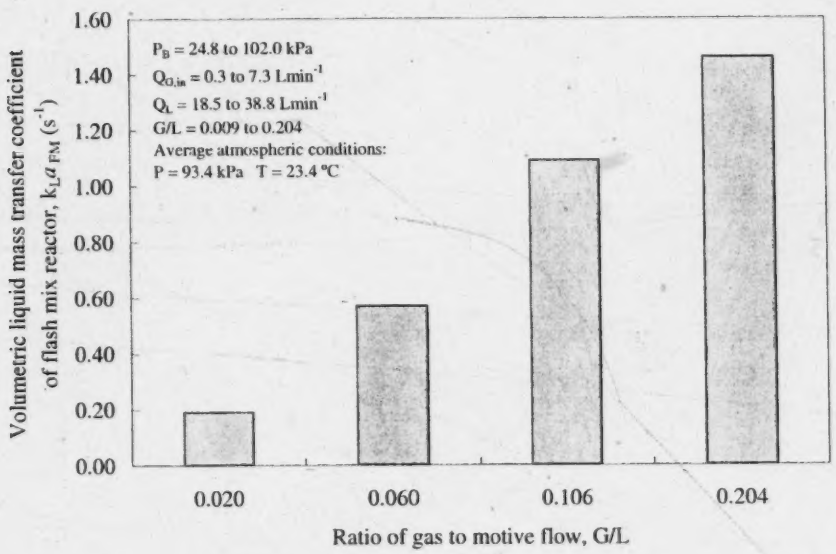

Figure 4-12 Volumetric liquid mass transfer coefficient of flash mix reactor at four ratios of gas to motive flow.

The modeling of the volumetric liquid mass transfer coefficient of the flash mix reactor with respect to the superficial velocities of the gas and liquid phases was attempted, however the resulting R^2 value was low. This was due to the fact that the bubbles inside the flash mix reactor were a variety of sizes, leading to a variety of *a* values. This range of interfacial area values led to a wide scatter of $k_L a_{FM}$ values at separate values of G/L ratio. The only way in which to normalize the volumetric liquid mass transfer coefficients would be to divide by the interfacial area. Since for this research it was not possible to measure the size of the bubbles to determine the values of *a*, the $k_L a$ values could not be normalized to achieve a better correlation with the ratio of gas to motive flow.

The applied ozone dose, $C_{L,a}$, was calculated for each run using Equation 4-20. In Figure 4-13, the residual ozone concentration sampled at the exit of the flash mix reactor was plotted against the applied ozone dose with a 45 ° line indicating complete mass transfer from the gas phase to the liquid phase through the injector, the connecting tubing, and the flash mix reactor. It was observed that as the applied ozone dose increased, the difference between the residual ozone concentration and the applied ozone dose also increased.

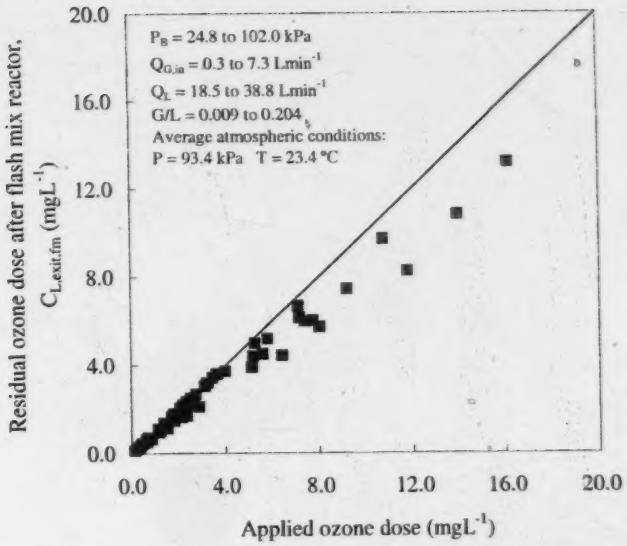

Figure 4-13 Residual concentration of ozone in the liquid phase sampled after the flash mix reactor versus the applied ozone dose.

4.7.4 Ozone Transfer Efficiency

The ozone transfer efficiency of the flash mix reactor, OTE_{FM}, was calculated for the gas phase with Equation 4-22, as previously applied to the injector. The range of OTE_{FM} values achieved was quite large: from 7.5 to 72.5 % with an average of 40.4 %. Ejection versus injection conditions did not show any difference in OTE_{FM} ranges. Neither $C_{G,0}$ nor P_B had an effect on OTE_{FM}. At the same G/L ratio a large range of OTE_{FM} values was observed. There was no effect on the ozone transfer efficiency through the flash mix reactor from the velocity of the gas or of the liquid. To minimize the scatter of

OTE_{FM} values, normalization of the data with respect to the gas flow rate was performed and illustrated in

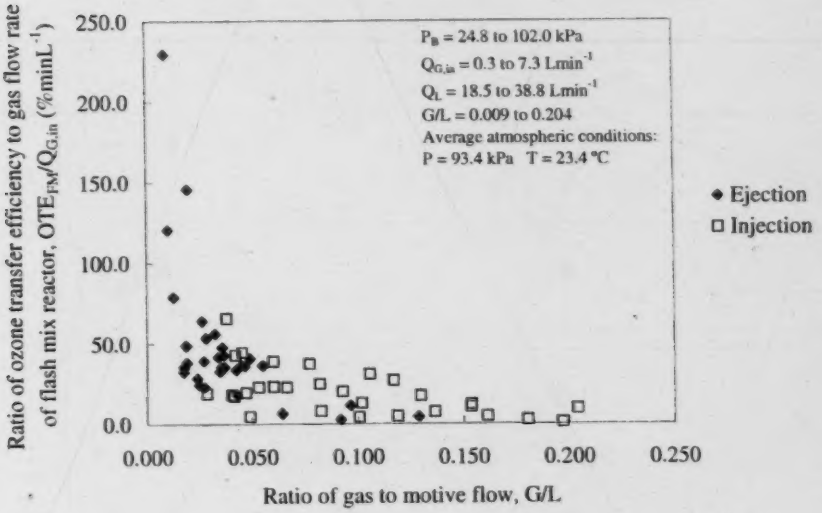

Figure 4-14. This figure shows that as the gas flow rate increased, the ozone transfer efficiency of the flash mix reactor decreased due to the lower residence time of the gas phase in the reactor.

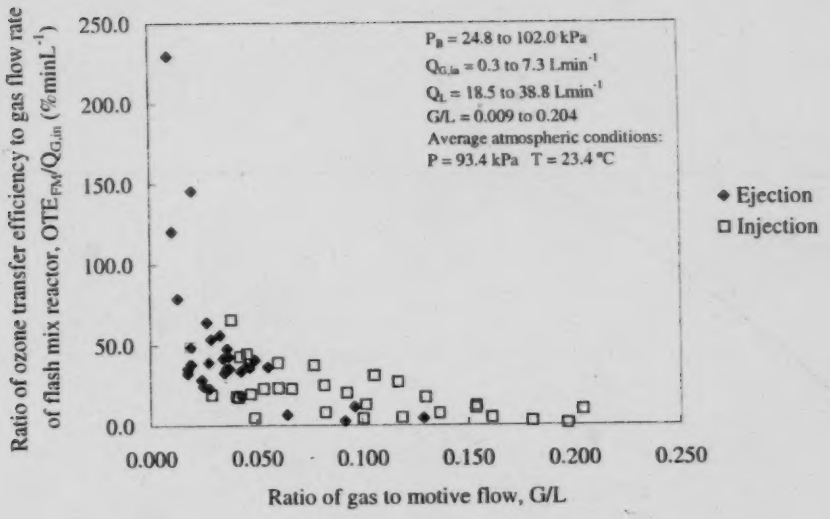

Figure 4-14 Ratio of ozone transfer efficiency to gas flow rate of flash mix reactor versus ratio of gas to motive flow.

The data of ozone transfer efficiency should be analyzed with several considerations in mind. As seen in Equation 4-22, one factor was the concentration of ozone in the gas phase upstream of the flash mix reactor and downstream of the injector. From the high $k_L a_{inj}$ and OTE_{inj} values observed it was clear that a significant portion of the mass transfer of ozone from gas to liquid occurred in the injector. The mass of ozone remaining in the gas phase was dependent on the G/L ratio and on the mass of ozone originally present in the feed gas. Therefore there was clearly a wide range of $C_{G,0}$ values available at the inlet of the flash mix reactor, resulting in the large scatter of OTE_{FM} values.

4.8 Opposing Jets Reactor

The total number of ozone mass transfer runs used to model the opposing jets reactor was 84.

4.8.1 Mixing Regime

The volume of the opposing jets reactor was determined to be approximately 0.21 L. The liquid passed through the opposing jets reactor at flow rates ranging from 18.5 to 37.7 $L \cdot min^{-1}$. The range of liquid retention times for the opposing jets was therefore 0.3 to 0.7 s. This maximum retention time was higher than those of the injector and of the flash mix reactor, but was lower than the interval of recording of the data logger (1 s), meaning that the actual peak conductivity or concentration could still have been missed. The exit age distribution curve for the opposing jets is illustrated in Figure 4-15.

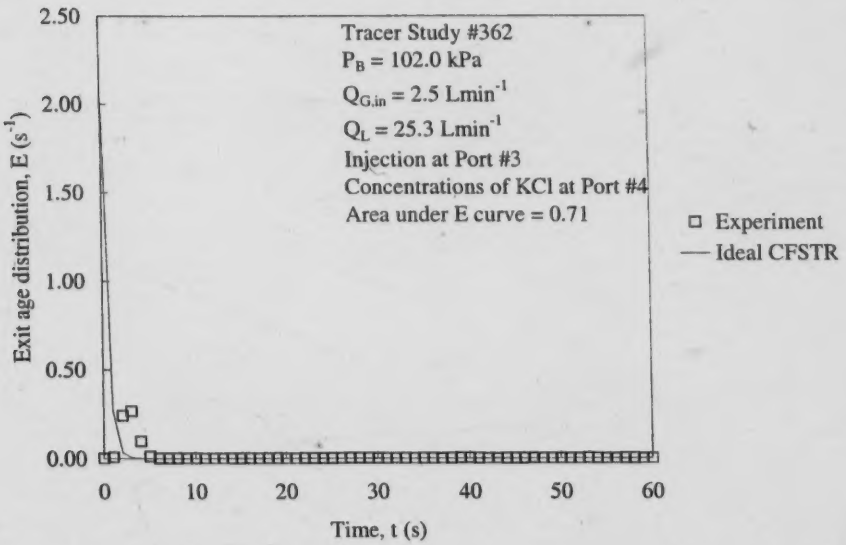

Figure 4-15 Hydrodynamic modeling of opposing jets by injection of nonreactive tracer potassium chloride (KCl) as a continuous flow stirred tank reactor.

The area under the exit age distribution curve in Figure 4-15 is equal to 0.71. This indicates that only 71 % of the mass of the tracer was recovered and that the peak concentration of KCl was not recorded by the data logger. Although the peak concentration of the tracer was not observed in Figure 4-15, the shape of the experimental exit age distribution through the opposing jets reactor was similar to that of the ideal CFSTR. The geometry of the opposing jets indicated that the assumption of CFSTR flow was correct: there were two jets of liquid that opposed each other by 180 ° in a small chamber before exiting the vessel. Visual observations with the injection of dye made it clear that the mixing was

instantaneous at the point where the jets collided and that the opposing jets reactor could be modeled as a CFSTR.

4.8.2 Theoretical Analysis

To apply the CFSTR model to the analysis of the opposing jets reactor, the same assumptions were made as for the mass transfer analysis of the flash mix reactor. The length of the opposing jets reactor used was taken to be the length (in the direction of flow) where the mixing of the two jets occurred and was equal to 0.07 m (Figure 3-6). The value of $C_{L,0}$ was equal to the concentration of dissolved ozone in the liquid sampled upstream of the opposing jets reactor at the exit of the injector (port #2). It was assumed that no mass transfer of ozone occurred in the steady state tubing between the exit of the injector and the inlet of the flash mixer and therefore the concentration and flow rate of the gas modeled at the exit of the injector were used as the inlet conditions for the flash mix reactor. The value of $C_{L,exit}$ was equal to the concentration of dissolved ozone in the liquid sampled downstream of the opposing jets reactor (port #4).

The analysis of data from the mass transfer experiments with the opposing jets reactor followed exactly the same steps as outlined in Section 4.7.2 for the flash mix reactor. The only value changed on the spreadsheet was the volume of the CFSTR, which was taken as the cylinder from the point of intersection of the jets to the exit: V = 0.111 L.

4.8.3 Mass Transfer of Ozone

The average $k_L a_{OJ}$ value under ejection was 0.32 s^{-1} and the average under injection conditions was 0.26 s^{-1}. Therefore for this reactor ejection conditions resulted in slightly higher values of $k_L a_{OJ}$. Neither $C_{G,0}$ nor P_B had an effect on $k_L a_{OJ}$. The range of $k_L a_{OJ}$ was from 0.001 to 1.95 s^{-1} with an average of 0.30 s^{-1}. In terms of a relationship with the G/L ratio, there was an apparent correlation that existed with the volumetric liquid mass transfer coefficient of the opposing jets reactor, though not as strongly correlated as the data from the injector.

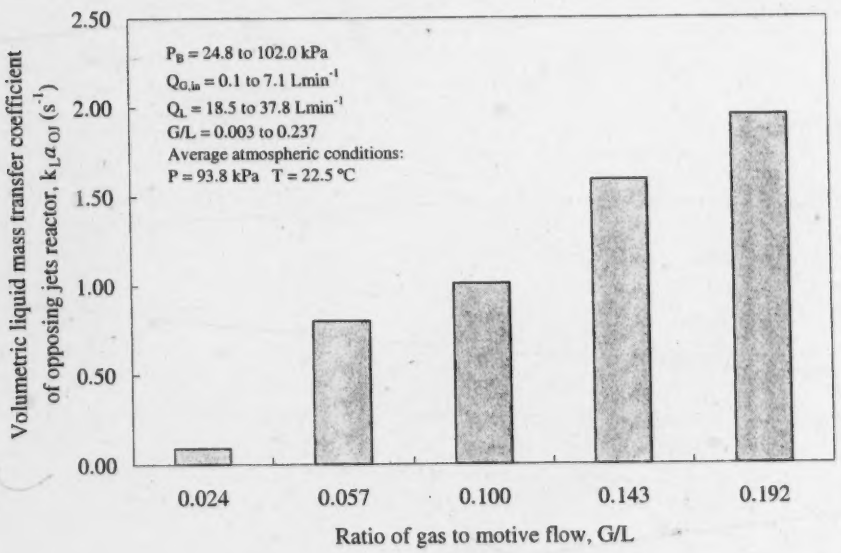

Figure 4-16 shows that an increasing trend was evident.

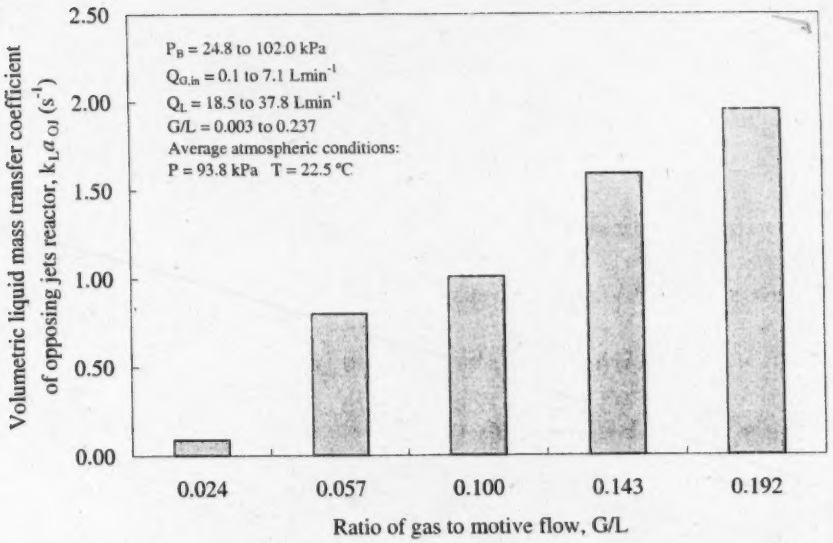

Figure 4-16 Volumetric liquid mass transfer coefficient of opposing jets reactor at five ratios of gas to motive flow.

As was done with the flash mix reactor, the modeling of the opposing jets reactor itself was attempted. Again the resulting R^2 value was low. The low coefficient of determination was the byproduct of the scatter of $k_L a_{OJ}$ values which was caused by the range in bubble sizes and thus the variation in interfacial area, *a*.

The applied ozone dose, $C_{L,a}$, was calculated for each run using Equation 4-20. In Figure 4-17, the residual ozone concentration sampled at the exit of the opposing jets reactor was plotted against the applied ozone dose with a 45 ° line indicating complete mass transfer from the gas phase to the liquid phase through the injector, the connecting tubing, and the opposing jets reactor. It was observed that as the

applied ozone dose increased, the difference between the residual ozone concentration and the applied ozone dose also increased.

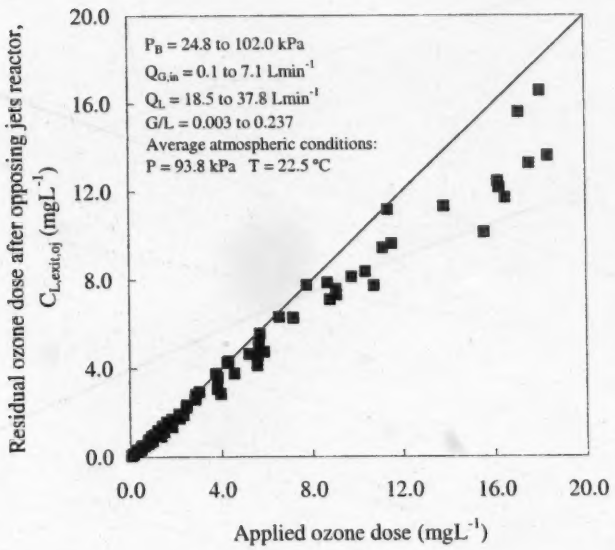

Figure 4-17 Residual concentration of ozone in the liquid phase sampled after the opposing jets reactor versus the applied ozone dose.

4.8.4 Ozone Transfer Efficiency

The ozone transfer efficiency of the opposing jets reactor, OTE_{OJ}, was calculated for the gas phase with Equation 4-22, as previously applied to the injector and to the flash mix reactor. The range of OTE_{OJ} values achieved was large: from 6.1 to 78.0 % with an average of 42.5 %. There was no difference in OTE_{OJ} ranges between runs performed under ejection conditions versus injection conditions.

Neither $C_{G,0}$ nor P_B had an effect on OTE_{OJ}. At the same G/L ratio there existed a large range of OTE_{OJ} values. There was no visible effect of either the velocity of the gas or the velocity of the liquid on the ozone transfer efficiency through the opposing jets reactor. To minimize the scatter in OTE_{OJ} data with respect to the ratio of gas to motive flow, the ozone transfer efficiency values were normalized by dividing through by the feed gas flow rate for each run, as shown in Figure 4-18. Figure 4-18 shows that the normalized OTE_{OJ} decreased with increasing G/L ratio due to the lower residence time of the gas phase in the reactor.

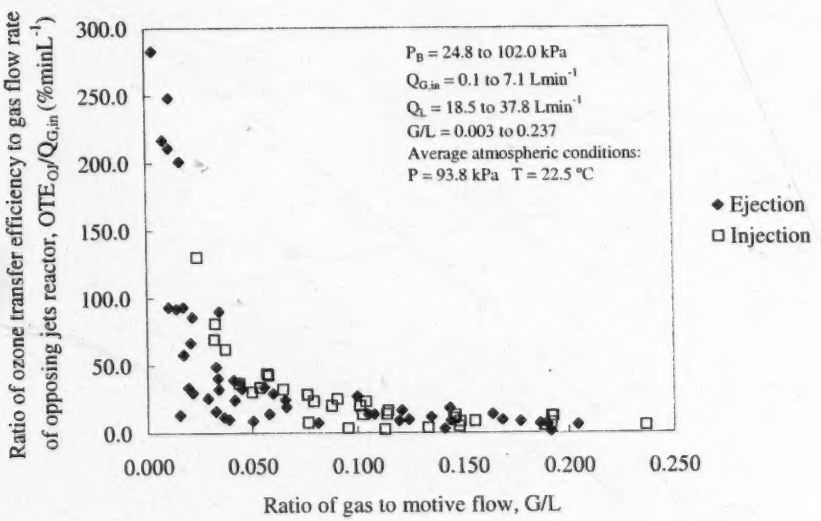

Figure 4-18 Ratio of ozone transfer efficiency to gas flow rate of opposing jets reactor versus ratio of gas to motive flow.

4.9 Comparison of Ozonation Systems

One principle goal of this research was to compare the flash mix system to the opposing jets system to determine which system is more efficient at dissolving ozone from the gas phase to the liquid phase. It was not possible to compare the entire systems using the volumetric liquid mass transfer coefficient because this parameter was only calculated for the injector, the flash mix reactor, and the opposing jets reactor separately from the entire systems. Comparing the $k_L a$ values of the flash mix and opposing jets reactors would not be accurate due to the cases where the injector had previously performed the majority of the mass transfer of ozone. The performance of the injector was modeled using data from both systems. The systems were compared using the ozone transfer efficiency of the systems, $OTE_{sys,liq}$. Table 4-2 shows that the flash mix system and the opposing jets system were operated under very similar hydraulic ranges.

Table 4-2 Ranges of hydraulic parameters for the flash mix and opposing jets systems.

Parameter	Flash Mix	Opposing Jets
Gas inlet pressure, P_{in} (kPa)	-73.8 to 50.3	-68.9 to 71.7
System back pressure, P_B (kPa)	24.8 to 102.0	24.8 to 102.0
Liquid flow rate, Q_L ($Lmin^{-1}$)	18.5 to 38.8	18.5 to 37.8
Feed gas flow rate, $Q_{G,in}$ ($Lmin^{-1}$)	0.3 to 7.3	0.1 to 7.1
Gas to motive flow ratio, G/L	0.009 to 0.204	0.003 to 0.237

Using the 60 runs from the flash mix system mass transfer experiments and the 84 runs from the opposing jets system mass transfer experiments, the average, minimum, and maximum values for the ozone transfer efficiency of the system, the ozone transfer efficiency of each individual reactor, and the volumetric liquid mass transfer coefficient of each reactor were determined and are represented in Table 4-3.

Table 4-3 Ranges and averages of ozone mass transfer results from flash mix system runs and opposing jets system runs.

Parameter	Reactor	Average	Minimum	Maximum
Ozone transfer efficiency of system in liquid phase, $OTE_{sys,liq}$ (%)	*FM*	88.0	63.0	100.0
	OJ	87.2	64.5	100.0
Ozone transfer efficiency of reactor, OTE_{FM} or OTE_{OJ} (%)	*FM*	40.4	7.5	72.5
	OJ	42.5	6.1	78.0
Volumetric liquid mass transfer coefficient, $k_L a_{FM}$ or $k_L a_{OJ}$ (s^{-1})	*FM*	0.33	0.01	1.46
	OJ	0.30	0.001	1.95

Table 4-3 shows that in terms of the performance of the two systems there was not much difference. The average OTE of the flash mix system was 88.0 %, which was only slightly higher than the average OTE of the opposing jets system, 87.2 %. The maximum value of OTE for both systems was 100 %. As discussed by Laplanche *et al.* (1991), the experimental values of dissolved ozone in water may have been overevaluated due to the presence of microbubbles of air that contained ozone trapped during sampling. The average OTE of the flash mix reactor itself was also within 5 % of the average OTE of the opposing jets reactor.

Similarly, the average volumetric liquid mass transfer coefficients of the two systems were within 14 %.

4.9.1 Ozone Transfer Efficiency

The ozone transfer efficiency was previously calculated for the injector, the flash mix reactor, and the opposing jets reactor. The OTE was also calculated for the entire system using the following equation:

$$OTE_{sys,liq} = \frac{Residual\ ozone\ dose}{Applied\ ozone\ dose} * 100\% \qquad \text{Equation 4-28}$$

This equation represents the percent decrease of mass of ozone in the liquid phase through the entire system. The OTE of the entire system in the gas phase, $OTE_{sys,gas}$, was also calculated by again applying Equation 4-22. However since the concentrations of ozone in the gas phase were determined using the mathematical model equations, it was more accurate to compare the systems using $OTE_{sys,liq}$ because its equation only contained values that were determined experimentally. In general, $OTE_{sys,gas}$ values for both systems were lower than the $OTE_{sys,liq}$ values due to the entrapment of gas bubbles in the liquid samples that may have increased the residual concentration of ozone and due to assumptions made while theoretically calculating the concentrations of ozone in the gas phase.

This trend is shown in Figure 4-19. It can be concluded from Figure 4-19 that, for both the flash mix and opposing jets systems, the mathematical modeling of the OTE in the gas phase closely approximated the experimentally determined OTE values in the liquid phase.

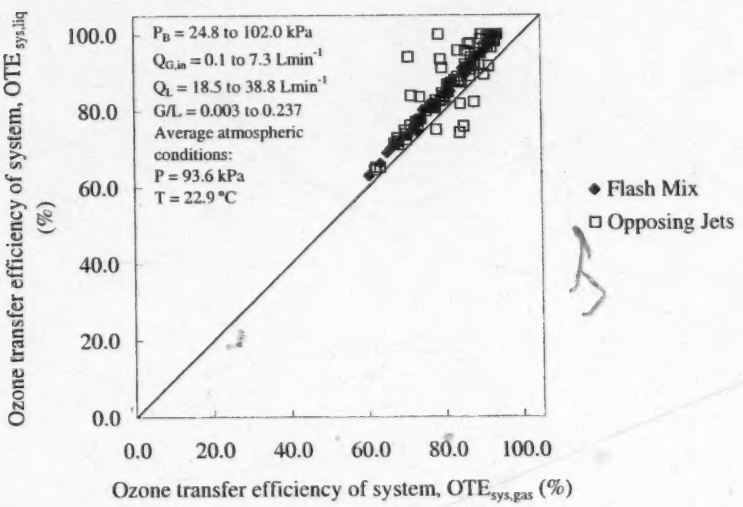

Figure 4-19 Ozone transfer efficiency of system in liquid phase versus ozone transfer efficiency of system in gas phase for flash mix and opposing jets systems.

The $OTE_{sys,liq}$ of the flash mix system ranged from 63.0 to 100.0 % with an average of 88.0% for the 60 runs analyzed. The ozone transfer efficiency of the flash mix system appeared to decrease with increasing gas to motive flow ratio. This result agreed with the relationship between the OTE of the injector and the G/L ratio. As with the injector and the flash mix reactor itself, $OTE_{sys,liq}$ was normalized by dividing through by the feed gas flow rate. The decreasing

exponential relationship between the normalized ozone transfer efficiency of the flash mix system and the ratio of gas to motive flow is shown in Figure 4-20.

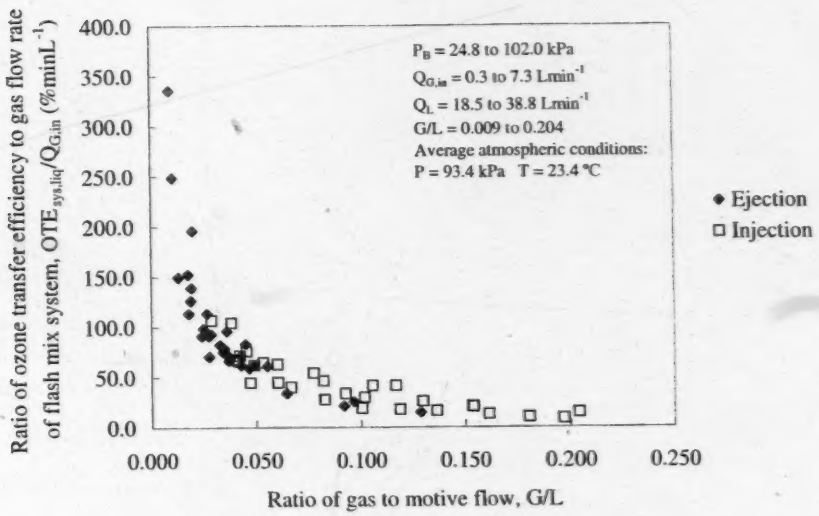

Figure 4-20 Ratio of zone transfer efficiency to gas flow rate of flash mix system versus ratio of gas to motive flow.

The ozone transfer efficiency of the opposing jets system ranged from 64.5 to 100.0 % with an average of 87.2% for the 84 runs analyzed. It was observed that the ozone transfer efficiency of the opposing jets system decreased as the gas to motive flow ratio increased. This relationship was the same result from the analyses of the injector and the flash mix system. The plot of $OTE_{sys,liq}$ versus $Q_{G,in}$ revealed that an increasing flow rate of gas resulted in a decreasing ozone transfer efficiency for the opposing jets system due to the lower retention time of

the gas phase within the reactor with the higher $Q_{G,in}$ values. Therefore the $OTE_{sys,liq}$ values for the opposing jets system were normalized with respect to $Q_{G,in}$ and plotted against the G/L ratio in Figure 4-21.

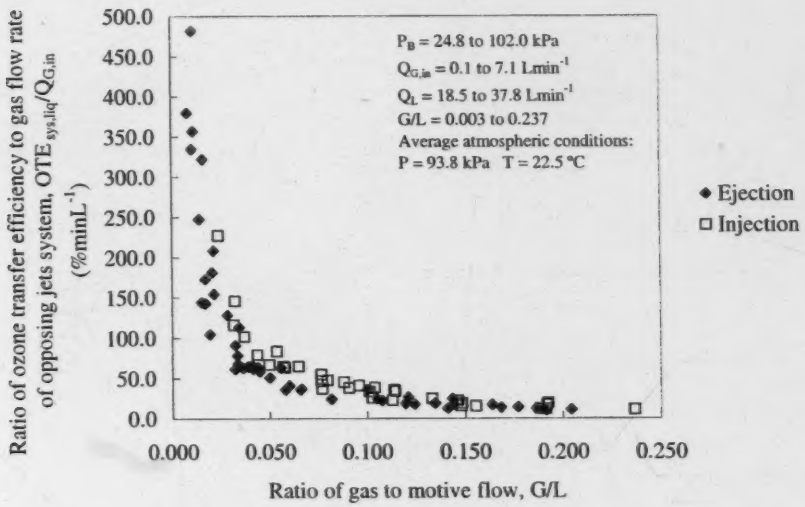

Figure 4-21 Ratio of ozone transfer efficiency to gas flow rate of opposing jets system versus ratio of gas to motive flow.

The normalized ratios of ozone transfer efficiency to feed gas flow rate were plotted against their respective ratios of gas to motive flow for the injector only, the flash mix reactor, the opposing jets reactor, the flash mix system, and the opposing jets system (Figure 4-10, Figure 4-14, Figure 4-18, Figure 4-20, and Figure 4-21, respectively). Each of these curves showed a decreasing exponential relationship between $OTE/Q_{G,in}$ and G/L. It was therefore desired to the natural logarithm of these five curves and to fit an equation to each. Figure 4-22

illustrates the resulting trend lines for the five data sets with their respective equations. The slopes for all curves were approximately equal. Figure 4-22 shows that in terms of the normalized ozone transfer efficiency, the opposing jets system had the highest overall values.

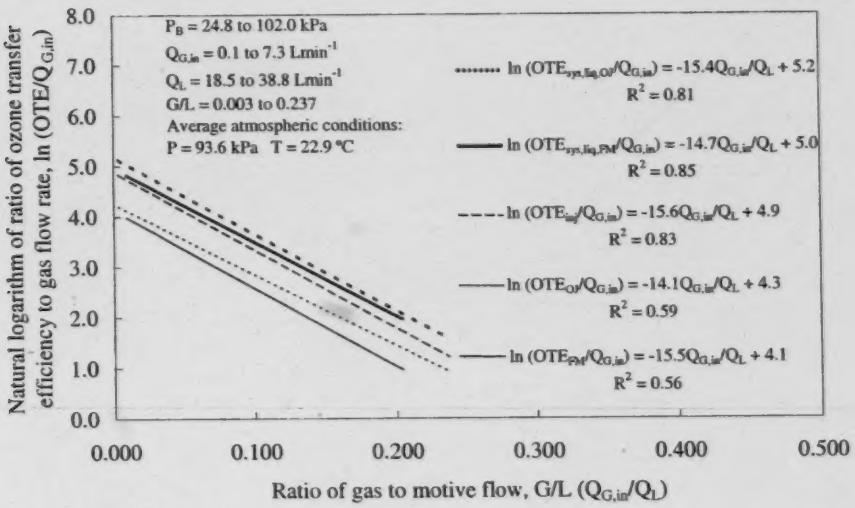

Figure 4-22 Natural logarithm of ratio of ozone transfer efficiency to gas flow rate versus ratio of gas to motive flow for injector, flash mix reactor, opposing jets reactor, flash mix system, and opposing jets system.

4.9.2 Comparison with Static Inline Mixer

The doctoral thesis of Craik (2001) investigated the effect of gas-liquid contacting conditions in a static mixer on ozone transfer efficiency and reduction of *Bacillus subtilis* spores. The mass transfer experiments of Craik occurred at system back

pressures (in this case, caused by a column of water) of 4.1, 13.8, and 22.8 kPa (0.6, 2.0, and 3.3 psig). The mass transfer experiments involved the calculation of the ozone transfer efficiency using the following equation (Craik *et al.* 2002):

$$OTE = \frac{C_{oz,f} - C_{oz,o}}{C_{oz,f}} \times 100\% \qquad \text{Equation 4-29}$$

where: $C_{oz,f}$ = concentration of ozone in the feed gas [$g \cdot NL^{-1}$]

$C_{oz,o}$ = concentration of ozone in the off-gas [$g \cdot NL^{-1}$]

These transfer efficiency measurements took into account the ozone transfer that occurred not only in the static mixer, but also in the bubble column and in the interconnecting tubing and piping. The highest P_B that this system operated under was 22.8 kPa (3.3 psig) and the lowest P_B exerted in the experiments with the flash mix and opposing jets systems was 24.8 kPa (3.6 psig). Therefore the OTE values for the static mix, flash mix, and opposing jets systems were compared at these two system back pressures. From Figure 4-23 it is observed that the ozone transfer efficiency values of the static mixer system were lower than those of the flash mix system and those of the opposing jets system, and higher than the OTE values of the injector alone. The maximum G/L ratio used in the experiments with the static mixer was 0.04 and therefore a comparison at the higher range of the G/L ratios used in the flash mix and opposing jets experiments was not possible.

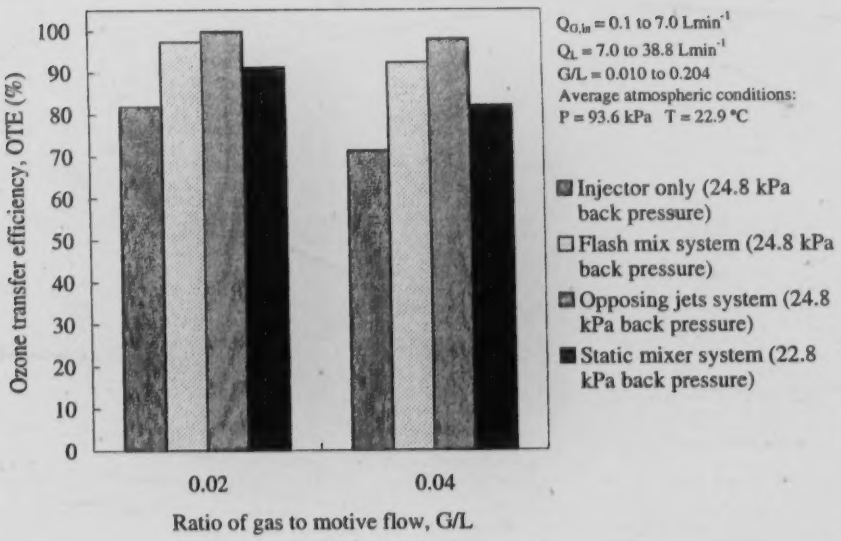

Figure 4-23 Ozone transfer efficiency of injector only, flash mix, opposing jets, and static mixer systems versus ratio of gas to motive flow.

4.9.3 Overall System Performance

As previously discussed, in certain mass transfer runs the injector did almost all of the mass transfer of ozone from the gas to the liquid phase, leaving little ozone for the flash mix or opposing jets reactors to dissolve. It was therefore attempted to relate the ozone transfer efficiencies of each individual component (i.e. of the injector and of either the flash mix or opposing jets reactor) to the ozone transfer efficiency of the system as a whole. Figure 4-24 and Figure 4-25 show the OTE of the injector versus the OTE of the flash mix reactor and opposing jets reactor, respectively, at various ranges of ozone transfer efficiencies of the system.

The trend lines for each range of $OTE_{sys,liq}$ values have negative slopes, which correctly indicates that higher values of OTE_{inj} corresponded to lower values of OTE_{FM} and OTE_{OJ}. From these figures, optimum use of both the injector and the flash mix or opposing jets reactor can be approximated based on the desired $OTE_{sys,liq}$.

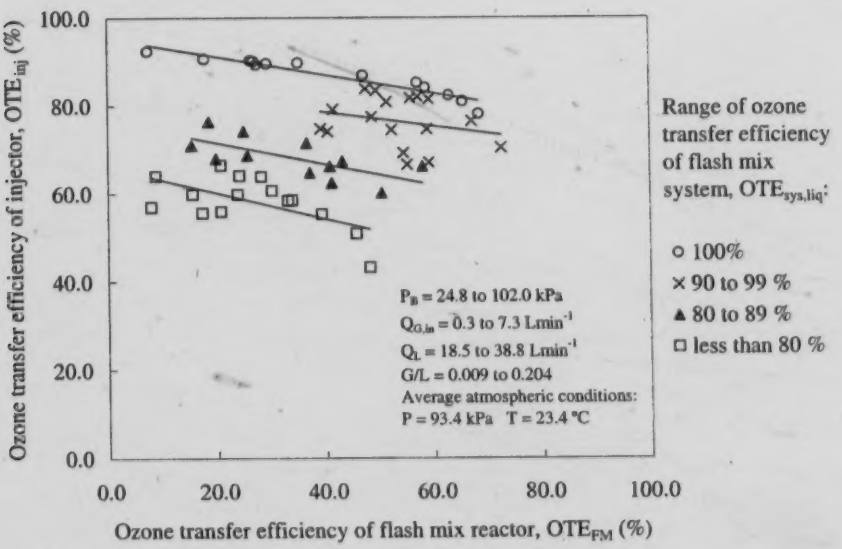

Figure 4-24 Ozone transfer efficiency of the injector versus ozone transfer efficiency of the flash mix reactor at various ranges of ozone transfer efficiency of the flash mix system.

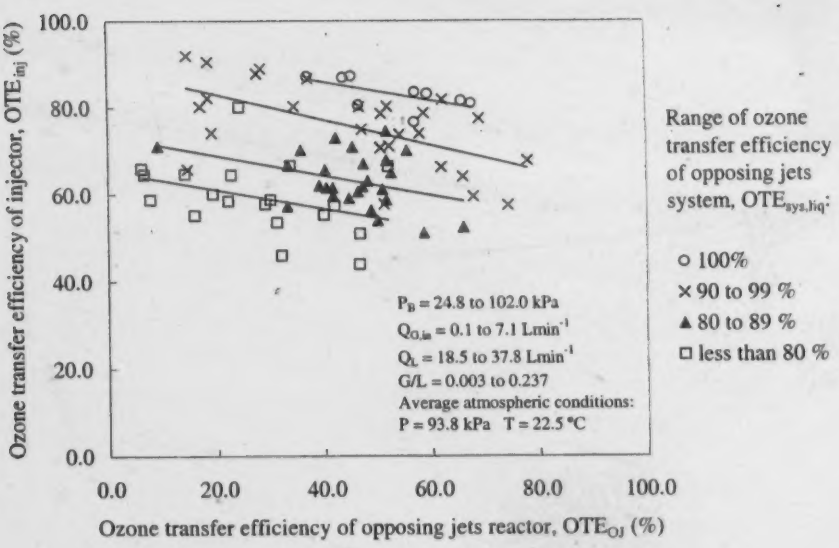

Figure 4-25 Ozone transfer efficiency of the injector versus ozone transfer efficiency of the opposing jets reactor at various ranges of ozone transfer efficiency of the opposing jets system.

For example, for an $OTE_{sys,liq}$ between 90 and 99 %, Figure 4-24 shows that the OTE of the flash mix reactor varied between approximately 38 and 75 %, while the OTE for the injector ranged from about 70 to 78 %. If maximum use of the flash mix reactor were desired (i.e. 75 %), then the OTE of the injector would be approximately 70 %.

5. CONCLUSIONS AND RECOMMENDATIONS

The values of volumetric liquid mass transfer coefficients for the injector were modeled using a relationship in the form of $k_L a = \alpha u_G^{\beta} u_L^{\gamma}$. The resulting model was $k_L a_{inj} = 50 u_G^{1.0} u_L^{-0.5}$ and the values predicted by this model were compared to other $k_L a$ values of researchers who modeled their gas-liquid contacting systems in this form or as $k_L a = \alpha u_G^{\beta}$. The $k_L a$ values of the injector alone exceeded the model results of other ozone dissolution system designs reported in the literature. The range of experimentally modeled $k_L a_{inj}$ values was from 0.28 to 30.17 s^{-1}.

The ozone transfer efficiency of the flash mix system ranged from 63.0 to 100.0 % and that of the opposing jets system ranged from 64.5 to 100.0 %. Both systems produced higher ozone transfer efficiencies compared to the static mixer system studied by Craik (2001). Furthermore, the average OTE values of the flash mix and opposing jets systems were very high at 88.0 and 87.2 %.

The OTE data of the injector, the flash mix reactor, the flash mix system, the opposing jets reactor, and the opposing jets system were normalized by dividing through by the feed gas flow rate. These normalized values resulted in exponentially decreasing curves with respect to the ratio of gas to motive flow. When normalized further by taking the natural logarithm, a linear relationship

ensued and the curve of the opposing jets system achieved the highest $OTE/Q_{G,in}$ values at each ratio of gas to motive flow.

With respect to the auto-decomposition of the ozone gas, the kinetics of the reaction between the tap water and the ozone was found to be first order. Tracer studies revealed that the injector could be modeled as an ideal plug flow reactor and the flash mix and opposing jets reactors could be modeled as continuous flow stirred tank reactors.

In terms of future research with these reactors, the sample water could be maintained at a higher temperature to better simulate the application of these units in an environment such as swimming pools or hot tubs. Other applications for these gas-liquid contacting devices could be considered and mass transfer experiments should be performed using wastewaters from various industries or contaminated ground water supplies.

6. REFERENCES

Alexander, B.F. and Y.T. Shah. 1976. Gas-liquid mass transfer coefficients for cocurrent upflow in packed beds. Can. J. Chem. Eng. 54:556-559.

American Public Health Association, American Water Works Association, and Water Environment Federation. 1995. Standard Methods for the Examination of Water and Wastewater. 19th edition. Edited by Greenberg, A.E., L.S. Clesceri, and A.D. Eaton. American Public Health Association, Washington, DC, U.S.A.

American Public Health Association, American Water Works Association, and Water Environment Federation. 1998. Standard Methods for the Examination of Water and Wastewater. 20th edition. Edited by Greenberg, A.E., L.S. Clesceri, and A.D. Eaton. American Public Health Association, Washington, DC, U.S.A.

American Water Works Association. 1999. Water Quality and Treatment: A Handbook of Community Water Supplies, 5th Ed. McGraw-Hill, Inc., New York, NY, U.S.A.

Beltrán, F.J, J.F. García-Araya, and P.M. Álvarez. 2001. Domestic Wastewater Ozonation: A Kinetic Model Approach. Ozone Sci. Eng. 23:219-228.

Beltrán, F.J., L.A. Fernández, P. Álvarez, and E. Rodriguez. 1998. Comparison of Ozonation Kinetic Data from Film and Danckwerts Theories. Ozone Sci. Eng. 20:403-420.

Bińi, A.K., B. Duczmal, and P. Machniewski. 2001. Hydrodynamics and ozone mass transfer in a tall bubble column. Chem. Eng. Sci. 56:6233-6240.

Bouaifi, M., G. Hebrard, D. Bastoul, and M. Roustan. 2001. A comparative study of gas hold-up, bubble size, interfacial area and mass transfer coefficients in stirred gas-liquid reactors and bubble columns. Chem. Eng. Proc. 40:97-111.

Briens, C.L., L.X. Huynh, J.F. Large, A. Catros, J.R. Bernard, and M.A. Bergougnou. 1992. Hydrodynamics and gas-liquid mass transfer in a downward venturi-bubble column combination. Chem. Eng. Sci. 47(13/14):3549-3556.

Brodard, E., J.P. Duguet, J. Mallevialle, and M. Roustan. 1986. A New Method to Dissolve Ozone Into Water: Deep U Tube. Environmental Technology Letters. 7:469-478.

Chen, Y.H., C.Y. Chang, C.Y. Chiu, W.H. Huang, Y.H. Yu, P.C. Chiang, Y. Ku, and J.N. Chen. 2002. Dynamic Model of Ozone Contacting Process with Oxygen Mass Transfer in Bubble Columns. J. Env. Eng. 11:1036-1045.

Craik, S.A. 2001. Improving the design of ozone contactors for microorganism reduction with a static mixer: Ph.D. thesis. University of Alberta, Edmonton, AB, Canada.

Craik, S.A., G. Finch, J. Leparc, and M.S. Chandrakanth. 2002. The Effect of Ozone Gas-Liquid Contacting Conditions in a Static Mixer on Microorganism Reduction. Ozone Sci. Eng. 23:99-103.

Danckwerts, P.V. 1970. Gas-liquid reactions. McGraw-Hill, Inc., New York, NY, U.S.A. 276 p.

Deckwer, W.D. 1992. Bubble Column Reactors. V. Cottrell (translator), R.W. Field (editor). John Wiley & Sons Ltd., Chichester, England. 533 p.

Deckwer, W.D. and A. Schumpe. 1993. Improved tools for bubble column reactor design and scale-up. Chem. Eng. Sci. 48(5):889-911.

Deckwer, W.D. and A. Schumpe. 1987. Bubble columns – the state of the art and current trends. Int. Chem. Eng. 27:3:405-422.

Deckwer, W.D., K. Nguyen-Tien, B.G. Kelkar, and Y.T. Shah. 1974. Mixing and mass transfer in tall bubble columns. Chem. Eng. Sci. 29:2177-2188.

Farines, V., S. Baig, J. Albet, J. Molinier, and C. Legay. 2003. Ozone transfer from gas to water in a co-current upflow packed bed reactor containing silica gel. Chem. Eng. J. 91:67-73.

Gamal El-Din, M. 2001. Theoretical analysis and experimental investigation of the performance of ozone bubble columns: Ph.D. thesis. University of Alberta, Edmonton, AB, Canada.

Gamal El-Din, M. and D.W. Smith. 2003. Mass transfer analysis in ozone bubble columns. J. Environ. Eng. Sci. 2:63-76.

Gamal El-Din, M. and D.W. Smith. 2002. Theoretical analysis and experimental verification of ozone mass transfer in bubble columns. Environ. Technol. 23:135-147.

Gamal El-Din, M. and D.W. Smith. 2001. Designing Ozone Bubble Columns: A Spreadsheet Approach to Axial Dispersion Model. Ozone Sci. Eng. 23:369-384.

Hermanowicz, S., W.D. Bellamy, and L.C. Fung. 1999. Variability of ozone reaction kinetics in batch and continuous flow reactors. Wat. Res. 33(9):2130-2138.

Heyouni, A., M. Roustan, and Z. Do-Quang. 2002. Hydrodynamics and mass transfer in gas-liquid flow through static mixers. Chem. Eng. Sci. 57:3325-3333.

Hsu, Y.-C., T.-Y. Chen, J.-H. Chen, and C.-W. Lay. 2002. Ozone Transfer into Water in a Gas-Inducing Reactor. Ind. Eng. Chem. Res. 41:120-127.

Huang, W.H., C.Y. Chang, C.Y. Chiu, S.J. Lee, Y.H. Yu, H.T. Liou, Y. Ku, and J.N. Chen. 1998. A refined model for ozone mass transfer in a bubble column. J. Environ. Sci. Health. A33(3):441-460.

Huynh, L.X., C.L. Briens, J.F. Large, A. Catros, J.R. Bernard, and M.A. Bergougnou. 1991. Hydrodynamics and mass transfer in an upward venturi/bubble column combination. Can. J. Chem. Eng. 69:711-72.

Jakubowski, C.A., B.W. Atkinson, P. Dennis, and G.M. Evans. 2003. Ozone Mass Transfer in a Confined Plunging Liquid Jet Contactor. Ozone Sci. Eng. 25:1-12.

Kaštánek, F., J. Zahradník, J. Kratochvíl, and J. Čermák. 1993. Chemical reactors for gas-liquid systems. Ellis Horwood Limited, Czech Republic. 406 p.

Kawagoe, M., T. Otake, and C.W. Robinson. 1989. Gas-phase mixing in bubble columns. Journal of Chemical Engineering of Japan. 22:2:136-142.

Kim, J.-H., R.B. Tomiak, and B.J. Mariñas. 2002. Inactivation of *Cryptosporidium* Oocysts in a Pilot-Scale Ozone Bubble-Diffuser Contactor. I: Model Development. J. Env. Eng. 6:514-521.

Kuo, C.H. 1982. Mass Transfer in Ozone Absorption. Environmental Progress. 1(3):189-195.

Langlais, B., D.A. Reckhow, and D.R. Brink editors. 1991. Ozone in Water Treatment – Application and Engineering. Lewis Publishers, Inc., Chelsea, MI, U.S.A. 569 p.

Laplanche, A., N. Le Sauze, G. Martin, and B. Langlais. 1991. Simulation of ozone transfer in water. Comparison with a pilot unit. Ozone Sci. Eng. 13:535-559.

Larachi, F., A. Laurent, N. Midoux, and G. Wild. 1991. Some experimental liquid saturation results in fixed-bed reactors operated under elevated pressure in cocurrent upflow and downflow of the gas and the liquid. Ind. Eng. Chem. Res. 30:2404-2410.

Levenspiel, O. 1999. Chemical Reaction Engineering. 3rd edition. John Wiley & Sons, New York, NY, U.S.A. 668 p.

Mariñas, B.J., S. Liang, and E.M. Aieta. 1993. Modeling Hydrodynamics and Ozone Residual Distribution in a Pilot-Scale Ozone Bubble –Diffuser Contactor. Journal AWWA. 90-99.

Martin, N. and C. Galey. 1994. Use Of Static Mixer For Oxidation And Disinfection By Ozone. Ozone Sci. Eng. 16:455-473.

Martin, N., M. Benezet-Toulze, C. Laplace, M. Faivre, and B. Langlais. 1992. Design And Efficiency Of Ozone Contactors For Disinfection. Ozone Sci. Eng. 14:391-405.

Mazzei, A.L and L.J. Bollyky. 1991. Optimizing Mass Transfer Efficiency and Ozone Utilization with High Efficiency Venturi Injectors. Proceedings of the International Ozone Association, Pan American Committee. Toronto, ON, Canada. 197-223.

Nakao, K., H. Takeuchi, H. Kataoka, H. Kaji, T. Otake, and T. Miyauchi. 1983. Mass Transfer Characteristics of Bubble Columns in Recirculation Flow Regime. Ind. Eng. Chem. Process Des. Dev. 22:577-582.

Oke, N.J., D.W. Smith, and H. Zhou. 1998. An Empirical Analysis of Ozone Decay Kinetics in Natural Waters. Ozone Sci. Eng. 20:361-379.

Radhakrishnan, V.R. and A.K. Mitra. 1984. Pressure Drop, Holdup and Interfacial Area in Vertical Two-Phase Flow of Multi-Jet Ejector Induced Dispersions. Can. J. Chem. Eng. 62:170-178.

Richard, Y. 1994. Ozone water demand test. Ozone Sci. Eng. 16:355-365.

Roustan, M., R.Y. Wang, and D. Wolbert. 1996. Modeling Hydrodynamics And Mass Transfer Parameters In A Continuous Ozone Bubble Column. Ozone Sci. Eng. 18:99-115.

Roustan, M., C. Beck, O. Wable, J.P. Duguet, and J. Mallevialle. 1993. Modeling Hydraulics of Ozone Contactors. Ozone Sci. Eng. 15: 213-226.

Roustan, M., J.P. Duguet, B. Brette, E. Brodard, and J. Mallevialle. 1987. Mass balance analysis of ozone in conventional bubble contactors. Ozone Sci. Eng. 9:289-297.

Salazar, J.A., K.D. Wisecarver, Y.T. Shah, and B. Solari. 1993. Gas-liquid mass transfer in jet bubble column. Chem. Eng. Comm. 124:177-188.

Sawyer, C.N., P.L. McCarty, and G.F. Parkin. 1994. Chemistry for Environmental Engineering, 4th Ed. McGraw-Hill, Inc., New York, NY, U.S.A. 658 p.

Schulz, C.R. and P.W. Prendiville. 1993. Designing High Concentration Ozone Contactors For Drinking Water Treatment Plants. Ozone Sci. Eng. 15:245-266.

Schulz, C.R., G.C. Schafran, L.B. Garrett, and R.A. Hawkins. 1995. Evaluating a high-efficiency ozone injection contactor. J. AWWA. 8:85-99.

Sheffer, S. and G.L. Esterson. 1982. Mass transfer and reaction kinetics in the ozone/tap water system. Wat. Res. 16:383-389.

Shetty, S.A., M.V. Kantak, and B.G. Kelkar. 1992. Gas-Phase Backmixing in Bubble-Column Reactors. AIChE Journal. 38:7:1013-1026.

Smith, D.W. and M. Gamal El-Din. 2002. Theoretical analysis and experimental verification of ozone mass transfer in bubble columns. Env. Tech. 23:135-147.

Smith, D.W. and H. Zhou. 1994. Theoretical Analysis Of Ozone Disinfection Performance In A Bubble Column. Ozone Sci. Eng. 16:429-441.

Sotelo, J.L., F.J. Beltrán, F.J. Benitez, and J. Beltrán-Heredia. 1989. Henry's Law Constant for the Ozone-Water System. Wat. Res. 23(10):1239-1246.

Thalasso, F., H. Naveau, and E.-J. Nyns. 1995. Design and performance of a bioreactor equipped with a Venturi injector for high gas transfer rates. Chem. Eng. J. 57:B1-B5.

Valentin, F.H.H. 1967. Absorption in gas-liquid dispersions: some aspects of bubble technology. E. & F. N. Spon Ltd., London, Great Britain. 212 p.

Voigt, J. and K. Schügerl. 1979. Absorption of oxygen in countercurrent multistage bubble columns – I. Chem. Eng. Sci. 23:1221-1229.

von Gunten, U. 2003. Ozonation of drinking water: Part I. Oxidation kinetics and product formation. Wat. Res. 37:1443-1467.

Wright, P.C., V. Meeyoo, and W.K. Soh. 1998. A Study Of Ozone Mass Transfer In A Cocurrent Downflow Jet Pump Contactor. Ozone Sci. Eng. 20(1):17-33.

Xu, F. and C. Liu. 1990. Mass Balance Analysis of Ozone in a Conventional Bubble Column. Ozone Sci. Eng. 12(3):269-279.

Yurteri, C. and M.D. Gurol. 1988. Ozone Consumption in Natural Waters: Effects of Background Organic Matter, pH and Carbonate Species. Ozone Sci. Eng. 10:277-290.

Zahradník, J. and M. Fialová. 1996. The effect of bubbling regime on gas and liquid phase mixing in bubble column reactors. Chem. Eng. Sci. 51:2491-2500.

Zhou, H. 1995. Investigation of ozone disinfection kinetics and contactor performance modeling: Ph.D. thesis. University of Alberta, Edmonton, AB, Canada.

Zhou, H. and D.W. Smith. 2000*a*. Ozone mass transfer in water and wastewater treatment: Experimental observations using a 2D-laser particle dynamics analyzer. Wat. Res. 34:909-921.

Zhou, H. and D.W. Smith. 2000*b*. Integrated modeling of ozonation processes in water treatment. In Proceedings of the Water Supply and Water Quality IV International Conference. Krakow, Poland. 1-12.

APPENDIX A – Summary Table of Kinetics Experiments

Table A-1 Summary of tap water kinetics experiments.

Trial	Temp., T (ºC)	k_1 (min^{-1})	R^2	$\ln(k_1)$	T - 20 (ºC)	pH	Alkalinity (mg $CaCO_3$/L)
1	6.00	4.07E-02	93%	-3.20	-14.00	8.21	107.64
2	5.94	3.98E-02	95%	-3.22	-14.06	8.40	107.64
3	6.87	4.47E-02	96%	-3.11	-13.13	8.47	107.64
4	15.17	9.15E-02	99%	-2.39	-4.83	8.58	107.64
5	15.67	1.15E-01	100%	-2.16	-4.33	8.57	107.64
6	21.12	2.68E-01	94%	-1.32	1.12	8.54	107.64
7	21.17	3.30E-01	96%	-1.11	1.17	8.56	107.64
8	20.21	1.78E-01	78%	-1.72	0.21	7.53	106.12
9	18.85	8.47E-02	90%	-2.47	-1.15	7.80	106.12
10	18.81	8.41E-02	89%	-2.48	-1.19	7.84	106.12
11	11.84	6.53E-02	90%	-2.73	-8.16	7.91	106.12
12	10.85	5.27E-02	90%	-2.94	-9.15	7.94	106.12
13	31.01	3.58E-01	85%	-1.03	11.01	8.07	106.12
14	32.37	3.03E-01	92%	-1.19	12.37	7.96	106.12
15	26.33	1.88E-01	93%	-1.67	6.33	7.84	105.76
16	25.11	2.29E-01	76%	-1.47	5.11	7.89	105.76
17	21.17	2.49E-01	96%	-1.39	1.17	7.83	105.76

APPENDIX B – Tables from Hydraulic Performance Study

Table A-2 Hydraulic performance study data from flash mix system.

Experiment		Environment				Gas				Liquid				
Date	Run #	P_0 at MSL (mm Hg)	P_{act} at actual elevation (mm Hg)	Air temp. (°C)	Water temp. (°C)	Output pressure of gas tank (psi)	Rotameter #	Calibrated rotameter injector throat inlet gas flowrate (SLPM)	Calibrated injector throat pressure (psig)	Calibrated flowmeter injector inlet liquid flowrate (GPM)	Calibrated injector inlet pressure (psi)	Calibrated injector outlet pressure (psi)	Calibrated system back-pressure (psi)	G/L ratio
12-Nov-02	31	763.6	705.1	24.0	6.5	50	1	0.5	2.3	3.8	7.4	7.1	3.6	0.031
12-Nov-02	32	763.6	705.1	24.0	6.5	50	1	1.0	3.3	3.8	8.4	8.1	3.6	0.072
12-Nov-02	33	763.6	705.1	24.0	6.5	50	1	0.5	-3.1	6.7	11.9	10.1	3.6	0.018
12-Nov-02	34	763.6	705.1	24.0	6.5	50	1	0.4	-10.9	10.2	21.8	15.2	3.6	0.011
12-Nov-02	35	763.6	705.1	24.0	6.5	50	1	0.3	-11.9	10.2	21.3	15.2	3.6	0.007
12-Nov-02	36	763.6	705.1	24.0	6.5	50	1	1.1	-8.0	9.9	21.3	14.2	3.6	0.028
12-Nov-02	37	763.6	705.1	24.0	6.5	50	1	1.0	-8.1	8.9	18.3	13.2	3.6	0.030
12-Nov-02	38	763.6	705.1	24.0	6.5	50	1	0.5	-8.0	8.9	17.3	13.2	3.6	0.016
12-Nov-02	39	763.6	705.1	24.0	6.5	50	2	5.5	-1.7	9.7	27.3	14.2	3.6	0.149
12-Nov-02	40	763.6	705.1	24.0	6.5	50	2	2.8	-5.6	9.7	26.3	14.7	3.6	0.076
12-Nov-02	41	763.6	705.1	24.0	6.5	50	2	7.5	0.0	9.7	28.3	14.2	3.6	0.204
12-Nov-02	42	763.6	705.1	24.0	6.5	50	2	2.8	3.8	5.5	12.4	10.1	3.6	0.138
12-Nov-02	43	762.1	703.6	24.0	14.0	50	2	1.3	-1.2	6.7	13.4	10.6	3.6	0.053
12-Nov-02	44	762.1	703.6	24.0	14.0	50	2	3.9	1.8	6.7	15.4	11.1	3.6	0.153
12-Nov-02	45	762.1	703.6	24.0	14.0	50	2	5.2	2.5	6.7	17.3	11.1	3.6	0.204
12-Nov-02	46	762.1	703.6	24.0	14.0	50	2	2.6	0.5	6.7	14.4	10.1	3.6	0.101
12-Nov-02	47	762.1	703.6	24.0	14.0	50	2	3.2	1.3	6.7	14.9	10.1	3.6	0.127
12-Nov-02	48	762.1	703.6	24.0	14.0	50	1	0.9	-1.7	6.7	13.4	10.6	3.6	0.035
12-Nov-02	49	762.1	703.6	24.0	14.0	50	1	1.1	-1.2	6.7	13.4	10.6	3.6	0.043
12-Nov-02	50	762.1	703.6	24.0	14.0	50	1	1.6	2.3	5.1	10.4	9.1	3.6	0.080
12-Nov-02	51	762.1	703.6	24.0	14.0	50	1	1.0	1.5	5.1	10.4	9.1	3.6	0.051
12-Nov-02	52	762.1	703.6	24.0	14.0	50	1	0.1	0.0	5.1	9.4	9.6	3.6	0.005
12-Nov-02	53	762.1	703.6	24.0	14.0	50	2	4.1	3.5	5.1	11.9	9.1	3.6	0.209
12-Nov-02	54	762.1	703.6	24.0	14.0	50	2	2.1	2.8	5.1	10.9	9.1	3.6	0.110
12-Nov-02	55	762.1	703.6	24.0	14.0	50	2	1.6	5.1	2.2	6.4	7.1	3.6	0.198
12-Nov-02	56	762.1	703.6	24.0	14.0	50	2	1.7	5.8	4.9	13.4	12.1	6.7	0.089
12-Nov-02	57	762.1	703.6	24.0	14.0	50	2	2.3	5.8	4.9	13.4	12.1	6.7	0.125
12-Nov-02	58	762.1	703.6	24.0	14.0	50	1	1.6	5.8	4.9	13.4	12.1	6.7	0.086
12-Nov-02	59	762.1	703.6	24.0	14.0	50	1	1.0	5.1	4.9	13.4	12.1	6.7	0.052
12-Nov-02	60	762.1	703.6	24.0	14.0	50	1	1.0	1.0	6.7	15.8	13.2	6.7	0.038
12-Nov-02	61	762.1	703.6	24.0	14.0	50	1	1.6	2.3	6.7	16.3	13.2	6.7	0.062
12-Nov-02	62	762.1	703.6	24.0	14.0	50	2	2.1	2.8	6.7	16.3	13.2	6.7	0.085
12-Nov-02	63	762.1	703.6	24.0	14.0	50	2	4.2	4.3	6.7	17.3	13.2	6.7	0.165
12-Nov-02	64	762.1	703.6	24.0	14.0	50	2	6.6	3.5	8.2	24.3	16.2	6.7	0.212
12-Nov-02	65	762.1	703.6	24.0	14.0	50	2	3.9	2.3	8.2	24.3	16.2	6.7	0.126
12-Nov-02	66	762.1	703.6	24.0	14.0	50	2	5.3	3.3	8.2	24.3	16.2	6.7	0.170
12-Nov-02	67	762.1	703.6	24.0	14.0	50	2	1.3	-1.7	8.2	19.3	16.2	6.7	0.042
12-Nov-02	69	762.1	703.6	24.0	14.0	50	1	0.8	-3.6	8.7	19.3	15.7	6.7	0.024
12-Nov-02	70	762.1	703.6	24.0	14.0	50	1	1.3	-2.2	8.7	20.3	15.2	6.7	0.040
12-Nov-02	71	762.1	703.6	24.0	14.0	50	1	0.5	-5.6	8.7	18.8	15.2	6.7	0.015
12-Nov-02	72	762.1	703.6	24.0	14.0	50	1	1.6	-1.7	8.7	20.3	15.2	6.7	0.047
12-Nov-02	73	762.1	703.6	24.0	14.0	50	1	0.8	-6.5	9.7	21.8	16.2	6.7	0.022
12-Nov-02	74	762.1	703.6	24.0	14.0	50	1	1.0	-5.6	9.7	22.3	16.2	6.7	0.028
12-Nov-02	75	762.1	703.6	24.0	14.0	50	1	1.3	-4.1	9.7	22.3	16.2	6.7	0.035
12-Nov-02	76	762.1	703.6	24.0	14.0	50	2	1.1	-4.6	9.7	22.8	17.2	6.7	0.031
12-Nov-02	77	762.1	703.6	24.0	14.0	50	2	2.3	-2.2	9.7	23.3	16.2	6.7	0.063
12-Nov-02	78	762.1	703.6	24.0	14.0	50	2	3.6	0.0	9.7	24.3	15.7	6.7	0.098
12-Nov-02	79	762.1	703.6	24.0	14.0	50	2	5.0	1.3	9.7	27.3	17.2	6.7	0.134
12-Nov-02	80	762.1	703.6	24.0	14.0	50	2	6.2	1.5	9.7	28.3	17.2	6.7	0.167
12-Nov-02	81	762.1	703.6	24.0	14.0	50	2	7.5	2.3	9.7	28.3	16.2	6.7	0.204
12-Nov-02	82	762.1	703.6	24.0	14.0	50	2	6.9	2.0	9.7	28.3	16.2	6.7	0.186
13-Nov-02	83	762.1	703.6	23.5	16.0	50	1	1.5	-2.6	10.0	28.3	21.2	10.7	0.039
13-Nov-02	84	762.1	703.6	23.5	16.0	50	1	1.2	-3.6	10.0	28.3	21.7	10.7	0.033
13-Nov-02	85	762.1	703.6	23.5	16.0	50	1	0.9	-4.6	10.0	28.3	21.7	10.7	0.025
13-Nov-02	86	762.1	703.6	24.0	5.0	50	2	1.2	-3.6	10.0	28.3	22.2	10.7	0.032
13-Nov-02	87	762.1	703.6	24.0	5.0	50	2	2.4	-1.2	10.0	29.3	21.2	10.7	0.064
13-Nov-02	88	762.1	703.6	24.0	5.0	50	2	3.1	0.0	10.0	29.3	21.2	10.7	0.081
13-Nov-02	89	762.1	703.6	24.0	5.0	50	2	3.9	1.8	10.0	30.8	21.7	10.7	0.102
13-Nov-02	90	762.1	703.6	24.0	5.0	50	2	5.3	3.3	10.0	31.3	21.2	10.7	0.140
13-Nov-02	91	762.1	703.6	24.0	5.0	50	2	4.6	3.0	10.0	31.3	21.2	10.7	0.122
13-Nov-02	92	762.1	703.6	24.0	5.0	50	2	3.0	5.3	7.7	23.3	18.2	10.7	0.102
13-Nov-02	93	762.1	703.6	24.0	5.0	50	2	1.6	4.6	7.7	22.8	18.7	10.7	0.056
13-Nov-02	94	762.1	703.6	24.0	5.0	50	2	0.4	3.3	7.7	20.3	18.2	10.7	0.015
13-Nov-02	95	762.1	703.6	24.0	5.0	50	2	0.7	3.5	7.7	20.3	17.7	10.7	0.024
13-Nov-02	96	762.1	703.6	24.0	5.0	50	2	1.0	4.0	7.7	20.8	17.2	10.7	0.033
13-Nov-02	97	762.1	703.6	23.5	5.0	50	1	1.2	6.1	7.2	19.3	17.2	10.7	0.046

Experiment		Environment				Gas				Liquid				
Date	Run #	P_0 at MSL (mm Hg)	P_{act} at actual elevation (mm Hg)	Air temp. (°C)	Water temp. (°C)	Output pressure of gas tank (psi)	Rotameter #	Calibrated rotameter injector throat inlet gas flowrate (SLPM)	Calibrated injector throat pressure (psig)	Calibrated flowmeter injector inlet liquid flowrate (GPM)	Calibrated injector inlet pressure (psi)	Calibrated injector outlet pressure (psi)	Calibrated system back-pressure (psi)	G/L ratio
13-Nov-02	98	762.1	703.6	23.5	5.0	50	1	1.0	5.3	7.2	19.3	17.2	10.7	0.036
13-Nov-02	99	762.1	703.6	23.5	5.0	50	1	0.7	4.8	7.2	19.3	18.2	10.7	0.027
13-Nov-02	100	762.1	703.6	23.5	5.0	50	1	0.5	4.3	7.2	19.3	18.7	10.7	0.018
13-Nov-02	101	762.1	703.6	23.5	5.0	50	1	0.4	4.0	7.2	19.3	18.7	10.7	0.013
13-Nov-02	102	762.1	703.6	23.5	5.0	50	1	1.3	0.0	10.0	31.3	24.7	14.8	0.036
13-Nov-02	103	762.1	703.6	23.5	5.0	50	1	1.5	0.5	10.0	31.3	24.7	14.8	0.039
13-Nov-02	104	762.1	703.6	23.5	5.0	50	2	1.4	0.5	10.0	31.3	25.2	14.8	0.038
13-Nov-02	105	762.1	703.6	23.5	5.0	50	2	2.2	3.0	10.0	31.3	24.7	14.8	0.057
13-Nov-02	106	762.1	703.6	23.0	9.0	50	2	1.7	5.8	8.2	26.3	23.2	14.8	0.054
13-Nov-02	107	762.1	703.6	23.0	9.0	50	2	3.0	5.6	8.7	28.3	23.2	14.8	0.091
13-Nov-02	108	762.1	703.6	23.0	9.0	50	2	2.3	5.8	9.2	31.8	26.8	16.8	0.067
14-Nov-02	109	763.6	705.1	23.5	9.0	50	1	0.9	-1.7	10.0	30.8	26.2	14.8	0.023
14-Nov-02	110	763.6	705.1	23.5	9.0	50	1	0.7	-1.9	10.0	29.3	24.7	14.8	0.018
14-Nov-02	111	763.6	705.1	23.5	9.0	50	1	0.5	-2.1	10.0	28.8	25.2	14.8	0.013
14-Nov-02	112	763.6	705.1	23.5	9.0	50	1	0.3	-3.1	10.0	28.8	25.2	14.8	0.007
14-Nov-02	113	763.6	705.1	23.5	9.0	50	1	0.1	-3.9	10.0	28.8	25.7	14.8	0.002
14-Nov-02	114	763.6	705.1	23.5	9.0	50	1	1.0	5.8	8.0	25.3	22.2	14.8	0.033
14-Nov-02	115	763.6	705.1	23.5	9.0	50	1	0.6	4.8	8.0	24.3	22.2	14.8	0.020
14-Nov-02	116	763.6	705.1	23.5	9.0	50	1	0.4	3.8	8.0	24.3	22.7	14.8	0.012
14-Nov-02	117	763.6	705.1	23.5	9.0	50	1	0.1	3.3	8.0	24.3	22.7	14.8	0.004
14-Nov-02	118	763.6	705.1	23.5	9.0	50	1	0.1	-2.6	8.7	20.3	18.2	10.7	0.003
14-Nov-02	119	763.6	705.1	23.5	9.0	50	1	0.3	-1.9	8.7	20.3	18.2	10.7	0.009
14-Nov-02	120	763.6	705.1	23.5	9.0	50	1	0.6	0.0	8.7	20.8	18.7	10.7	0.019
14-Nov-02	121	763.6	705.1	23.5	9.0	50	1	0.5	-0.9	8.7	20.3	18.2	10.7	0.015
14-Nov-02	122	763.6	705.1	23.5	9.0	50	1	0.4	-1.7	8.7	20.3	18.2	10.7	0.012
14-Nov-02	123	763.6	705.1	23.5	9.0	50	1	1.0	0.5	8.7	22.3	19.2	10.7	0.029
14-Nov-02	124	763.6	705.1	23.5	9.0	50	1	1.2	1.0	8.7	22.3	19.2	10.7	0.036
14-Nov-02	125	763.6	705.1	23.5	9.0	50	1	1.4	1.5	8.7	22.8	19.2	10.7	0.043
14-Nov-02	126	763.6	705.1	23.5	9.0	50	1	1.7	2.0	8.7	23.3	19.2	10.7	0.051
14-Nov-02	127	763.6	705.1	23.5	9.0	50	1	1.3	-4.8	8.7	18.3	12.1	3.6	0.038
14-Nov-02	128	763.6	705.1	23.5	9.0	50	1	0.9	-6.1	8.7	18.3	12.1	3.6	0.028
14-Nov-02	129	763.6	705.1	23.5	9.0	50	1	1.1	-5.3	8.7	18.3	12.1	3.6	0.034
14-Nov-02	130	763.6	705.1	23.5	9.0	50	1	1.4	-4.6	8.7	18.3	12.1	3.6	0.041
14-Nov-02	131	763.6	705.1	23.5	9.0	50	1	0.6	-7.3	8.7	17.3	12.1	3.6	0.019
14-Nov-02	132	763.6	705.1	23.5	9.0	50	1	0.5	-8.0	8.7	16.8	13.2	3.6	0.014
14-Nov-02	133	763.6	705.1	23.5	9.0	50	1	0.2	-9.7	8.7	15.8	13.7	3.6	0.007
14-Nov-02	134	763.6	705.1	23.5	9.0	50	1	0.0	-11.2	8.7	15.4	13.2	3.6	0.001
14-Nov-02	135	763.6	705.1	23.5	9.0	50	1	0.7	-9.2	10.0	21.3	14.7	3.6	0.017
14-Nov-02	136	763.6	705.1	23.5	9.0	50	1	0.8	-8.5	10.0	21.3	14.2	3.6	0.022
14-Nov-02	137	763.6	705.1	23.5	9.0	50	1	1.0	-7.8	10.0	21.3	14.2	3.6	0.027
14-Nov-02	138	763.6	705.1	23.5	9.0	50	2	0.8	-9.2	10.0	20.8	14.2	3.6	0.021
14-Nov-02	139	763.6	705.1	23.5	9.0	50	2	1.9	-6.1	10.0	21.3	13.7	3.6	0.050
14-Nov-02	140	763.6	705.1	23.5	9.0	50	2	3.1	-3.9	10.0	24.3	14.2	3.6	0.081

Table A-3 Hydraulic performance study data from opposing jets system.

Experiment		Environment				Gas				Liquid				
Date	Run #	P_0 at MSL (mm Hg)	P_{act} at actual elevation (mm Hg)	Air temp. (°C)	Water temp. (°C)	Output pressure of gas tank (psi)	Rotameter #	Calibrated rotameter injector throat inlet gas flowrate (SLPM)	Calibrated injector throat pressure (psig)	Calibrated flowmeter injector inlet liquid flowrate (GPM)	Calibrated injector inlet pressure (psi)	Calibrated injector outlet pressure (psi)	Calibrated system back-pressure (psi)	G/L ratio
5-Feb-03	200	771.1	712.6	23.2	14.0	50	1	0.1	-3.4	5.1	7.4	8.1	3.6	0.005
5-Feb-03	201	771.1	712.6	23.2	14.0	50	1	0.4	-1.7	5.1	8.4	8.1	3.6	0.021
5-Feb-03	202	771.1	712.6	23.2	14.0	50	1	0.6	0.0	5.1	8.4	8.1	3.6	0.032
5-Feb-03	203	771.1	712.6	23.2	14.0	50	1	0.9	0.0	5.1	9.4	8.1	3.6	0.048
5-Feb-03	204	771.1	712.6	23.2	14.0	50	1	0.2	-2.9	5.1	7.9	8.1	3.6	0.010
5-Feb-03	205	771.1	712.6	23.2	14.0	50	1	0.3	-1.9	5.1	7.9	8.1	3.6	0.016
5-Feb-03	206	771.1	712.6	23.2	14.0	50	1	1.3	0.5	5.1	9.4	8.1	3.6	0.066
5-Feb-03	207	771.1	712.6	23.2	14.0	50	1	1.5	1.0	5.1	9.4	8.1	3.6	0.078
5-Feb-03	208	771.1	712.6	23.2	14.0	50	2	1.5	1.0	5.1	9.4	8.1	3.6	0.075
5-Feb-03	209	771.1	712.6	23.2	14.0	50	2	2.1	1.5	5.1	9.4	7.6	3.6	0.107
5-Feb-03	210	771.1	712.6	23.2	14.0	50	2	4.0	2.5	5.1	10.4	7.6	3.6	0.204
5-Feb-03	211	771.1	712.6	23.2	14.0	50	2	5.3	3.3	5.1	10.9	8.1	3.6	0.273
5-Feb-03	212	771.1	712.6	23.2	14.0	50	2	6.7	3.8	5.1	10.9	8.1	3.6	0.342
5-Feb-03	213	771.1	712.6	23.2	14.0	50	2	8.0	4.3	5.1	11.4	8.1	3.6	0.413
5-Feb-03	214	771.1	712.6	23.2	14.0	50	2	7.7	2.8	6.7	16.3	9.1	3.6	0.305
5-Feb-03	215	771.1	712.6	23.2	14.0	50	2	6.3	2.0	6.7	15.8	9.1	3.6	0.250
5-Feb-03	216	771.1	712.6	23.2	14.0	50	2	5.0	1.0	6.7	15.4	9.1	3.6	0.196
5-Feb-03	217	771.1	712.6	23.2	14.0	50	2	3.7	0.5	6.7	14.9	8.6	3.6	0.147
5-Feb-03	218	771.1	712.6	23.2	14.0	50	2	3.1	0.0	6.7	14.4	8.6	3.6	0.123
5-Feb-03	219	771.1	712.6	23.2	14.0	50	2	2.4	-1.4	6.7	13.9	8.6	3.6	0.095
5-Feb-03	220	771.1	712.6	23.2	14.0	50	2	1.3	-2.6	6.7	11.4	8.1	3.6	0.050
5-Feb-03	221	771.1	712.6	23.2	14.0	50	1	1.3	-2.1	6.7	11.4	8.1	3.6	0.053
5-Feb-03	222	771.1	712.6	23.2	14.0	50	1	1.0	-3.1	6.7	11.4	8.1	3.6	0.040
5-Feb-03	223	771.1	712.6	23.2	14.0	50	1	0.8	-3.6	6.7	10.9	8.1	3.6	0.032
5-Feb-03	224	771.1	712.6	23.2	14.0	50	1	0.4	-4.6	6.7	10.4	8.1	3.6	0.017
5-Feb-03	225	771.1	712.6	23.2	14.0	50	1	0.2	-5.6	6.7	9.9	8.1	3.6	0.010
5-Feb-03	226	771.1	712.6	23.2	14.0	50	1	0.1	-12.6	8.7	10.4	8.1	3.6	0.002
5-Feb-03	227	771.1	712.6	23.2	14.0	50	1	0.2	-11.9	8.7	10.9	8.1	3.6	0.005
5-Feb-03	228	771.1	712.6	23.2	14.0	50	1	0.4	-10.0	8.7	11.9	8.1	3.6	0.012
5-Feb-03	229	771.1	712.6	23.2	14.0	50	1	0.6	-9.0	8.7	12.4	8.1	3.6	0.017
5-Feb-03	230	771.1	712.6	23.2	14.0	50	1	0.8	-8.7	8.7	13.9	8.1	3.6	0.023
5-Feb-03	231	772.6	714.1	23.2	10.0	50	1	0.9	-8.0	8.7	14.4	8.1	3.6	0.029
5-Feb-03	232	772.6	714.1	23.2	10.0	50	1	1.2	-7.3	8.7	14.9	8.1	3.6	0.035
5-Feb-03	233	772.6	714.1	23.2	10.0	50	2	0.9	-8.0	8.7	13.9	8.1	3.6	0.028
5-Feb-03	234	772.6	714.1	23.2	10.0	50	2	1.9	-5.8	8.7	15.4	8.1	3.6	0.059
5-Feb-03	235	772.6	714.1	23.2	10.0	50	2	3.0	-4.6	8.7	17.3	8.1	3.6	0.091
5-Feb-03	236	772.6	714.1	23.2	10.0	50	2	4.2	-3.1	8.7	18.3	8.1	3.6	0.128
5-Feb-03	237	772.6	714.1	23.2	10.0	50	2	5.5	-1.9	8.7	18.8	8.1	3.6	0.166
5-Feb-03	238	772.6	714.1	23.2	10.0	50	2	6.8	-0.9	8.7	19.3	8.1	3.6	0.206
5-Feb-03	239	772.6	714.1	23.2	10.0	50	2	8.2	0.0	8.7	19.8	8.1	3.6	0.247
5-Feb-03	240	772.6	714.1	22.8	5.0	50	2	6.5	-3.6	9.7	25.3	9.1	3.6	0.177
5-Feb-03	241	772.6	714.1	22.8	5.0	50	2	4.6	-5.6	9.7	24.8	9.6	3.6	0.124
5-Feb-03	242	772.6	714.1	22.8	5.0	50	2	2.3	-8.2	9.7	21.3	9.1	3.6	0.063
5-Feb-03	243	772.6	714.1	22.8	5.0	50	2	0.4	-12.9	9.7	19.8	9.6	3.6	0.010
5-Feb-03	244	772.6	714.1	22.8	5.0	50	1	0.6	-11.4	9.7	20.3	9.6	3.6	0.017
5-Feb-03	245	772.6	714.1	22.8	5.0	50	1	0.8	-10.9	9.7	20.3	9.6	3.6	0.021
5-Feb-03	246	772.6	714.1	22.8	5.0	50	1	0.5	-11.9	9.7	20.3	9.6	3.6	0.014
5-Feb-03	247	772.6	714.1	22.8	5.0	50	1	0.4	-12.4	9.7	19.8	9.6	3.6	0.010
5-Feb-03	248	772.6	714.1	22.8	5.0	50	1	0.3	-12.6	9.7	16.3	9.1	3.6	0.007
5-Feb-03	249	772.6	714.1	22.8	5.0	50	1	0.2	-12.9	9.7	16.3	9.1	3.6	0.005
5-Feb-03	250	772.6	714.1	22.8	5.0	50	1	0.1	-13.4	9.7	16.3	9.1	3.6	0.002
5-Feb-03	251	772.6	714.1	22.8	5.0	50	1	0.5	3.0	4.9	10.4	10.1	6.7	0.025
5-Feb-03	252	772.6	714.1	22.8	5.0	50	1	0.8	3.5	4.9	10.4	10.1	6.7	0.044
5-Feb-03	253	772.6	714.1	22.8	5.0	50	1	1.1	3.8	4.9	10.9	10.1	6.7	0.057
5-Feb-03	254	772.6	714.1	22.8	5.0	50	1	1.6	4.8	4.9	11.9	10.6	6.7	0.085
5-Feb-03	255	772.6	714.1	22.8	5.0	50	1	2.0	5.3	4.9	11.9	10.6	6.7	0.106
5-Feb-03	256	772.6	714.1	22.8	5.0	50	1	0.2	3.3	4.9	10.9	11.1	6.7	0.013
5-Feb-03	257	772.6	714.1	22.8	5.0	50	2	1.7	5.3	4.9	11.9	10.6	6.7	0.090
5-Feb-03	258	772.6	714.1	22.8	5.0	50	2	2.4	5.8	4.9	12.9	11.6	6.7	0.127
5-Feb-03	259	772.6	714.1	22.8	5.0	50	2	4.4	6.3	4.9	13.9	11.6	6.7	0.239
5-Feb-03	260	772.6	714.1	22.8	5.0	50	2	7.4	7.8	4.9	14.4	11.6	6.7	0.400
5-Feb-03	261	772.6	714.1	22.8	5.0	50	2	7.0	5.3	6.7	18.8	12.1	6.7	0.275

Experiment		Environment				Gas				Liquid				
Date	Run #	P_0 at MSL (mm Hg)	P_{act} at actual elevation (mm Hg)	Air temp. (°C)	Water temp. (°C)	Output pressure of gas tank (psi)	Rotameter #	Calibrated rotameter injector throat inlet gas flowrate (SLPM)	Calibrated injector throat pressure (psig)	Calibrated flowmeter injector inlet liquid flowrate (GPM)	Calibrated injector inlet pressure (psi)	Calibrated injector outlet pressure (psi)	Calibrated system back-pressure (psi)	G/L ratio
5-Feb-03	262	772.6	714.1	22.8	5.0	50	2	4.2	4.0	6.7	17.8	12.1	6.7	0.165
5-Feb-03	263	772.6	714.1	22.8	5.0	50	2	2.1	2.3	6.7	17.3	12.1	6.7	0.084
5-Feb-03	264	772.6	714.1	22.8	5.0	50	2	2.7	2.3	6.7	15.4	11.1	6.7	0.108
5-Feb-03	265	772.6	714.1	22.8	5.0	50	1	1.5	0.8	6.7	14.4	11.1	6.7	0.060
5-Feb-03	266	772.6	714.1	22.8	5.0	50	1	0.9	0.0	6.7	13.9	11.1	6.7	0.037
5-Feb-03	267	772.6	714.1	22.8	5.0	50	1	0.7	-0.9	6.7	13.4	11.6	6.7	0.028
5-Feb-03	268	772.6	714.1	22.8	5.0	50	1	0.5	-1.2	6.7	13.4	11.6	6.7	0.020
5-Feb-03	269	772.6	714.1	22.8	5.0	50	1	0.4	-1.7	6.7	13.4	11.6	6.7	0.016
5-Feb-03	270	772.6	714.1	22.8	5.0	50	1	0.2	-2.1	6.7	12.9	11.6	6.7	0.008
5-Feb-03	271	772.6	714.1	22.8	5.0	50	1	0.4	-7.5	8.7	14.4	11.6	6.7	0.013
5-Feb-03	272	772.6	714.1	22.8	5.0	50	1	0.5	-7.0	8.7	14.9	11.6	6.7	0.016
5-Feb-03	273	772.6	714.1	22.8	5.0	50	1	0.7	-7.0	8.7	16.3	12.1	6.7	0.020
5-Feb-03	274	772.6	714.1	22.8	5.0	50	1	1.1	-5.3	8.7	17.3	12.1	6.7	0.035
5-Feb-03	275	772.6	714.1	22.8	5.0	50	1	1.4	-4.6	8.7	17.3	12.1	6.7	0.041
5-Feb-03	276	772.6	714.1	22.8	5.0	50	2	1.1	-5.6	8.7	16.8	12.1	6.7	0.033
5-Feb-03	277	772.6	714.1	22.8	5.0	50	2	3.5	-1.2	8.7	18.8	12.1	6.7	0.106
5-Feb-03	278	772.6	714.1	22.8	5.0	50	2	4.8	0.0	8.7	21.3	12.1	6.7	0.145
5-Feb-03	279	772.6	714.1	22.8	5.0	50	2	6.1	0.8	8.7	21.8	12.1	6.7	0.184
5-Feb-03	280	772.6	714.1	22.8	5.0	50	2	6.8	1.3	8.7	22.3	12.1	6.7	0.205
5-Feb-03	281	772.6	714.1	22.8	5.0	50	2	7.5	1.8	8.7	22.3	12.1	6.7	0.226
5-Feb-03	282	772.6	714.1	22.8	5.0	50	2	6.6	-1.7	9.7	26.3	12.1	6.7	0.179
5-Feb-03	283	772.6	714.1	22.8	5.0	50	2	5.9	-2.1	9.7	26.3	12.1	6.7	0.161
5-Feb-03	284	772.6	714.1	22.8	5.0	50	2	5.2	-3.1	9.7	26.3	12.1	6.7	0.141
5-Feb-03	285	772.6	714.1	22.8	5.0	50	2	4.0	-4.3	9.7	25.8	12.1	6.7	0.108
5-Feb-03	286	772.6	714.1	22.8	5.0	50	2	2.8	-5.6	9.7	24.3	12.1	6.7	0.077
5-Feb-03	287	772.6	714.1	22.8	5.0	50	2	1.6	-8.0	9.7	23.3	12.6	6.7	0.045
5-Feb-03	288	772.6	714.1	22.8	5.0	50	2	0.7	-10.0	9.7	18.3	12.1	6.7	0.020
5-Feb-03	289	772.6	714.1	22.8	5.0	50	1	1.0	-8.0	9.7	19.3	12.1	6.7	0.028
5-Feb-03	290	772.6	714.1	22.8	5.0	50	1	0.8	-8.7	9.7	19.3	12.1	6.7	0.022
5-Feb-03	291	772.6	714.1	22.8	5.0	50	1	0.6	-9.7	9.7	18.3	12.1	6.7	0.017
5-Feb-03	292	772.6	714.1	22.8	5.0	50	1	0.5	-10.4	9.7	18.3	12.1	6.7	0.013
5-Feb-03	293	772.6	714.1	22.8	5.0	50	1	0.2	-11.9	9.7	17.8	12.1	6.7	0.006
5-Feb-03	294	772.6	714.1	22.8	5.0	50	1	0.1	-12.9	9.7	17.3	12.1	6.7	0.003
5-Feb-03	295	772.6	714.1	22.8	5.0	50	1	0.4	1.0	7.2	16.3	15.2	10.7	0.016
5-Feb-03	296	772.6	714.1	22.8	5.0	50	1	0.7	1.5	7.2	16.8	15.2	10.7	0.024
5-Feb-03	297	772.6	714.1	22.8	5.0	50	1	0.9	2.0	7.2	17.3	15.2	10.7	0.033
5-Feb-03	298	772.6	714.1	22.8	5.0	50	1	1.1	2.3	7.2	17.3	15.2	10.7	0.042
5-Feb-03	299	772.6	714.1	22.8	5.0	50	1	1.6	3.3	7.2	17.3	15.2	10.7	0.060
5-Feb-03	300	772.6	714.1	22.8	5.0	50	2	2.3	4.3	7.2	19.8	15.7	10.7	0.083
5-Feb-03	301	772.6	714.1	22.8	5.0	50	2	4.4	5.8	7.2	20.3	15.7	10.7	0.160
5-Feb-03	302	772.6	714.1	22.8	5.0	50	2	5.8	6.3	7.2	20.3	15.7	10.7	0.212
6-Feb-03	303	768.9	710.4	23.5	2.0	50	2	7.2	6.8	7.7	23.3	15.2	10.7	0.247
6-Feb-03	304	768.9	710.4	23.5	2.0	50	2	5.7	5.8	7.7	22.3	15.2	10.7	0.195
6-Feb-03	305	768.9	710.4	23.5	2.0	50	2	4.2	4.3	7.7	22.3	15.2	10.7	0.144
6-Feb-03	306	768.9	710.4	23.5	2.0	50	2	2.8	3.5	7.7	21.8	15.2	10.7	0.097
6-Feb-03	307	768.9	710.4	23.5	2.0	50	2	1.5	2.0	7.7	19.8	15.2	10.7	0.052
6-Feb-03	308	768.9	710.4	23.5	2.0	50	1	1.6	1.8	7.7	19.8	15.2	10.7	0.053
6-Feb-03	309	768.9	710.4	23.5	2.0	50	1	1.3	1.3	7.7	19.3	15.7	10.7	0.045
6-Feb-03	310	768.9	710.4	23.5	2.0	50	1	0.9	0.0	7.7	18.8	16.2	10.7	0.032
6-Feb-03	311	768.9	710.4	23.5	2.0	50	1	0.6	0.0	7.7	18.3	16.2	10.7	0.022
6-Feb-03	312	768.9	710.4	23.5	2.0	50	1	0.4	-0.9	7.7	18.3	16.2	10.7	0.014
6-Feb-03	313	768.9	710.4	23.5	2.0	50	1	0.3	-1.7	7.7	18.3	16.2	10.7	0.010
6-Feb-03	314	768.9	710.4	23.5	2.0	50	1	0.2	-1.9	7.7	18.3	16.2	10.7	0.007
6-Feb-03	315	768.9	710.4	23.5	2.0	50	1	0.1	-2.1	7.7	17.8	16.2	10.7	0.003
6-Feb-03	316	767.4	708.9	23.5	2.0	50	1	0.1	-5.8	8.7	17.8	15.2	10.7	0.002
6-Feb-03	317	767.4	708.9	23.5	2.0	50	1	0.2	-5.1	8.7	17.8	15.2	10.7	0.008
6-Feb-03	318	767.4	708.9	23.5	2.0	50	1	0.3	-4.3	8.7	17.8	15.2	10.7	0.010
6-Feb-03	319	767.4	708.9	23.5	2.0	50	1	0.4	-3.9	8.7	17.8	15.2	10.7	0.013
6-Feb-03	320	767.4	708.9	23.5	2.0	50	1	0.5	-3.5	8.7	17.8	15.2	10.7	0.016
6-Feb-03	321	767.4	708.9	23.5	2.0	50	1	0.8	-2.6	8.7	18.3	14.7	10.7	0.026
6-Feb-03	322	767.4	708.9	23.5	2.0	50	1	1.1	-2.1	8.7	20.3	16.2	10.7	0.032
6-Feb-03	323	767.4	708.9	23.5	2.0	50	1	1.3	-1.7	8.7	20.3	15.2	10.7	0.038

Experiment		Environment				Gas				Liquid				
Date	Run #	P_0 at MSL (mm Hg)	P_{act} at actual elevation (mm Hg)	Air temp. (°C)	Water temp. (°C)	Output pressure of gas tank (psi)	Rotameter #	Calibrated rotameter injector throat inlet gas flowrate (SLPM)	Calibrated injector throat pressure (psig)	Calibrated flowmeter injector inlet liquid flowrate (GPM)	Calibrated injector inlet pressure (psi)	Calibrated injector outlet pressure (psi)	Calibrated system back-pressure (psi)	G/L ratio
6-Feb-03	324	767.4	708.9	23.5	2.0	50	1	1.5	-1.2	8.7	20.3	15.2	10.7	0.045
6-Feb-03	325	767.4	708.9	23.5	2.0	50	2	1.3	-1.4	8.7	20.8	16.2	10.7	0.040
6-Feb-03	326	767.4	708.9	23.5	2.0	50	2	2.5	0.0	8.7	21.3	15.2	10.7	0.077
6-Feb-03	327	767.4	708.9	23.5	2.0	50	2	3.9	1.8	8.7	22.3	15.2	10.7	0.117
6-Feb-03	328	767.4	708.9	23.5	2.0	50	2	5.1	2.3	8.7	23.3	15.2	10.7	0.156
6-Feb-03	329	767.4	708.9	23.5	2.0	50	2	6.7	4.3	8.7	23.8	15.2	10.7	0.204
6-Feb-03	330	767.4	708.9	22.8	2.0	50	2	8.3	5.3	8.7	24.3	14.2	10.7	0.250
6-Feb-03	331	767.4	708.9	22.8	2.0	50	2	4.8	0.0	10.0	27.8	16.2	10.7	0.126
6-Feb-03	332	767.4	708.9	22.8	2.0	50	2	3.9	-1.7	10.0	27.3	16.2	10.7	0.104
6-Feb-03	333	767.4	708.9	22.8	2.0	50	2	3.4	-2.1	10.0	26.3	16.2	10.7	0.089
6-Feb-03	334	767.4	708.9	22.8	2.0	50	2	2.7	-3.6	10.0	25.3	15.2	10.7	0.070
6-Feb-03	335	767.4	708.9	22.8	2.0	50	2	2.1	-4.6	10.0	28.8	15.7	10.7	0.055
6-Feb-03	336	767.4	708.9	22.8	2.0	50	2	1.0	-7.0	10.0	22.3	16.2	10.7	0.026
6-Feb-03	337	767.4	708.9	22.8	2.0	50	2	6.2	1.3	10.0	28.3	15.2	10.7	0.163
6-Feb-03	338	767.4	708.9	22.8	2.0	50	2	7.6	2.3	10.0	28.3	15.2	10.7	0.200
6-Feb-03	339	767.4	708.9	22.8	2.0	50	1	1.2	-6.1	10.0	23.3	16.2	10.7	0.033
6-Feb-03	340	767.4	708.9	22.8	2.0	50	1	1.1	-6.5	10.0	22.8	16.2	10.7	0.028
6-Feb-03	341	767.4	708.9	22.8	2.0	50	1	0.7	-8.0	10.0	22.8	16.2	10.7	0.020
6-Feb-03	342	767.4	708.9	22.8	2.0	50	1	0.6	-9.0	10.0	21.8	16.2	10.7	0.015
6-Feb-03	343	767.4	708.9	22.8	2.0	50	1	0.2	-7.5	10.0	23.3	20.2	14.8	0.006
6-Feb-03	344	767.4	708.9	22.8	2.0	50	1	0.4	-6.5	10.0	23.3	20.2	14.8	0.010
6-Feb-03	345	767.4	708.9	22.8	2.0	50	1	0.6	-5.1	10.0	23.8	19.7	14.8	0.015
6-Feb-03	346	767.4	708.9	22.8	2.0	50	1	0.8	-4.6	10.0	24.3	19.7	14.8	0.020
6-Feb-03	347	767.4	708.9	22.8	2.0	50	1	1.1	-3.9	10.0	25.3	19.7	14.8	0.030
6-Feb-03	348	767.4	708.9	22.8	2.0	50	1	1.3	-2.6	10.0	26.3	19.7	14.8	0.035
6-Feb-03	349	767.4	708.9	22.8	2.0	50	2	1.2	-3.6	10.0	25.8	19.7	14.8	0.032
6-Feb-03	350	767.4	708.9	22.8	2.0	50	2	1.8	-1.7	10.0	27.3	19.7	14.8	0.049
6-Feb-03	351	767.4	708.9	22.8	2.0	50	2	2.5	0.0	10.0	27.3	19.2	14.8	0.067
6-Feb-03	352	767.4	708.9	22.8	2.0	50	2	3.9	1.8	9.7	29.3	19.2	14.8	0.105
6-Feb-03	353	766.6	708.1	23.0	2.0	50	2	5.4	3.8	9.7	30.3	19.7	14.8	0.146
6-Feb-03	354	766.6	708.1	23.0	2.0	50	2	7.6	9.3	8.0	28.3	19.7	14.8	0.253
6-Feb-03	355	766.6	708.1	23.0	2.0	50	2	4.5	7.3	8.0	26.3	19.7	14.8	0.150
6-Feb-03	356	766.6	708.1	23.0	2.0	50	2	1.6	4.3	8.0	24.3	19.2	14.8	0.054
6-Feb-03	357	766.6	708.1	23.0	2.0	50	1	0.9	2.3	8.0	22.8	19.2	14.8	0.030
6-Feb-03	358	766.6	708.1	23.0	2.0	50	1	0.6	1.8	8.0	22.3	20.2	14.8	0.018
6-Feb-03	359	766.6	708.1	23.0	2.0	50	1	0.3	0.8	8.0	20.8	19.2	14.8	0.011
6-Feb-03	360	766.6	708.1	23.0	2.0	50	1	0.1	0.0	8.0	20.8	19.2	14.8	0.004
6-Feb-03	361	766.6	708.1	23.0	2.0	50	1	1.3	3.0	8.0	22.8	19.2	14.8	0.042
6-Feb-03	362	766.6	708.1	23.0	2.0	50	2	2.6	9.3	6.7	22.3	19.2	14.8	0.101
6-Feb-03	363	766.6	708.1	23.0	2.0	50	2	4.8	10.4	6.7	22.8	18.2	14.8	0.191
6-Feb-03	364	766.6	708.1	23.0	2.0	50	2	7.2	11.4	6.7	23.3	18.2	14.8	0.285
6-Feb-03	365	766.6	708.1	23.0	2.0	50	2	3.3	9.8	6.7	22.3	18.7	14.8	0.131
6-Feb-03	366	766.6	708.1	23.0	2.0	50	2	2.0	12.6	5.1	20.3	19.2	14.8	0.100
6-Feb-03	367	766.6	708.1	23.0	2.0	50	2	2.7	12.9	5.1	20.3	19.2	14.8	0.141
6-Feb-03	368	766.6	708.1	23.0	2.0	50	2	3.5	13.1	5.1	20.8	19.2	14.8	0.182
6-Feb-03	369	766.6	708.1	23.0	2.0	50	2	4.3	13.4	5.1	21.3	18.7	14.8	0.223
6-Feb-03	370	766.6	708.1	23.0	2.0	50	2	5.2	13.6	5.1	21.3	18.7	14.8	0.264

APPENDIX C – Tracer Study Data

Table A-4 Tracer study data from modeling of degas separator.

Time, t (s)	δt_i (s)	Concn, C (mg/L)	E (s^{-1})	$E_{avg,i}$ (s^{-1})	$\delta t_i * E_{avg,i}$	E_{CFSTR} (s^{-1})
0		0.405	3.75E-04			1.25E-01
1	1	5.464	5.07E-03	2.72E-03	2.72E-03	1.10E-01
2	1	11.535	1.07E-02	7.88E-03	7.88E-03	9.73E-02
3	1	24.964	2.32E-02	1.69E-02	1.69E-02	8.59E-02
4	1	37.382	3.47E-02	2.89E-02	2.89E-02	7.58E-02
5	1	44.189	4.10E-02	3.78E-02	3.78E-02	6.69E-02
6	1	50.811	4.71E-02	4.41E-02	4.41E-02	5.90E-02
7	1	52.927	4.91E-02	4.81E-02	4.81E-02	5.21E-02
8	1	55.227	5.12E-02	5.02E-02	5.02E-02	4.60E-02
9	1	54.767	5.08E-02	5.10E-02	5.10E-02	4.06E-02
10	1	51.915	4.82E-02	4.95E-02	4.95E-02	3.58E-02
11	1	49.708	4.61E-02	4.71E-02	4.71E-02	3.16E-02
12	1	44.649	4.14E-02	4.38E-02	4.38E-02	2.79E-02
13	1	41.797	3.88E-02	4.01E-02	4.01E-02	2.46E-02
14	1	37.382	3.47E-02	3.67E-02	3.67E-02	2.17E-02
15	1	33.979	3.15E-02	3.31E-02	3.31E-02	1.92E-02
16	1	30.759	2.85E-02	3.00E-02	3.00E-02	1.69E-02
17	1	27.816	2.58E-02	2.72E-02	2.72E-02	1.49E-02
18	1	24.412	2.26E-02	2.42E-02	2.42E-02	1.32E-02
19	1	23.308	2.16E-02	2.21E-02	2.21E-02	1.16E-02
20	1	19.997	1.86E-02	2.01E-02	2.01E-02	1.03E-02
21	1	17.422	1.62E-02	1.74E-02	1.74E-02	9.07E-03
22	1	16.594	1.54E-02	1.58E-02	1.58E-02	8.00E-03
23	1	14.478	1.34E-02	1.44E-02	1.44E-02	7.06E-03
24	1	12.546	1.16E-02	1.25E-02	1.25E-02	6.24E-03
25	1	10.983	1.02E-02	1.09E-02	1.09E-02	5.50E-03
26	1	9.879	9.16E-03	9.68E-03	9.68E-03	4.86E-03
27	1	9.879	9.16E-03	9.16E-03	9.16E-03	4.29E-03
28	1	8.407	7.80E-03	8.48E-03	8.48E-03	3.78E-03
29	1	7.579	7.03E-03	7.42E-03	7.42E-03	3.34E-03
30	1	6.660	6.18E-03	6.60E-03	6.60E-03	2.95E-03
31	1	5.924	5.50E-03	5.84E-03	5.84E-03	2.60E-03
32	1	4.912	4.56E-03	5.03E-03	5.03E-03	2.30E-03
33	1	4.912	4.56E-03	4.56E-03	4.56E-03	2.03E-03
34	1	4.360	4.04E-03	4.30E-03	4.30E-03	1.79E-03
35	1	3.992	3.70E-03	3.87E-03	3.87E-03	1.58E-03
36	1	3.624	3.36E-03	3.53E-03	3.53E-03	1.39E-03
37	1	3.624	3.36E-03	3.36E-03	3.36E-03	1.23E-03
38	1	3.624	3.36E-03	3.36E-03	3.36E-03	1.09E-03
39	1	3.624	3.36E-03	3.36E-03	3.36E-03	9.58E-04
40	1	2.152	2.00E-03	2.68E-03	2.68E-03	8.46E-04
41	1	2.520	2.34E-03	2.17E-03	2.17E-03	7.46E-04
42	1	2.152	2.00E-03	2.17E-03	2.17E-03	6.59E-04
43	1	2.520	2.34E-03	2.17E-03	2.17E-03	5.81E-04
44	1	2.152	2.00E-03	2.17E-03	2.17E-03	5.13E-04
45	1	1.417	1.31E-03	1.66E-03	1.66E-03	4.53E-04
46	1	1.049	9.73E-04	1.14E-03	1.14E-03	4.00E-04
47	1	2.152	2.00E-03	1.48E-03	1.48E-03	3.53E-04
48	1	1.417	1.31E-03	1.66E-03	1.66E-03	3.11E-04
49	1	1.417	1.31E-03	1.31E-03	1.31E-03	2.75E-04
50	1	0.405	3.75E-04	8.45E-04	8.45E-04	2.43E-04
51	1	1.417	1.31E-03	8.45E-04	8.45E-04	2.14E-04
52	1	1.049	9.73E-04	1.14E-03	1.14E-03	1.89E-04
53	1	1.417	1.31E-03	1.14E-03	1.14E-03	1.67E-04
54	1	1.049	9.73E-04	1.14E-03	1.14E-03	1.47E-04
55	1	1.049	9.73E-04	9.73E-04	9.73E-04	1.30E-04
56	1	1.049	9.73E-04	9.73E-04	9.73E-04	1.15E-04
57	1	0.405	3.75E-04	6.74E-04	6.74E-04	1.01E-04
58	1	0.405	3.75E-04	3.75E-04	3.75E-04	8.93E-05
59	1	0.405	3.75E-04	3.75E-04	3.75E-04	7.88E-05
60	1	0.405	3.75E-04	3.75E-04	3.75E-04	6.96E-05
					Σ 8.39E-01	

Table A-5 Tracer study data from modeling of injector.

Time, t (s)	δt_i (s)	Concn, C (mg/L)	E (s^{-1})	$E_{avg,i}$ (s^{-1})	$\delta t_i * E_{avg,i}$	E_{CFSTR} (s^{-1})
0		0.535	1.61E-03			4.63E+00
1	1	186.031	5.60E-01	2.81E-01	2.81E-01	4.52E-02
2	1	33.201	9.99E-02	3.30E-01	3.30E-01	4.42E-04
3	1	8.717	2.62E-02	6.31E-02	6.31E-02	4.31E-06
4	1	3.308	9.95E-03	1.81E-02	1.81E-02	4.21E-08
5	1	3.546	1.07E-02	1.03E-02	1.03E-02	4.11E-10
6	1	2.359	7.10E-03	8.88E-03	8.88E-03	4.02E-12
7	1	2.359	7.10E-03	7.10E-03	7.10E-03	3.92E-14
8	1	2.170	6.53E-03	6.81E-03	6.81E-03	3.83E-16
9	1	0.794	2.39E-03	4.46E-03	4.46E-03	3.74E-18
10	1	0.155	4.67E-04	1.43E-03	1.43E-03	3.65E-20
11	1	1.057	3.18E-03	1.82E-03	1.82E-03	3.57E-22
12	1	0.155	4.67E-04	1.82E-03	1.82E-03	3.49E-24
13	1	1.911	5.75E-03	3.11E-03	3.11E-03	3.40E-26
14	1	1.674	5.04E-03	5.39E-03	5.39E-03	3.33E-28
15	1	0.725	2.18E-03	3.61E-03	3.61E-03	3.25E-30
16	1	2.480	7.46E-03	4.82E-03	4.82E-03	3.17E-32
17	1	1.341	4.04E-03	5.75E-03	5.75E-03	3.10E-34
18	1	1.057	3.18E-03	3.61E-03	3.61E-03	3.03E-36
19	1	1.341	4.04E-03	3.61E-03	3.61E-03	2.95E-38
20	1	1.531	4.61E-03	4.32E-03	4.32E-03	2.89E-40
21	1	1.911	5.75E-03	5.18E-03	5.18E-03	2.82E-42
22	1	1.531	4.61E-03	5.18E-03	5.18E-03	2.75E-44
23	1	3.572	1.07E-02	7.68E-03	7.68E-03	2.69E-46
24	1	1.674	5.04E-03	7.89E-03	7.89E-03	2.63E-48
25	1	3.856	1.16E-02	8.32E-03	8.32E-03	2.56E-50
26	1	1.911	5.75E-03	8.68E-03	8.68E-03	2.50E-52
27	1	1.674	5.04E-03	5.39E-03	5.39E-03	2.45E-54
28	1	2.196	6.61E-03	5.82E-03	5.82E-03	2.39E-56
29	1	3.999	1.20E-02	9.32E-03	9.32E-03	2.33E-58
30	1	2.196	6.61E-03	9.32E-03	9.32E-03	2.28E-60
31	1	2.196	6.61E-03	6.61E-03	6.61E-03	2.23E-62
32	1	2.765	8.32E-03	7.46E-03	7.46E-03	2.17E-64
33	1	2.765	8.32E-03	8.32E-03	8.32E-03	2.12E-66
34	1	2.480	7.46E-03	7.89E-03	7.89E-03	2.07E-68
35	1	2.765	8.32E-03	7.89E-03	7.89E-03	2.02E-70
36	1	1.911	5.75E-03	7.03E-03	7.03E-03	1.98E-72
37	1	1.674	5.04E-03	5.39E-03	5.39E-03	1.93E-74
38	1	3.050	9.18E-03	7.11E-03	7.11E-03	1.89E-76
39	1	2.196	6.61E-03	7.89E-03	7.89E-03	1.84E-78
40	1	1.911	5.75E-03	6.18E-03	6.18E-03	1.80E-80
41	1	2.480	7.46E-03	6.61E-03	6.61E-03	1.76E-82
42	1	0.535	1.61E-03	4.54E-03	4.54E-03	1.72E-84
43	1	1.531	4.61E-03	3.11E-03	3.11E-03	1.68E-86
44	1	1.911	5.75E-03	5.18E-03	5.18E-03	1.64E-88
45	1	3.050	9.18E-03	7.46E-03	7.46E-03	1.60E-90
46	1	3.050	9.18E-03	9.18E-03	9.18E-03	1.56E-92
47	1	1.911	5.75E-03	7.46E-03	7.46E-03	1.53E-94
48	1	3.856	1.16E-02	8.68E-03	8.68E-03	1.49E-96
49	1	2.480	7.46E-03	9.53E-03	9.53E-03	1.45E-98
50	1	3.050	9.18E-03	8.32E-03	8.32E-03	1.42E-100
51	1	3.856	1.16E-02	1.04E-02	1.04E-02	1.39E-102
52	1	3.856	1.16E-02	1.16E-02	1.16E-02	1.36E-104
53	1	3.856	1.16E-02	1.16E-02	1.16E-02	1.32E-106
54	1	3.572	1.07E-02	1.12E-02	1.12E-02	1.29E-108
55	1	3.572	1.07E-02	1.07E-02	1.07E-02	1.26E-110
56	1	3.334	1.00E-02	1.04E-02	1.04E-02	1.23E-112
57	1	1.911	5.75E-03	7.89E-03	7.89E-03	1.20E-114
58	1	3.572	1.07E-02	8.25E-03	8.25E-03	1.18E-116
59	1	1.911	5.75E-03	8.25E-03	8.25E-03	1.15E-118
60	1	3.856	1.16E-02	8.68E-03	8.68E-03	1.12E-120
					Σ 1.08E+00	

Table A-6 Tracer study data from modeling of flash mix reactor.

Time, t (s)	δt_i (s)	Concn, C (mg/L)	E (s^{-1})	$E_{avg,i}$ (s^{-1})	$\delta t_i * E_{avg,i}$	E_{CFSTR} (s^{-1})
0		168.725	2.65E-01			6.71E+00
1	1	326.826	5.14E-01	3.89E-01	3.89E-01	8.20E-03
2	1	9.085	1.43E-02	2.64E-01	2.64E-01	1.00E-05
3	1	0.985	1.55E-03	7.91E-03	7.91E-03	1.23E-08
4	1	0.985	1.55E-03	1.55E-03	1.55E-03	1.50E-11
5	1	0.370	5.82E-04	1.07E-03	1.07E-03	1.83E-14
6	1	0.370	5.82E-04	5.82E-04	5.82E-04	2.24E-17
7	1	0.245	3.85E-04	4.83E-04	4.83E-04	2.74E-20
8	1	0.245	3.85E-04	3.85E-04	3.85E-04	3.35E-23
9	1	0.985	1.55E-03	9.67E-04	9.67E-04	4.10E-26
10	1	0.245	3.85E-04	9.67E-04	9.67E-04	5.02E-29
11	1	0.245	3.85E-04	3.85E-04	3.85E-04	6.13E-32
12	1	0.245	3.85E-04	3.85E-04	3.85E-04	7.50E-35
13	1	0.245	3.85E-04	3.85E-04	3.85E-04	9.17E-38
14	1	0.370	5.82E-04	4.83E-04	4.83E-04	1.12E-40
15	1	0.370	5.82E-04	5.82E-04	5.82E-04	1.37E-43
16	1	0.370	5.82E-04	5.82E-04	5.82E-04	1.68E-46
17	1	0.245	3.85E-04	4.83E-04	4.83E-04	2.05E-49
18	1	0.370	5.82E-04	4.83E-04	4.83E-04	2.51E-52
19	1	0.245	3.85E-04	4.83E-04	4.83E-04	3.07E-55
20	1	0.370	5.82E-04	4.83E-04	4.83E-04	3.75E-58
21	1	0.963	1.51E-03	1.05E-03	1.05E-03	4.59E-61
22	1	0.963	1.51E-03	1.51E-03	1.51E-03	5.61E-64
23	1	0.370	5.82E-04	1.05E-03	1.05E-03	6.86E-67
24	1	0.370	5.82E-04	5.82E-04	5.82E-04	8.39E-70
25	1	0.963	1.51E-03	1.05E-03	1.05E-03	1.03E-72
26	1	0.963	1.51E-03	1.51E-03	1.51E-03	1.26E-75
27	1	0.370	5.82E-04	1.05E-03	1.05E-03	1.53E-78
28	1	0.245	3.85E-04	4.83E-04	4.83E-04	1.88E-81
29	1	0.370	5.82E-04	4.83E-04	4.83E-04	2.30E-84
30	1	0.245	3.85E-04	4.83E-04	4.83E-04	2.81E-87
31	1	0.245	3.85E-04	3.85E-04	3.85E-04	3.43E-90
32	1	0.245	3.85E-04	3.85E-04	3.85E-04	4.20E-93
33	1	0.245	3.85E-04	3.85E-04	3.85E-04	5.13E-96
34	1	0.245	3.85E-04	3.85E-04	3.85E-04	6.28E-99
35	1	0.963	1.51E-03	9.49E-04	9.49E-04	7.68E-102
36	1	0.370	5.82E-04	1.05E-03	1.05E-03	9.39E-105
37	1	0.370	5.82E-04	5.82E-04	5.82E-04	1.15E-107
38	1	0.245	3.85E-04	4.83E-04	4.83E-04	1.40E-110
39	1	0.245	3.85E-04	3.85E-04	3.85E-04	1.72E-113
40	1	0.245	3.85E-04	3.85E-04	3.85E-04	2.10E-116
41	1	0.370	5.82E-04	4.83E-04	4.83E-04	2.57E-119
42	1	0.370	5.82E-04	5.82E-04	5.82E-04	3.14E-122
43	1	0.370	5.82E-04	5.82E-04	5.82E-04	3.84E-125
44	1	0.985	1.55E-03	1.07E-03	1.07E-03	4.70E-128
45	1	0.245	3.85E-04	9.67E-04	9.67E-04	5.74E-131
46	1	0.370	5.82E-04	4.83E-04	4.83E-04	7.02E-134
47	1	0.370	5.82E-04	5.82E-04	5.82E-04	8.59E-137
48	1	0.985	1.55E-03	1.07E-03	1.07E-03	1.05E-139
49	1	0.245	3.85E-04	9.67E-04	9.67E-04	1.28E-142
50	1	0.370	5.82E-04	4.83E-04	4.83E-04	1.57E-145
51	1	0.963	1.51E-03	1.05E-03	1.05E-03	1.92E-148
52	1	0.963	1.51E-03	1.51E-03	1.51E-03	2.35E-151
53	1	0.245	3.85E-04	9.49E-04	9.49E-04	2.87E-154
54	1	0.985	1.55E-03	9.67E-04	9.67E-04	3.51E-157
55	1	0.985	1.55E-03	1.55E-03	1.55E-03	4.30E-160
56	1	0.985	1.55E-03	1.55E-03	1.55E-03	5.25E-163
57	1	0.985	1.55E-03	1.55E-03	1.55E-03	6.42E-166
58	1	0.370	5.82E-04	1.07E-03	1.07E-03	7.86E-169
59	1	0.985	1.55E-03	1.07E-03	1.07E-03	9.61E-172
60	1	0.607	9.54E-04	1.25E-03	1.25E-03	1.17E-174
					Σ 7.06E-01	

Table A-7 Tracer study data from modeling of opposing jets reactor.

Time, t (s)	δt_i (s)	Concn, C (mg/L)	E (s^{-1})	$E_{avg,i}$ (s^{-1})	$\delta t_i * E_{avg,i}$	E_{CFSTR} (s^{-1})
0		0.573	3.45E-04			2.02E+00
1	1	13.689	8.24E-03	4.29E-03	4.29E-03	2.69E-01
2	1	401.003	2.41E-01	1.25E-01	1.25E-01	3.58E-02
3	1	444.681	2.68E-01	2.54E-01	2.54E-01	4.77E-03
4	1	162.999	9.81E-02	1.83E-01	1.83E-01	6.36E-04
5	1	20.821	1.25E-02	5.53E-02	5.53E-02	8.47E-05
6	1	2.547	1.53E-03	7.03E-03	7.03E-03	1.13E-05
7	1	2.547	1.53E-03	1.53E-03	1.53E-03	1.50E-06
8	1	2.802	1.69E-03	1.61E-03	1.61E-03	2.01E-07
9	1	0.573	3.45E-04	1.02E-03	1.02E-03	2.67E-08
10	1	2.547	1.53E-03	9.39E-04	9.39E-04	3.56E-09
11	1	0.573	3.45E-04	9.39E-04	9.39E-04	4.75E-10
12	1	0.573	3.45E-04	3.45E-04	3.45E-04	6.32E-11
13	1	0.573	3.45E-04	3.45E-04	3.45E-04	8.43E-12
14	1	2.547	1.53E-03	9.39E-04	9.39E-04	1.12E-12
15	1	2.547	1.53E-03	1.53E-03	1.53E-03	1.50E-13
16	1	2.802	1.69E-03	1.61E-03	1.61E-03	1.99E-14
17	1	0.573	3.45E-04	1.02E-03	1.02E-03	2.66E-15
18	1	2.547	1.53E-03	9.39E-04	9.39E-04	3.54E-16
19	1	2.802	1.69E-03	1.61E-03	1.61E-03	4.72E-17
20	1	0.573	3.45E-04	1.02E-03	1.02E-03	6.29E-18
21	1	0.573	3.45E-04	3.45E-04	3.45E-04	8.38E-19
22	1	2.547	1.53E-03	9.39E-04	9.39E-04	1.12E-19
23	1	2.802	1.69E-03	1.61E-03	1.61E-03	1.49E-20
24	1	2.802	1.69E-03	1.69E-03	1.69E-03	1.98E-21
25	1	2.802	1.69E-03	1.69E-03	1.69E-03	2.64E-22
26	1	2.547	1.53E-03	1.61E-03	1.61E-03	3.52E-23
27	1	5.476	3.29E-03	2.41E-03	2.41E-03	4.70E-24
28	1	5.476	3.29E-03	3.29E-03	3.29E-03	6.26E-25
29	1	5.476	3.29E-03	3.29E-03	3.29E-03	8.34E-26
30	1	2.802	1.69E-03	2.49E-03	2.49E-03	1.11E-26
31	1	2.547	1.53E-03	1.61E-03	1.61E-03	1.48E-27
32	1	4.775	2.87E-03	2.20E-03	2.20E-03	1.97E-28
33	1	2.802	1.69E-03	2.28E-03	2.28E-03	2.63E-29
34	1	0.573	3.45E-04	1.02E-03	1.02E-03	3.51E-30
35	1	2.802	1.69E-03	1.02E-03	1.02E-03	4.67E-31
36	1	2.802	1.69E-03	1.69E-03	1.69E-03	6.23E-32
37	1	0.573	3.45E-04	1.02E-03	1.02E-03	8.30E-33
38	1	2.802	1.69E-03	1.02E-03	1.02E-03	1.11E-33
39	1	5.476	3.29E-03	2.49E-03	2.49E-03	1.47E-34
40	1	5.476	3.29E-03	3.29E-03	3.29E-03	1.96E-35
41	1	2.802	1.69E-03	2.49E-03	2.49E-03	2.62E-36
42	1	0.573	3.45E-04	1.02E-03	1.02E-03	3.49E-37
43	1	0.573	3.45E-04	3.45E-04	3.45E-04	4.65E-38
44	1	2.547	1.53E-03	9.39E-04	9.39E-04	6.19E-39
45	1	2.547	1.53E-03	1.53E-03	1.53E-03	8.26E-40
46	1	2.802	1.69E-03	1.61E-03	1.61E-03	1.10E-40
47	1	4.775	2.87E-03	2.28E-03	2.28E-03	1.47E-41
48	1	0.573	3.45E-04	1.61E-03	1.61E-03	1.95E-42
49	1	0.573	3.45E-04	3.45E-04	3.45E-04	2.60E-43
50	1	2.802	1.69E-03	1.02E-03	1.02E-03	3.47E-44
51	1	0.573	3.45E-04	1.02E-03	1.02E-03	4.62E-45
52	1	0.573	3.45E-04	3.45E-04	3.45E-04	6.16E-46
53	1	5.476	3.29E-03	1.82E-03	1.82E-03	8.21E-47
54	1	2.802	1.69E-03	2.49E-03	2.49E-03	1.09E-47
55	1	0.573	3.45E-04	1.02E-03	1.02E-03	1.46E-48
56	1	0.573	3.45E-04	3.45E-04	3.45E-04	1.94E-49
57	1	2.547	1.53E-03	9.39E-04	9.39E-04	2.59E-50
58	1	2.547	1.53E-03	1.53E-03	1.53E-03	3.45E-51
59	1	0.573	3.45E-04	9.39E-04	9.39E-04	4.60E-52
60	1	0.573	3.45E-04	3.45E-04	3.45E-04	6.13E-53
					Σ 7.05E-01	

APPENDIX D – Raw Data Sheets

Table A-8 Raw data calculation sheet for flash mix reactor run #033.

RUN #: 33 DATE: December 5, 2002

Port # - trial	Ozone conc'n (% w/w)	Volume of indigo solution (mL)	Volume of sample, V (mL)	Absorbance of sample @ 600 nm	Abs. blank - Abs. sample, ΔA	Ozone conc'n (mg/L)	Avg. ozone conc'n (mg/L)
2-1	7.09	10.0	14.6	0.122	0.083	1.354	
2-2	7.09	10.0	28.0	0.059	0.146	1.241	**1.298**
4-1	7.11	10.0	21.6	0.055	0.151	1.659	
4-2	7.11	10.0	21.9	0.052	0.154	1.669	**1.664**
5-1	7.11	10.0	21.6	0.054	0.151	1.664	
5-2	7.11	10.0	23.0	0.048	0.157	1.625	**1.645**

Run#: 33	Gauge	Actual		NOTES:
Liquid flow rate=	7.00	6.68	GPM (Q_L)	noticed water bubbling through flowmeter (at ~2:33) --> might have decreased liquid flow rate
Gas flow rate=	0.6		SLPM	
Gas rotameter #=	1			
System back pressure=	5.0	3.61	psi	
Gas inlet pressure=	-2.0	-3.38	in Hg	
		-1.66	psi	
Injector inlet pressure=	10.5	10.51	psi	
Injector exit pressure=	8.0	8.36	psi	
FM reactor exit pressure=		4.09	psi	from equation of head loss vs. Q_L

Actual temperature (°C)	24.00
Actual temperature (°K)	297.15
Actual experimental barometric pressure = P_{act} (mm Hg)	706.60
Actual experimental rotameter exit gauge pressure (psig)	-1.66
Actual experimental rotameter exit gauge pressure (mm Hg)	-85.78
Actual experimental rotameter exit absolute pressure (mm Hg)	620.83
$k_{rot,\ act,\ extra\text{-}dry\ O2}$	0.940
$k_{rot,\ act,\ air}$	1.048
Conc. of ozone product gas (% w/w) at experimental condns	7.09
Concentration of ozone product gas (% w/w) at STP	7.09
Density of ozone product gas (g/L) at STP	1.376
$k_{rot,\ act,\ O3}$	0.958
Rotameter reading (SLPM)	0.60
Actual ozone feed-gas flowrate (mL/min)	498.05
Actual ozone feed-gas flowrate (L/min)	0.498 ← Q_G
Actual air feed-gas flowrate (L/min)	0.545
Actual oxygen feed-gas flowrate (L/min)	0.489
STP ozone feed-gas flowrate (SMLPM)	401.37
STP ozone feed-gas flowrate (SLPM)	0.40
Ozone feed gas concentration, C_G (mg/L_{gas})	86.715 ←
Applied ozone dose (mg/L_{liq})	1.709 ← $= C_G * Q_G / Q_L$

	Injector inlet (*PG1*) P_{in}	Injector exit (*PG2*) P_{exit}	Injector throat (*PG31/4*) P_{throat}	Flash Mix exit (eqn) P_{ext}
Actual experimental gauge pressure (mm Hg)	543.71	432.41	-85.78	211.64
Actual experimental absolute pressure (mm Hg)	1250.31	1139.01	620.83	918.24
Actual experimental absolute pressure (kPa)	166.67	151.83	82.76	122.40

RUN #: 33 DATE: December 5, 2002

Absorbance of blank =	0.205	
path of cell, b =	1 cm	
factor, f =	0.42	
Air temperature=	24.0 °C	
Water temperature=	2.5 °C	
Atm. pressure=	102.0 kPa	
Actual atm. pressure=	706.60 mm Hg	
Ozone monitor temp.=	31.1 °C	
Wet test initial volume=	25.05 L	
Wet test final volume=	29.18 L	
Wet test total volume=	4.13 L	
Time of wet test=	16.82 min	
Gas temperature=	23.0 °C	
Ozone concentration=	7.09 %	
KI volume titrated=	400.0 mL	
Normality of $Na_2S_2O_3$=	0.500 N	
Titrant initial volume=	22.79 mL	
Titrant final volume=	24.05 mL	
Titrant total volume=	1.26 mL	
Conc'n of O_3 in offgas=	**3.66 mg/L** ← $C_{G,eff}$	
pH=	? pH units	
Temperature for pH=	? °C	
Normality of H_2SO_4=	0.107 N	0.107 N
Volume of H_2SO_4=	2.35 mL	mL
Volume of tap water=	100 mL	100 mL
Alkalinity=	125.73 mg/L	0.00 mg/L
Average alkalinity=	125.73 mg/L	

Table A-9 Raw data calculation sheet for opposing jets reactor run #201.

RUN #: 201 DATE: February 11, 2003

Port # - trial	Ozone conc'n (% w/w)	Volume of indigo solution (mL)	Volume of sample, V (mL)	Absorbance of sample @ 600 nm	Abs. blank - Abs. sample, ΔA	Ozone conc'n (mg/L)	Avg. ozone conc'n (mg/L)
2-1	1.20	10.0	79.1	0.128	0.079	0.238	
2-2	1.20	10.0	76.7	0.129	0.078	0.242	**0.240**
4-1	1.20	10.0	71.8	0.127	0.080	0.265	
4-2	1.20	10.0	52.0	0.146	0.061	0.279	**0.274**
4-3	1.20	10.0	73.3	0.122	0.085	0.276	
5-1	1.20	10.0	72.0	0.127	0.080	0.265	
5-2	1.20	10.0	55.0	0.146	0.061	0.264	**0.267**
5-3	1.20	10.0	74.0	0.122	0.085	0.273	

Run#: 201	Gauge	Actual	
Liquid flow rate=	5.50	5.15	GPM (Q_L)
Gas flow rate=	0.5		SLPM
Gas rotameter #=	1		
System back pressure=	5.0	3.61	psi
Gas inlet pressure=	0.0	0.00	psi
		0.00	psi
Injector inlet pressure=	7.5	7.53	psi
Injector exit pressure=	5.5	5.84	psi
OJ reactor exit pressure=		4.50	psi

NOTES:

from equation of head loss vs. Q_L

Actual temperature (°C)	23.00
Actual temperature (°K)	296.15
Actual experimental barometric pressure = P_{atm} (mm Hg)	707.35
Actual experimental rotameter exit gauge pressure (psig)	0.00
Actual experimental rotameter exit gauge pressure (mm Hg)	0.00
Actual experimental rotameter exit absolute pressure (mm Hg)	707.35
$k_{vol,\ act,\ extra\text{-}dry\ O2}$	1.005
$k_{vol,\ act,\ air}$	1.121
Conc. of ozone product gas (% w/w) at experimental condns	1.21
Concentration of ozone product gas (% w/w) at STP	1.21
Density of ozone product gas (g/L) at STP	1.348
$k_{vol,\ act,\ O2}$	1.000
Rotameter reading (SLPM)	0.50
Actual ozone feed-gas flowrate (mL/min)	416.69
Actual ozone feed-gas flowrate (L/min)	0.417 ← Q_G
Actual air feed-gas flowrate (L/min)	0.467
Actual oxygen feed-gas flowrate (L/min)	0.418
STP ozone feed-gas flowrate (SMLPM)	383.89
STP ozone feed-gas flowrate (SLPM)	0.38
Ozone feed gas concentration, C_G (mg/L_{gas})	14.732 ←
Applied ozone dose (mg/L_{liq})	0.315 ← $= C_G * Q_G / Q_L$

	Injector inlet (*PG1*) P_{in}	Injector exit (*PG2*) P_{exit}	Injector throat (*PG31/4*) P_{throat}	Opposing Jets exit (eqn) P_{exit}
Actual experimental gauge pressure (mm Hg)	389.27	302.12	0.00	232.89
Actual experimental absolute pressure (mm Hg)	1096.62	1009.47	707.35	940.24
Actual experimental absolute pressure (kPa)	146.18	134.56	94.29	125.33

RUN #: 201 DATE: February 11, 2003

Absorbance of blank =	0.207	
path of cell, b =	1 cm	
factor, f =	0.42	
Air temperature=	23.0 °C	
Water temperature=	2.0 °C	
Atm. pressure=	102.1 kPa	
Actual atm. pressure=	707.35 mm Hg	
Ozone monitor temp.=	31.7 °C	
Wet test initial volume=	19.17 L	
Wet test final volume=	21.21 L	
Wet test total volume=	2.04 L	
Time of wet test=	12.87 min	
Gas temperature=	22.6 °C	
Ozone concentration=	1.21 %	
KI volume titrated=	400.0 mL	
Normality of $Na_2S_2O_3$=	0.100 N	
Titrant initial volume=	16.40 mL	
Titrant final volume=	17.59 mL	
Titrant total volume=	1.19 mL	
Conc'n of O_3 in offgas=	**1.40 mg/L** ← $C_{G,off}$	
pH=	7.54 pH units	
Temperature for pH=	11.2 °C	
Normality of H_2SO_4=	0.107 N	0.107 N
Volume of H_2SO_4=	2.19 mL	2.19 mL
Volume of tap water=	100 mL	100 mL
Alkalinity=	117.17 mg/L	117.17 mg/L
Average alkalinity=	117.17 mg/L	

APPENDIX E – Data Analyses Sheets

Table A-10 Data analyses spreadsheets for flash mix run # 033.

Run # 33

Experimental values:

Liquid flow rate, Q_L (GPM)	6.7
Feed gas flow rate, $Q_{G,0}$ (L/min)	0.50
Feed gas pressure, P_0 (kPa)	82.8
Exit pressure, P_{exit} (kPa)	151.8
Feed gas temperature, T_0 (ºC)	24.0
Actual atmospheric pressure (mm Hg)	706.6
Liquid temperature, T_i (ºC)	2.5
Inlet concentration in gas phase at atmospheric pressure, $C_{G,0}$ (mg/L)	86.7
Exit concentration in liquid phase, $C_{L,11}$ (mg/L)	1.3
Liquid flow rate, Q_L (L/min)	25.3
Feed gas temperature, T_0 (K)	297.2
Liquid temperature, T_i (K)	275.7
Molar ratio of ozone gas in feed gas at inlet, y_0	0.0473

Constants:

Reaction rate constant, k_w (min^{-1})	0.032
Number of cells, N_{CFSTR}	11
Length of injector, L (m)	1.35E-01
Injector inlet nozzle area, A_0 (m^2)	3.22E-05
Injector exit nozzle area, A_{exit} (m^2)	3.14E-04
Injector average area, A_{avg} (m^2)	1.73E-04
Total volume, V (m^3)	2.34E-05
Total volume, V (L)	2.34E-02
Cell volume, V_{CFSTR} (L)	2.13E-03
Universal gas law constant, R (kPa-L/K-mol)	8.31E+00
Henry's law constant, H (kPa-L/mg)	0.22

Check

Injector inlet gas flow rate, $Q_{inert\ gases,0} * C_{inert\ gases,0}$ (mg/min)	763.3
Injector exit gas flow rate, $Q_{inert\ gases,exit} * C_{inert\ gases,exit}$ (mg/min)	763.3

Iteration #	1	2	3	4	5	
C_L^* (mg/L)	1.88E+01	1.69E+01	1.79E+01	1.79E+01	1.79E+01	
$k_L a_{inj}$ (min^{-1})	77.56	79.42	75.02	74.96	**74.96** ← SOLVER	
$K_1=Q_L+k_w V+k_L a V$	2.54E+01	2.54E+01	2.54E+01	2.54E+01	2.54E+01	
$K_2=k_L a C_L^* V$	3.10E+00	2.85E+00	2.85E+00	2.85E+00	2.85E+00	
$K_3=k_L a V$	1.65E-01	1.69E-01	1.59E-01	1.59E-01	1.59E-01	
Q_L/K_1	9.94E-01	9.93E-01	9.94E-01	9.94E-01	9.94E-01	$k_w C_{L,i} V_{CFSTR}$
$C_{L,11}$ eqn (mg/L)	1.30E+00	1.30E+00	1.30E+00	1.30E+00	1.30E+00	8.85E-05
$C_{L,11}$ dif. (mg/L)	0.0000	0.0000	0.0000	0.0000	0.0000	
$C_{L,1}$ (mg/L)	1.22E-01	1.12E-01	1.12E-01	1.12E-01	1.12E-01	8.31E-06
$C_{L,2}$ (mg/L)	2.43E-01	2.24E-01	2.23E-01	2.23E-01	2.23E-01	1.66E-05
$C_{L,3}$ (mg/L)	3.63E-01	3.34E-01	3.34E-01	3.34E-01	3.34E-01	2.48E-05
$C_{L,4}$ (mg/L)	4.83E-01	4.44E-01	4.43E-01	4.43E-01	4.43E-01	3.29E-05
$C_{L,5}$ (mg/L)	6.01E-01	5.53E-01	5.53E-01	5.53E-01	5.53E-01	4.10E-05
$C_{L,6}$ (mg/L)	7.19E-01	6.62E-01	6.61E-01	6.61E-01	6.61E-01	4.91E-05
$C_{L,7}$ (mg/L)	8.36E-01	7.69E-01	7.69E-01	7.69E-01	7.69E-01	5.70E-05
$C_{L,8}$ (mg/L)	9.53E-01	8.76E-01	8.76E-01	8.76E-01	8.76E-01	6.50E-05
$C_{L,9}$ (mg/L)	1.07E+00	9.83E-01	9.82E-01	9.82E-01	9.82E-01	7.29E-05
$C_{L,10}$ (mg/L)	1.18E+00	1.09E+00	1.09E+00	1.09E+00	1.09E+00	8.07E-05
y_6	0.0317	0.0335	0.0335	0.0335	0.0335	**5.37E-04 Sum**
$C_{L,6}^*$ (mg/L)	1.69E+01	1.79E+01	1.79E+01	1.79E+01	1.79E+01	
$y_{est} = y_{11}$	0.0131	0.0165	0.0165	0.0165	0.0165	
$C_{G,11}$ eqn_2 (mg/L)					52.4	
$Q_{G,est}=Q_{G,11}$ (L/min)					0.24	
OTE_{inj} (%)					70.4	

Run # 33

Experimental values:	from injector
Measured exit concentration in liquid phase, $C_{L,measured\ exit}$ (mg/L)	1.7
Air temperature (^{0}C)	24.0
Water temperature (^{0}C)	2.5
Actual atm. Pressure (mmHg)	706.6
System Exit pressure, P_{exit} (psi)	3.6
Inlet concentration in liquid phase, $C_{L,0}$ (mg/L)	1.3
Inlet pressure, P_0 (kPa)	151.8
Liquid flow rate, Q_L (L/min)	25.3
Exit pressure, P_{exit} (kPa)	122.4
Inlet temperature, T_0 (K)	275.7
Exit temperature, T_{exit} (K)	275.7

Constants

Reaction rate constant, k_w (min^{-1})	0.032
Number of cells, N_{CFSTR}	1
Total volume, V (L)	8.20E-02
Cell volume, V_{CFSTR} (L)	8.20E-02
Universal gas law constant, R (kPa-L/K-mol)	8.31E+00
Henry's law constant, H (kPa-L/mg)	0.22

Calculations (from gas and liquid mass balances)

$Q_{G,exit}$ * $C_{G,exit}$ (mg/min)	3.5
$Q_{G,exit}$ * y_{exit} (L/min)	0.0014
$Q_{G,exit}$ (L/min)	0.30
y_{exit}	0.0046
$C_{G,exit}$ (mg/L)	11.8
$k_L a_{lm/oj}$ (min^{-1})	11.2
$OTE_{lm/oj}$ (%)	72.5
$OTE_{sys,gas}$ (%)	91.9
Unused applied gaseous ozone mass rate (mg/min)	3.5
Unused applied gaseous ozone dose (mg/L_{liq})	0.1
Applied ozone dose (mg/L_{liq})	1.7
Residual ozone dose (mg/L_{liq})	1.7
Unused applied ozone dose = Applied - Residual (mg/L_{liq})	0.0
$OTE_{sys,liq}$ (%)	97.4
G/L ratio	0.02
$k_L a_{inj}/k_L a_{lm}$	6.7

Check

FM/OJ reactor inlet gas flow rate, $Q_{inert\ gases,0}$ * $C_{inert\ gases,0}$ (mg/min)	763.3
FM/OJ reactor exit gas flow rate, $Q_{inert\ gases,exit}$ * $C_{inert\ gases,exit}$ (mg/min)	763.3

The difference between the two unused applied ozone values is due to ozone auto-decomposition

Injector	**Sum of** $k_w C_{L,j} V_{CFSTR}/Q_L$	2.1E-05 mg/L
FM/OJ	$k_w C_{L,exit} V_{CFSTR}/Q_L$	1.7E-04 mg/L
Injector and FM/OJ reactor		0.000 mg/L

Table A-11 Data analyses spreadsheets for opposing jets run # 201.

Run # 201

Experimental values:

Liquid flow rate, Q_L (GPM)	5.1
Feed gas flow rate, $Q_{G,0}$ (L/min)	0.42
Feed gas pressure, P_0 (kPa)	94.3
Exit pressure, P_{exit} (kPa)	134.6
Feed gas temperature, T_0 (ºC)	23.0
Actual atmospheric pressure (mm Hg)	707.4
Liquid temperature, T_i (ºC)	2.0
Inlet concentration in gas phase at atmospheric pressure, $C_{G,0}$ (mg/L)	14.7
Exit concentration in liquid phase, $C_{L,11}$ (mg/L)	0.2
Liquid flow rate, Q_L (L/min)	19.5
Feed gas temperature, T_0 (K)	296.2
Liquid temperature, T_i (K)	275.2
Molar ratio of ozone gas in feed gas at inlet, y_0	0.0080

Constants:

Reaction rate constant, k_w (min^{-1})	0.031
Number of cells, N_{CFSTR}	11
Length of injector, L (m)	1.35E-01
Injector inlet nozzle area, A_0 (m^2)	3.22E-05
Injector exit nozzle area, A_{exit} (m^2)	3.14E-04
Injector average area, A_{avg} (m^2)	1.73E-04
Total volume, V (m^3)	2.34E-05
Total volume, V (L)	2.34E-02
Cell volume, V_{CFSTR} (L)	2.13E-03
Universal gas law constant, R (kPa-L/K-mol)	8.31E+00
Henry's law constant, H (kPa-L/mg)	0.22

Check

Injector inlet gas flow rate, $Q_{inert\ gases,0} * C_{inert\ gases,0}$ (mg/min)	760.2
Injector exit gas flow rate, $Q_{inert\ gases,exit} * C_{inert\ gases,exit}$ (mg/min)	760.2

Iteration #	1	2	3	4	5		
C_L^* (mg/L)	3.19E+00	2.41E+00	2.55E+00	2.55E+00	2.55E+00		
$k_L a_{inj}$ (min^{-1})	65.41	80.36	75.92	75.85	75.85	←	SOLVER
$K_1=Q_L+k_wV+k_La\,V$	1.96E+01	1.97E+01	1.96E+01	1.96E+01	1.96E+01		
$K_2=k_La\,C_L^*V$	4.43E-01	4.12E-01	4.11E-01	4.11E-01	4.11E-01		
$K_3=k_La\,V$	1.39E-01	1.71E-01	1.61E-01	1.61E-01	1.61E-01		
Q_L/K_1	9.93E-01	9.91E-01	9.92E-01	9.92E-01	9.92E-01	$k_wC_{L,i}V_{CFSTR}$	
$C_{L,11}$ eqn (mg/L)	2.40E-01	2.40E-01	2.40E-01	2.40E-01	2.40E-01	1.57E-05	
$C_{L,11}$ dif. (mg/L)	0.0000	0.0000	0.0000	0.0000	0.0000		
$C_{L,1}$ (mg/L)	2.26E-02	2.10E-02	2.09E-02	2.09E-02	2.09E-02	1.48E-06	
$C_{L,2}$ (mg/L)	4.50E-02	4.18E-02	4.17E-02	4.17E-02	4.17E-02	2.94E-06	
$C_{L,3}$ (mg/L)	6.73E-02	6.24E-02	6.22E-02	6.22E-02	6.22E-02	4.40E-06	
$C_{L,4}$ (mg/L)	8.94E-02	8.28E-02	8.26E-02	8.26E-02	8.26E-02	5.84E-06	
$C_{L,5}$ (mg/L)	1.11E-01	1.03E-01	1.03E-01	1.03E-01	1.03E-01	7.28E-06	
$C_{L,6}$ (mg/L)	1.33E-01	1.23E-01	1.23E-01	1.23E-01	1.23E-01	8.70E-06	
$C_{L,7}$ (mg/L)	1.55E-01	1.43E-01	1.43E-01	1.43E-01	1.43E-01	1.01E-05	
$C_{L,8}$ (mg/L)	1.76E-01	1.63E-01	1.63E-01	1.63E-01	1.63E-01	1.15E-05	
$C_{L,9}$ (mg/L)	1.98E-01	1.82E-01	1.82E-01	1.82E-01	1.82E-01	1.29E-05	
$C_{L,10}$ (mg/L)	2.19E-01	2.02E-01	2.02E-01	2.02E-01	2.02E-01	1.43E-05	
y_6	0.0046	0.0049	0.0049	0.0049	0.0049	**9.52E-05**	**Sum**
$C_{L,6}^*$ (mg/L)	2.41E+00	2.55E+00	2.55E+00	2.55E+00	2.55E+00		
$y_{exit} = y_{11}$	0.0019	0.0024	0.0024	0.0024	0.0024		
$C_{G,11}$ eqn$_2$ (mg/L)					6.8		
$Q_{G,exit}=Q_{G,11}$ (L/min)					0.27		
OTE_{inj} (%)					70.1		

Run # 201

Experimental values:	from injector
Measured exit concentration in liquid phase, $C_{L,measured\ exit}$ (mg/L)	0.3
Air temperature (^{0}C)	23.0
Water temperature (^{0}C)	2.0
Actual atm. Pressure (mmHg)	707.4
System Exit pressure, P_{exit} (psi)	3.6
Inlet concentration in liquid phase, $C_{L,0}$ (mg/L)	0.2
Inlet pressure, P_0 (kPa)	134.6
Liquid flow rate, Q_L (L/min)	19.5
Exit pressure, P_{exit} (kPa)	125.3
Inlet temperature, T_0 (K)	275.2
Exit temperature, T_{exit} (K)	275.2
Constants	
Reaction rate constant, k_w (min^{-1})	0.031
Number of cells, N_{CFSTR}	1
Total volume, V (L)	1.11E-01
Cell volume, V_{CFSTR} (L)	1.11E-01
Universal gas law constant, R (kPa-L /K-mol)	8.31E+00
Henry's law constant, H (kPa-L/mg)	0.22
Calculations (from gas and liquid mass balances)	
$Q_{G,exit} * C_{G,exit}$ (mg/min)	1.2
$Q_{G,exit} * y_{exit}$ (L/min)	0.0004
$Q_{G,exit}$ (L/min)	0.29
y_{exit}	0.0015
$C_{G,exit}$ (mg/L)	4.1
$k_L a_{fm/oj}$ (min^{-1})	1.6
$OTE_{fm/oj}$ (%)	35.7
$OTE_{sys,gas}$ (%)	80.8
Unused applied gaseous ozone mass rate (mg/min)	1.2
Unused applied gaseous ozone dose (mg/L $_{liq}$)	0.1
Applied ozone dose (mg/L $_{liq}$)	0.3
Residual ozone dose (mg/L $_{liq}$)	0.3
Unused applied ozone dose = Applied - Residual (mg/L $_{liq}$)	0.0
$OTE_{sys,liq}$ (%)	86.8
G/L ratio	0.02
$k_L a_{in}/k_L a_{fm}$	48.8
Check	
FM/OJ reactor inlet gas flow rate, $Q_{inert\ gases,0} * C_{inert\ gases,0}$ (mg/min)	760.2
FM/OJ reactor exit gas flow rate, $Q_{inert\ gases,exit} * C_{inert\ gases,exit}$ (mg/min)	760.2

The difference between the two unused applied ozone values is due to ozone auto-decomposition

Injector	**Sum of $k_w C_{L,i} V_{CFSTR}/Q_L$**	4.9E-06 mg/L
FM/OJ	**$k_w C_{L,exit} V_{CFSTR}/Q_L$**	4.8E-05 mg/L
Injector and FM/OJ reactor		0.000 mg/L

APPENDIX F – Summary of Mass Transfer Experiments

Table A-12 Summary of results from mass transfer experiments with flash mix system.

							CFSTR Modeling Data		
Run #	Gas inlet pressure (psi)	$Q_{G,0,inj}$ (L/min)	$C_{G,0,inj}$ (mg/L)	Q_L (gal/min)	Q_L (L/min)	G/L	$Q_{G,exit,sys}$ (L/min)	$C_{G,exit,sys}$ (mg/L)	Unused Applied Ozone Gaseous Mass Rate (mg/min)
33	-1.7	0.50	86.7	6.7	25.3	0.020	0.30	11.8	3.5
34	-9.5	0.69	47.9	10.2	38.8	0.018	0.18	49.7	8.9
35	-10.7	0.50	118.1	10.2	38.8	0.013	0.10	155.9	16.0
36	-6.8	1.39	13.3	10.0	37.8	0.037	0.57	4.3	2.5
40	-3.1	3.38	87.1	9.7	36.9	0.092	2.04	47.5	96.8
43	0.0	1.39	47.8	6.7	25.3	0.055	0.97	13.6	13.2
44	2.3	3.77	13.8	6.5	24.5	0.154	3.07	4.5	13.9
45	3.3	5.00	14.0	6.5	24.5	0.204	4.33	4.8	20.6
46	1.3	2.57	50.3	6.7	25.3	0.102	1.97	18.2	36.0
47	2.1	3.18	14.0	6.5	24.5	0.130	2.56	3.9	9.9
48	-1.2	0.91	48.5	6.7	25.3	0.036	0.58	14.1	8.2
49	0.0	1.13	88.3	6.7	25.3	0.045	0.79	15.5	12.2
50	2.8	1.50	118.8	5.1	19.5	0.077	1.26	31.6	39.6
54	3.3	2.06	48.9	5.1	19.5	0.106	1.78	10.4	18.6
57	6.8	2.16	49.5	4.9	18.5	0.117	1.87	8.1	15.2
60	2.3	0.96	47.1	6.7	25.3	0.038	0.70	4.2	3.0
61	3.0	1.52	87.3	6.7	25.3	0.060	1.15	12.1	13.8
62	3.8	2.07	13.9	6.7	25.3	0.082	1.69	1.6	2.7
63	4.8	3.88	48.0	6.7	25.3	0.153	3.28	12.6	41.2
69	-2.6	0.87	85.1	8.7	33.0	0.026	0.43	13.8	6.0
70	-1.4	1.40	48.5	8.7	33.0	0.042	0.79	6.0	4.7
71	-3.6	0.57	13.6	8.7	33.0	0.017	0.27	5.6	1.5
72	-1.2	1.62	14.1	8.7	33.0	0.049	0.95	1.6	1.5
73	-5.3	1.00	13.9	9.7	36.9	0.027	0.43	5.0	2.1
74	-4.6	1.20	83.6	9.7	36.9	0.033	0.54	14.5	7.8
75	7.3	1.74	14.0	9.7	36.9	0.047	1.79	3.7	6.7
76	-5.1	1.26	13.3	9.7	36.9	0.034	0.53	3.8	2.0
77	-2.6	2.37	86.7	9.7	36.9	0.064	1.31	38.6	50.5
78	-0.9	3.55	14.2	9.7	36.9	0.096	2.32	3.4	7.8
79	0.0	4.74	49.8	9.7	36.9	0.129	3.25	25.4	82.4
80	1.3	5.94	47.9	9.7	36.9	0.161	4.47	16.5	73.9
81	3.0	7.25	117.6	9.7	36.9	0.197	6.00	56.4	338.0
82	2.8	6.65	117.7	9.7	36.9	0.180	5.13	56.0	286.9
83	-0.9	1.61	14.4	10.0	37.8	0.043	0.88	1.9	1.7
84	-1.7	1.40	87.7	10.0	37.8	0.037	0.68	15.2	10.3
85	-2.6	1.07	48.5	10.0	37.8	0.028	0.47	8.4	4.0
86	-1.8	1.35	87.0	10.0	37.8	0.036	0.64	15.4	9.9
87	0.5	2.51	48.1	10.0	37.8	0.066	1.59	4.9	7.7
88	1.3	3.12	86.6	10.0	37.8	0.082	2.06	25.4	52.3
89	1.8	3.70	117.3	9.7	36.9	0.100	2.26	65.1	147.2
90	4.3	5.02	118.5	9.7	36.9	0.136	3.62	36.4	131.8
91	3.3	4.37	117.7	9.7	36.9	0.119	2.93	46.8	136.9
92	5.3	2.70	115.7	7.7	29.1	0.093	1.85	23.7	43.8
95	4.3	1.32	48.1	7.7	29.1	0.045	0.88	4.8	4.2
96	4.8	1.55	47.1	7.7	29.1	0.053	1.06	4.6	4.9
103	3.5	1.53	86.6	9.7	36.9	0.041	0.90	10.6	9.5
105	5.3	2.10	117.7	9.2	34.9	0.060	1.28	22.4	28.7
110	0.0	0.72	13.5	10.0	37.8	0.019	0.34	2.2	0.8
119	-2.2	0.30	13.7	8.7	33.0	0.009	0.13	2.1	0.3
123	0.7	0.94	13.9	8.7	33.0	0.029	0.53	1.9	1.0
125	2.0	1.39	86.7	8.7	33.0	0.042	0.87	10.4	9.1
126	2.8	1.61	48.0	8.7	33.0	0.049	1.02	5.4	5.5
128	-4.3	1.12	48.2	8.5	32.2	0.035	0.56	17.4	9.8
130	-3.6	1.54	50.0	8.7	33.0	0.047	0.86	13.4	11.5
131	-5.8	0.82	14.7	8.7	33.0	0.025	0.37	8.4	3.1
132	-6.8	0.62	14.7	8.7	33.0	0.019	0.24	10.2	2.5
133	-7.5	0.34	118.4	8.7	33.0	0.010	0.12	69.2	8.0
135	-8.0	0.90	48.4	10.0	37.8	0.024	0.30	33.6	10.2
136	-8.5	1.04	85.0	10.0	37.8	0.027	0.32	84.8	27.0
143	2.3	1.49	84.9	9.7	36.9	0.040	0.80	11.4	9.1

Run #	OTE_{inj} (%)	OTE_{tm} (%)	$\frac{OTE_{inj}}{OTE_{tm}}$	$OTE_{sys,liq}$ (%)	$OTE_{sys,gas}$ (%)	k_La_{inj} (min^{-1})	k_La_{tm} (min^{-1})	k_La_{tm} (s^{-1})	$\frac{k_La_{inj}}{k_La_{tm}}$
33	70.4	72.5	1.0	97.4	91.9	75.0	11.2	0.19	6.7
34	64.1	24.2	2.6	77.5	72.8	34.2	0.7	0.01	48.1
35	55.4	39.3	1.4	74.5	72.9	16.6	0.8	0.01	20.3
36	67.0	59.2	1.1	92.3	86.5	116.5	11.3	0.19	10.3
40	64.0	8.8	7.2	71.5	67.2	409.1	2.7	0.05	149.3
43	60.1	50.3	1.2	84.9	80.2	193.4	14.4	0.24	13.4
44	50.9	45.6	1.1	76.8	73.3	560.9	49.2	0.82	11.4
45	43.3	48.1	0.9	73.4	70.6	638.3	87.7	1.46	7.3
46	58.4	33.1	1.8	76.3	72.2	407.6	15.1	0.25	26.9
47	49.9	55.3	0.9	81.3	77.6	422.6	62.5	1.04	6.8
48	67.4	43.1	1.6	86.9	81.4	137.2	6.0	0.10	22.9
49	79.2	41.5	1.9	93.8	87.8	255.3	8.9	0.15	28.6
50	49.7	55.9	0.9	81.1	77.8	183.6	25.4	0.42	7.2
54	49.3	63.5	0.8	85.0	81.5	276.3	65.4	1.09	4.2
57	66.2	57.9	1.1	89.7	85.8	592.4	86.7	1.45	6.8
60	82.3	63.0	1.3	100.0	93.4	242.1	25.3	0.42	9.6
61	74.7	58.8	1.3	95.0	89.6	348.7	34.0	0.57	10.2
62	80.9	51.4	1.6	96.0	90.7	739.6	69.7	1.16	10.6
63	62.4	41.2	1.5	81.2	77.9	1002.1	53.5	0.89	18.7
69	81.7	55.7	1.5	98.5	91.9	142.0	7.9	0.13	17.9
70	86.9	47.0	1.8	100.0	93.0	302.7	13.0	0.22	23.2
71	76.3	18.6	4.1	87.4	80.7	76.4	0.8	0.01	97.8
72	81.0	65.5	1.2	100.0	93.4	315.5	39.2	0.65	8.1
73	74.8	39.3	1.9	91.1	84.7	110.3	3.6	0.06	30.6
74	76.4	67.1	1.1	98.2	92.3	145.7	16.3	0.27	8.9
75	58.5	33.8	1.7	77.4	72.6	255.3	12.9	0.22	19.7
76	74.5	52.3	1.4	94.2	87.8	141.4	8.0	0.13	17.7
77	70.9	15.5	4.6	80.6	75.4	318.3	3.3	0.06	96.3
78	74.1	40.5	1.8	90.0	84.6	669.1	30.5	0.51	22.0
79	55.9	20.8	2.7	69.0	65.1	552.2	12.6	0.21	44.0
80	63.8	28.2	2.3	77.8	74.0	1132.1	33.6	0.56	33.7
81	56.9	8.0	7.1	63.0	60.4	1263.4	8.5	0.14	147.8
82	55.6	17.3	3.2	66.2	63.3	981.8	17.5	0.29	56.1
83	89.6	29.3	3.1	100.0	92.6	338.8	6.5	0.11	52.0
84	83.5	49.4	1.7	98.3	91.6	227.6	10.2	0.17	22.4
85	82.0	57.1	1.4	99.2	92.3	152.2	9.2	0.15	16.6
86	83.9	47.5	1.8	98.3	91.5	218.3	8.8	0.15	24.7
87	85.2	57.1	1.5	100.0	93.6	583.3	75.2	1.25	7.8
88	74.2	25.0	3.0	85.9	80.6	571.4	11.0	0.18	51.8
89	59.8	15.6	3.8	70.1	66.1	446.7	5.8	0.10	76.8
90	64.7	37.2	1.7	81.6	77.8	915.1	40.9	0.68	22.4
91	66.4	20.8	3.2	77.5	73.4	745.8	12.1	0.20	61.5
92	69.2	54.5	1.3	90.5	86.0	541.9	45.7	0.76	11.9
95	84.1	58.6	1.4	100.0	93.4	334.5	27.7	0.46	12.1
96	89.7	35.2	2.6	100.0	93.3	504.5	15.5	0.26	32.5
103	90.3	26.4	3.4	100.0	92.8	372.6	5.9	0.10	62.8
105	77.5	48.6	1.6	94.1	88.4	414.9	21.0	0.35	19.8
110	89.3	27.4	3.3	100.0	92.2	128.6	1.8	0.03	72.7
119	78.1	68.4	1.1	100.0	93.1	40.4	3.7	0.06	10.8
123	90.7	17.9	5.1	100.0	92.4	217.9	1.8	0.03	124.0
125	81.5	59.2	1.4	98.8	92.4	289.4	23.5	0.39	12.3
126	92.3	7.5	12.4	100.0	92.9	484.6	1.8	0.03	274.5
128	71.4	36.6	2.0	87.7	81.9	141.6	4.3	0.07	32.8
130	66.6	55.1	1.2	90.3	85.0	188.9	15.2	0.25	12.4
131	68.0	19.9	3.4	80.2	74.3	84.1	1.1	0.02	73.4
132	60.6	30.1	2.0	77.7	72.5	47.4	1.3	0.02	36.2
133	66.2	40.9	1.6	84.4	80.0	26.9	1.0	0.02	27.1
135	68.7	25.7	2.7	82.1	76.7	65.6	1.3	0.02	49.9
136	59.8	23.8	2.5	73.1	69.4	56.2	1.2	0.02	45.3
143	90.1	26.9	3.3	100.0	92.8	336.0	5.2	0.09	64.9

Run #	Residual Ozone Dose$_{degas}$ (mg/L)	Residual Ozone Dose$_{im}$ (mg/L)	Residual Ozone Dose$_{inj}$ (mg/L)	Wet Test Meter Data: Applied Ozone Dose (mg/L)	Wet Test Total Volume (L)	Time of Wet Test Volume (min)	$Q_{G,exit,sys}$ (L/min)	$C_{G,exit,sys}$ (mg/L)	Unused Applied Ozone Gaseous Mass Rate (mg/min)
33	1.7	1.7	1.3	1.7	4.1	16.8	0.25	3.7	0.9
34	0.6	0.7	0.6	0.8	2.8	9.9	0.29	7.5	2.2
35	1.1	1.1	0.9	1.5	0.7	13.5	0.05	18.5	1.0
36	0.4	0.5	0.4	0.5	4.3	5.2	0.82	4.3	3.5
40	6.0	5.7	5.5	8.0	5.6	3.3	1.71	17.6	30.2
43	2.4	2.2	1.7	2.6	4.4	5.6	0.78	6.6	5.2
44	1.5	1.6	1.2	2.1	10.3	5.7	1.81	3.9	7.0
45	1.9	2.1	1.3	2.9	5.0	2.6	1.89	4.6	8.6
46	4.0	3.9	3.2	5.1	4.4	4.1	1.07	11.0	11.7
47	1.4	1.5	1.0	1.8	7.3	4.9	1.49	3.5	5.2
48	1.5	1.5	1.3	1.7	5.1	9.4	0.54	4.6	2.5
49	3.4	3.7	3.4	4.0	4.7	6.8	0.70	17.6	12.3
50	6.9	7.4	4.9	9.2	4.3	6.8	0.63	19.7	12.4
54	4.0	4.4	2.7	5.2	4.6	4.5	1.02	13.0	13.3
57	4.7	5.2	4.1	5.8	5.8	2.7	2.14	13.3	28.5
60	1.8	1.8	1.6	1.8	4.3	5.3	0.82	13.3	10.9
61	4.9	5.0	4.2	5.2	4.3	3.6	1.17	22.8	26.8
62	1.1	1.1	1.0	1.1	5.5	2.5	2.16	3.5	7.5
63	6.4	6.0	4.8	7.4	6.6	1.8	3.70	13.1	48.4
69	2.1	2.2	2.0	2.2	4.1	7.2	0.57	13.3	7.6
70	2.1	2.1	1.9	2.1	4.3	4.0	1.08	14.8	16.1
71	0.2	0.2	0.2	0.2	4.3	12.3	0.34	2.8	1.0
72	0.7	0.7	0.6	0.7	4.2	3.3	1.30	4.1	5.4
73	0.3	0.3	0.3	0.4	4.1	6.7	0.61	5.3	3.3
74	2.6	2.7	2.2	2.7	4.2	5.7	0.74	16.5	12.2
75	0.5	0.5	0.4	0.7	4.2	4.7	0.89	1.2	1.1
76	0.4	0.4	0.4	0.5	4.9	6.5	0.75	4.7	3.5
77	4.6	4.5	4.2	5.6	4.6	2.9	1.56	25.3	39.6
78	1.2	1.2	1.1	1.4	8.7	3.2	2.73	2.1	5.6
79	4.5	4.4	3.8	6.4	4.5	1.2	3.75	10.7	40.2
80	5.5	6.0	5.2	7.7	4.5	0.9	5.18	11.1	57.3
81	16.3	14.6	13.8	23.1	5.3	0.9	5.70	34.6	197.2
82	13.8	14.0	12.4	21.2	6.1	1.2	5.09	35.1	178.5
83	0.6	0.6	0.6	0.6	4.3	3.4	1.25	5.7	7.1
84	3.0	3.2	2.9	3.2	4.1	4.7	0.86	26.0	22.4
85	1.3	1.4	1.2	1.4	4.8	7.4	0.65	6.5	4.2
86	2.9	3.0	2.8	3.1	4.5	5.3	0.85	15.5	13.2
87	3.2	3.2	2.9	3.2	5.9	2.7	2.16	5.8	12.5
88	6.7	6.1	5.7	7.1	6.6	3.2	2.08	22.5	46.7
89	8.6	8.3	7.5	11.8	4.3	1.8	2.43	11.8	28.8
90	12.8	13.2	11.1	16.1	4.9	1.1	4.36	32.1	140.1
91	10.8	10.8	9.8	14.0	4.9	1.3	3.82	24.2	92.6
92	9.2	9.7	7.9	10.7	4.1	1.7	2.42	26.7	64.6
95	2.2	2.2	2.0	2.2	4.2	3.6	1.16	4.8	5.5
96	2.5	2.5	2.4	2.5	5.3	3.6	1.48	5.6	8.3
103	3.6	3.6	3.5	3.6	4.6	3.9	1.18	21.1	25.0
105	6.8	6.7	5.9	7.1	4.0	2.9	1.40	11.7	16.5
110	0.3	0.3	0.2	0.3	4.0	10.7	0.37	6.1	2.3
119	0.1	0.1	0.1	0.1	0.0		0.00	0.0	0.0
123	0.4	0.4	0.4	0.4	5.5	7.7	0.71	2.7	1.9
125	3.6	3.6	3.2	3.6	4.9	5.0	0.99	9.9	9.8
126	2.3	2.3	2.3	2.3	5.8	4.3	1.36	4.5	6.2
128	1.5	1.5	1.3	1.7	4.2	7.7	0.54	3.1	1.7
130	2.0	2.1	1.7	2.3	4.4	8.3	0.53	6.0	3.2
131	0.3	0.3	0.3	0.4	4.0	12.2	0.33	0.7	0.2
132	0.2	0.2	0.2	0.3	3.1	12.1	0.26	0.7	0.2
133	1.0	1.0	0.9	1.2	1.7	17.5	0.10	15.3	1.5
135	0.9	1.0	0.9	1.2	4.1	9.4	0.44	13.7	6.0
136	1.7	1.7	1.5	2.3	3.9	8.1	0.49	4.1	2.0
143	3.4	3.4	3.3	3.4	4.3	5.7	0.76	31.5	23.9

Table A-13 Summary of results from mass transfer experiments with opposing jets system.

Run #	Gas inlet pressure (psi)	$Q_{G,0,Inj}$ (L/min)	$C_{G,0,Inj}$ (mg/L)	Q_L (gal/min)	Q_L (L/min)	G/L	CFSTR Modeling Data: $Q_{G,exit,sys}$ (L/min)	CFSTR Modeling Data: $C_{G,exit,sys}$ (mg/L)	CFSTR Modeling Data: Unused Applied Ozone Gaseous Mass Rate (mg/min)
201	0.0	0.42	14.7	5.1	19.5	0.021	0.29	4.1	1.2
202	0.5	0.63	49.0	5.1	19.5	0.032	0.44	10.0	4.4
204	0.0	0.21	86.4	5.1	19.5	0.011	0.14	9.5	1.3
205	0.0	0.31	86.7	5.1	19.5	0.016	0.21	8.9	1.8
206	1.3	1.26	86.4	5.1	19.5	0.065	0.93	26.9	24.9
207	1.5	1.48	49.9	5.1	19.5	0.076	1.13	15.4	17.4
209	1.8	2.02	13.9	5.1	19.5	0.104	1.64	4.4	7.3
210	2.8	3.75	110.4	5.1	19.5	0.192	2.95	42.1	123.9
215	2.0	5.98	109.8	6.7	25.3	0.237	4.50	53.6	241.0
216	1.3	4.84	12.0	6.7	25.3	0.192	3.68	3.2	11.7
217	0.0	3.62	12.5	6.7	25.3	0.143	2.52	2.9	7.3
218	0.0	3.05	48.6	6.7	25.3	0.121	2.13	16.0	34.1
219	0.0	2.52	86.8	6.7	25.3	0.100	1.69	16.8	28.5
221	-1.7	1.41	13.6	6.7	25.3	0.056	0.86	3.9	3.3
223	-3.1	0.87	87.0	6.7	25.3	0.034	0.45	11.9	5.4
225	-4.8	0.28	85.4	6.7	25.3	0.011	0.12	13.3	1.7
232	-7.5	1.35	13.9	8.7	33.0	0.041	0.41	7.5	3.1
234	-5.8	2.18	12.9	8.7	33.0	0.066	0.89	7.9	7.0
236	-2.6	4.44	85.5	8.7	33.0	0.135	2.40	31.6	75.7
237	-3.1	5.40	110.2	8.7	33.0	0.164	2.81	23.2	65.1
238	-1.2	6.74	85.9	8.7	33.0	0.204	4.13	37.6	155.3
240	-3.1	6.99	47.8	9.7	36.9	0.190	3.78	20.0	75.5
241	-4.6	5.20	110.2	9.7	36.9	0.141	2.40	90.2	216.2
242	-7.0	3.00	48.6	9.7	36.9	0.081	1.02	46.2	47.1
245	-10.0	1.19	13.7	9.7	36.9	0.032	0.23	22.7	5.2
251	3.5	0.44	13.3	4.9	18.5	0.024	0.33	1.3	0.4
253	4.7	0.99	84.9	4.9	18.5	0.054	0.77	24.4	18.8
255	4.8	1.77	112.3	4.9	18.5	0.096	1.41	45.2	63.7
258	5.1	2.10	49.0	4.9	18.5	0.114	1.73	17.9	30.9
262	2.8	3.75	111.2	6.7	25.3	0.148	2.58	51.6	133.2
263	1.3	2.00	13.2	6.7	25.3	0.079	1.31	2.1	2.8
264	1.8	2.55	110.1	6.7	25.3	0.101	1.63	32.8	53.5
265	0.5	1.46	48.6	6.7	25.3	0.058	0.91	10.0	9.1
266	0.5	0.93	48.4	6.7	25.3	0.037	0.56	8.8	4.9
267	0.0	0.72	85.1	6.7	25.3	0.028	0.41	21.7	8.9
268	0.0	0.52	13.3	6.7	25.3	0.021	0.31	2.8	0.9
271	-8.0	0.50	86.5	8.7	33.0	0.015	0.12	113.7	14.2
275	-5.1	1.48	13.4	8.7	33.0	0.045	0.57	6.7	3.8
276	-6.3	1.20	49.9	8.7	33.0	0.036	0.39	46.3	18.1
277	-1.9	3.46	86.1	8.7	33.0	0.105	1.76	34.2	60.1
278	0.0	4.75	12.0	8.7	33.0	0.144	2.82	4.6	12.8
279	0.0	5.84	49.6	8.7	33.0	0.177	3.43	18.9	64.6
280	0.0	6.31	110.8	8.7	33.0	0.191	3.62	73.7	266.1
282	-0.9	6.86	11.3	9.7	36.9	0.186	3.93	4.2	16.4
285	-3.1	4.40	86.6	9.7	36.9	0.119	2.02	43.7	88.1
287	-6.5	2.14	13.1	9.7	36.9	0.058	0.68	11.8	8.1
289	-8.0	1.24	50.1	9.7	36.9	0.034	0.31	40.7	12.8
297	2.3	0.86	49.6	7.2	27.2	0.032	0.50	5.8	2.9
299	4.0	1.55	13.5	7.2	27.2	0.057	1.01	1.3	1.3
300	4.3	2.08	85.6	7.2	27.2	0.076	1.33	11.7	15.6
301	6.3	3.97	48.9	7.2	27.2	0.146	2.77	10.9	30.2
306	3.3	2.63	85.8	7.7	29.1	0.090	1.61	10.0	6.9
309	1.8	1.27	85.7	7.7	29.1	0.044	0.69	2.7	0.9
311	0.0	0.62	13.3	7.7	29.1	0.021	0.32	14.7	2.7
312	-1.2	0.40	85.6	7.7	29.1	0.014	0.18	9.3	1.2
313	-2.4	0.30	49.0	7.7	29.1	0.010	0.13	3.0	0.1
315	-2.6	0.10	13.7	7.7	29.1	0.003	0.04	4.4	0.3
317	-6.8	0.26	14.3	8.7	33.0	0.008	0.07	4.3	0.8
320	-4.8	0.56	14.3	8.7	33.0	0.017	0.19	3.3	1.4
322	-3.1	1.07	13.8	8.7	33.0	0.032	0.42	15.8	9.6
324	-3.1	1.45	47.9	8.7	33.0	0.044	0.60	11.8	15.1
326	0.5	2.53	49.8	8.7	33.0	0.077	1.29	32.5	67.1
327	2.0	3.72	86.2	8.7	33.0	0.113	2.07	49.5	140.3
328	2.3	4.88	109.3	8.7	33.0	0.148	2.84	37.3	147.1
329	4.3	6.21	86.2	8.7	33.0	0.188	3.95	49.5	116.0
331	0.0	4.69	111.6	10.0	37.8	0.124	2.35	17.0	31.3
332	-1.2	4.07	48.4	10.0	37.8	0.108	1.85	4.9	3.8

							CFSTR Modeling Data		
Run #	Gas inlet pressure (psi)	$Q_{G,0,inj}$ (L/min)	$C_{G,0,inj}$ (mg/L)	Q_L (gal/min)	Q_L (L/min)	G/L	$Q_{G,exit,sys}$ (L/min)	$C_{G,exit,sys}$ (mg/L)	Unused Applied Ozone Gaseous Mass Rate (mg/min)
335	-4.6	2.27	12.5	10.0	37.8	0.060	0.77	25.6	79.1
337	0.8	5.87	110.1	10.0	37.8	0.155	3.09	42.4	160.5
338	1.3	7.05	110.7	9.7	36.9	0.191	3.80	5.2	2.4
339	-5.3	1.46	13.1	10.0	37.8	0.039	0.46	74.7	10.4
342	-8.5	0.73	49.1	10.0	37.8	0.019	0.14	26.9	4.7
345	-5.1	0.64	48.5	10.0	37.8	0.017	0.17	20.9	9.0
347	-2.6	1.26	85.1	10.0	37.8	0.033	0.43	13.3	9.8
350	-1.4	1.89	48.8	10.0	37.8	0.050	0.74	33.1	35.1
351	0.0	2.49	85.8	10.0	37.8	0.066	1.06	2.2	4.2
352	2.3	3.77	11.4	9.7	36.9	0.102	1.93	28.2	80.1
355	7.6	4.01	85.3	8.0	30.1	0.133	2.63	10.1	8.7
356	5.1	1.50	85.1	8.0	30.1	0.050	0.86	1.7	1.2
362	9.3	2.22	49.1	6.7	25.3	0.088	1.58	9.2	4.1
432	-7.5	1.36	14.0	8.7	33.0	0.041	0.44	55.2	173.1
437	-2.2	5.55	109.1	8.7	33.0	0.168	3.14	11.2	31.3
501	5.8	3.95	49.3	7.2	27.2	0.145	2.80	6.7	0.6
565	10.4	2.89	49.7	6.7	25.3	0.114	2.16	8.8	19.0

Run #	OTE_{aq} (%)	OTE_{sg} (%)	$\frac{OTE_{aq}}{OTE_{sg}}$	$OTE_{sg,abs}$ (%)	$OTE_{sg,open}$ (%)	k_La_{aq} (min^{-1})	k_La_{sg} (min^{-1})	k_La_{sg} (s^{-1})	$\frac{k_La_{aq}}{k_La_{sg}}$
201	70.1	35.7	2.0	86.8	80.8	75.8	1.6	0.03	48.8
202	70.6	50.7	1.4	91.2	85.5	120.8	4.8	0.08	25.2
204	86.9	43.8	2.0	100.0	92.6	53.0	1.1	0.02	49.0
205	81.8	62.4	1.3	99.9	93.1	71.0	3.7	0.06	19.5
206	61.5	40.5	1.5	81.5	77.1	212.3	6.8	0.11	31.1
207	59.6	41.8	1.4	80.8	76.5	250.5	9.1	0.15	27.5
209	51.0	46.7	1.1	77.7	73.9	289.9	17.4	0.29	16.7
210	43.9	40.6	0.9	72.5	70.1	480.3	36.4	0.61	13.2
215	46.0	32.0	1.4	65.1	63.3	894.5	27.9	0.46	32.1
216	51.1	58.7	0.9	82.9	79.8	931.0	116.8	1.95	7.3
217	52.4	66.0	0.8	87.5	83.8	531.7	95.5	1.59	5.6
218	53.9	50.1	1.1	80.7	77.0	438.1	27.4	0.46	16.0
219	59.5	67.9	0.9	90.8	87.0	408.3	60.6	1.01	6.7
221	67.0	47.5	1.4	88.1	82.7	236.5	8.5	0.14	28.0
223	67.7	78.0	0.9	98.0	92.9	125.0	19.1	0.32	6.5
225	77.4	69.1	1.1	99.2	93.0	43.2	2.7	0.04	16.0
232	64.9	52.7	1.2	88.9	83.4	117.7	4.5	0.07	26.4
234	57.3	41.9	1.4	79.9	75.2	201.6	6.3	0.11	32.0
236	58.7	51.8	1.1	83.6	80.1	620.3	33.3	0.55	18.6
237	57.5	74.3	0.8	91.9	89.1	748.2	25.5	0.42	29.4
238	55.3	40.0	1.4	75.7	73.2	1138.2	38.2	0.64	29.8
240	59.1	44.7	1.3	80.6	77.4	1135.0	43.3	0.72	26.2
241	55.2	15.8	3.5	65.2	62.3	541.6	4.6	0.08	118.2
242	58.5	22.2	2.6	71.9	67.7	245.8	2.8	0.05	88.3
245	60.1	19.2	3.1	72.8	67.8	59.6	0.5	0.01	118.7
251	83.5	57.3	1.5	100.0	93.0	119.5	5.3	0.09	22.4
253	66.6	33.3	2.0	82.7	77.8	195.3	4.1	0.07	47.8
255	65.9	6.1	10.8	72.0	68.0	408.1	1.0	0.02	412.5
258	57.8	29.1	2.0	73.9	70.0	403.2	8.3	0.14	48.7
262	53.5	31.2	1.7	71.0	68.0	571.1	13.7	0.23	41.8
263	80.1	46.9	1.7	95.0	89.4	606.6	19.4	0.32	31.3
264	61.1	51.0	1.2	84.8	81.0	421.9	21.5	0.36	19.6
265	66.2	62.0	1.1	92.3	87.2	241.8	18.1	0.30	13.3
266	74.0	58.0	1.3	95.0	89.1	178.4	8.7	0.15	20.5
267	82.2	18.5	4.4	92.1	85.5	157.0	0.9	0.02	168.5
268	80.2	34.6	2.3	93.9	87.0	109.3	1.6	0.03	66.5
271	64.6	6.6	9.8	71.4	66.9	35.8	0.1	0.00	445.6
275	63.1	48.3	1.3	86.2	80.9	149.7	5.2	0.09	28.9
276	64.7	14.1	4.6	74.7	69.6	109.5	0.6	0.01	184.1
277	61.7	47.3	1.3	83.9	79.8	476.3	18.2	0.30	26.1
278	61.5	41.6	1.5	81.7	77.5	853.7	26.3	0.44	32.4
279	56.3	48.9	1.2	81.0	77.7	927.8	47.3	0.79	19.6
280	58.8	7.7	7.6	64.5	61.9	1113.6	3.3	0.06	334.4
282	60.6	46.4	1.3	82.5	78.9	1321.8	52.6	0.88	25.1
285	62.0	39.2	1.6	80.8	76.9	567.8	14.5	0.24	39.2
287	58.8	30.1	2.0	76.1	71.1	166.4	2.8	0.05	59.7
289	65.7	40.3	1.6	84.5	79.5	93.0	2.0	0.03	47.1
297	83.2	59.6	1.4	100.0	93.2	199.9	9.1	0.15	22.0
299	80.9	67.7	1.2	100.0	93.8	420.4	48.1	0.80	8.7
300	78.7	58.9	1.3	96.5	91.2	571.8	37.2	0.62	15.4
301	67.8	51.8	1.3	87.9	84.5	1227.1	63.1	1.05	19.4
306	81.5	65.9	1.2	100.0	93.7	281.4	19.2	0.32	14.6
309	80.5	46.8	1.7	100.0	89.6	116.7	2.8	0.05	42.2
311	90.5	18.5	4.9	96.6	92.3	86.6	0.4	0.01	213.4
312	87.1	37.1	2.3	100.0	91.9	54.6	0.7	0.01	76.2
313	87.8	27.7	3.2	99.4	91.2	18.0	0.1	0.00	126.2
315	88.9	28.5	3.1	99.1	92.1	33.9	0.2	0.00	136.8
317	76.6	57.2	1.3	100.0	90.0	68.4	2.4	0.04	28.7
320	80.2	52.1	1.5	96.7	90.5	168.3	4.7	0.08	35.6
322	71.1	52.3	1.4	97.3	86.2	186.1	6.8	0.11	27.3
324	73.7	54.3	1.4	91.9	88.0	477.8	19.8	0.33	24.2
326	74.2	19.1	3.9	93.4	79.1	904.9	5.9	0.10	154.5
327	71.0	9.1	7.8	83.6	73.7	1289.7	3.4	0.06	376.7
328	64.4	22.6	2.8	77.1	72.5	1810.5	15.5	0.26	116.5
329	66.5	33.8	2.0	75.0	77.8	775.6	14.0	0.23	55.6
331	70.9	45.4	1.6	81.8	84.1	685.9	19.1	0.32	36.0
332	70.0	55.6	1.3	89.0	86.7	255.7	10.2	0.17	25.1

Run #	OTE_{aq} (%)	OTE_{aq} (%)	$\frac{OTE_{aq}}{OTE_{aq}}$	$OTE_{aq,aq}$ (%)	$OTE_{aq,gas}$ (%)	k_La_{aq} (min^{-1})	k_La_{aq} (min^{-1})	k_La_{aq} (s^{-1})	$\frac{k_La_{aq}}{k_La_{aq}}$
335	64.1	66.0	1.0	92.5	87.8	1039.3	13.8	0.23	75.5
337	57.7	51.3	1.1	91.2	79.4	1118.5	61.2	1.02	18.3
338	74.5	51.8	1.4	82.2	87.7	164.4	4.8	0.08	33.9
339	65.7	14.6	4.5	94.1	70.7	42.8	0.2	0.00	196.8
342	80.1	24.4	3.3	75.8	84.9	72.1	0.5	0.01	138.1
345	86.6	37.3	2.3	91.7	91.6	208.2	2.7	0.04	78.2
347	78.5	50.9	1.5	98.7	89.4	295.7	8.3	0.14	35.5
350	80.2	17.1	4.7	95.7	83.6	459.7	2.3	0.04	198.4
351	75.4	60.8	1.2	89.5	90.4	839.9	56.0	0.93	15.0
352	70.7	50.7	1.4	95.6	85.6	1243.4	51.7	0.86	24.1
355	92.0	14.7	6.3	98.3	93.1	491.8	2.3	0.04	214.2
356	87.2	45.4	1.9	100.0	93.0	336.3	8.2	0.14	41.1
362	61.7	44.2	1.4	100.0	78.7	114.7	3.3	0.06	34.4
432	57.2	33.2	1.7	83.8	71.4	826.4	18.7	0.31	44.3
437	66.4	52.1	1.3	74.2	83.9	1134.5	62.1	1.03	18.3
501	73.0	42.2	1.7	87.4	84.4	30.0	0.6	0.01	50.0
565	74.9	47.2	1.6	97.8	86.8	1518.3	47.1	0.78	32.3

Run #	Residual Ozone Dose$_{design}$ (mg/L)	Residual Ozone Dose$_{inj}$ (mg/L)	Residual Ozone Dose$_{inj}$ (mg/L)	Applied Ozone Dose (mg/L)	Wet Test Meter Data: Wet Test Total Volume (L)	Wet Test Meter Data: Time of Wet Test Volume (min)	Wet Test Meter Data: $Q_{G,exit,wet}$ (L/min)	Wet Test Meter Data: $C_{G,exit,wet}$ (mg/L)	Unused Applied Ozone Gaseous Mass Rate (mg/min)
201	0.3	0.3	0.2	0.3	2.0	12.9	0.16	1.4	0.2
202	1.4	1.4	1.2	1.6	1.4	8.0	0.18	10.7	1.9
204	0.9	0.9	0.9	0.9	1.6	14.8	0.11	2.4	0.3
205	1.4	1.4	1.2	1.4	1.1	12.7	0.08	4.1	0.3
206	4.6	4.6	3.7	5.6	4.2	9.6	0.44	20.9	9.2
207	3.1	3.1	2.4	3.8	4.3	8.7	0.50	17.1	8.6
209	1.1	1.1	0.8	1.4	4.5	7.0	0.64	4.0	2.6
210	12.4	15.3	9.8	21.2	4.3	4.1	1.05	14.4	15.2
215	14.3	16.9	12.4	26.0	5.0	2.9	1.76	26.9	47.4
216	1.7	1.9	1.2	2.3	5.2	2.3	2.33	3.8	8.9
217	1.3	1.6	1.0	1.8	4.8	2.5	1.96	3.2	6.3
218	4.0	4.7	3.4	5.9	4.8	2.8	1.72	13.3	22.8
219	6.4	7.9	5.5	8.7	6.3	7.5	0.84	9.4	7.9
221	0.7	0.7	0.5	0.8	4.6	8.7	0.52	2.7	1.4
223	2.3	2.9	2.2	3.0	4.5	9.5	0.47	8.6	4.1
225	0.8	0.9	0.8	0.9	0.3	15.6	0.02	218.5	4.8
232	0.4	0.5	0.4	0.6	5.8	6.9	0.85	2.9	2.5
234	0.6	0.7	0.5	0.9	4.1	3.5	1.19	0.8	0.9
236	7.7	9.6	7.2	11.5	3.5	2.0	1.74	21.9	38.1
237	10.9	16.6	10.9	18.0	4.9	3.9	1.25	29.9	37.3
238	10.9	13.3	10.1	17.5	4.6	2.1	2.17	17.4	37.7
240	6.0	7.3	5.6	9.1	5.4	2.0	2.72	14.3	39.0
241	10.4	10.1	9.0	15.5	4.8	3.5	1.38	25.8	35.5
242	2.6	2.8	2.5	4.0	5.2	4.3	1.23	7.0	8.6
245	0.3	0.3	0.3	0.4	5.6	10.9	0.51	0.8	0.4
251	0.3	0.3	0.3	0.3	4.2	11.6	0.37	5.4	2.0
253	3.8	3.8	3.3	4.6	5.2	5.9	0.88	22.6	19.9
255	7.7	7.7	7.5	10.7	5.3	3.3	1.62	18.0	29.0
258	4.1	4.1	3.4	5.6	5.8	3.1	1.90	12.8	24.4
262	11.7	11.7	9.3	16.5	4.6	1.5	3.14	33.5	105.2
263	0.9	1.0	0.9	1.0	5.3	3.1	1.74	2.3	4.1
264	8.2	9.4	7.2	11.1	4.4	2.3	1.95	26.3	51.4
265	2.3	2.6	2.0	2.8	4.2	3.6	1.17	6.8	8.0
266	1.7	1.7	1.4	1.8	4.4	6.8	0.65	6.6	4.3
267	2.2	2.2	2.1	2.4	4.5	10.3	0.44	15.1	6.6
268	0.3	0.3	0.2	0.3	4.2	12.4	0.34	2.1	0.7
271	0.9	0.9	0.9	1.3	1.6	10.1	0.16	1.3	0.2
275	0.5	0.5	0.4	0.6	4.2	4.3	1.00	1.1	1.1
276	1.3	1.4	1.3	1.8	4.8	7.3	0.66	7.9	5.2
277	6.7	7.6	5.9	9.0	7.1	2.7	2.60	8.1	21.1
278	1.4	1.4	1.1	1.7	7.5	2.0	3.68	3.2	11.7
279	6.5	7.1	5.2	8.8	4.5	0.9	4.80	14.4	69.0
280	13.8	13.7	13.0	21.2	4.5	0.9	5.13	33.1	169.7
282	1.6	1.7	1.4	2.1	6.8	1.2	5.48	3.2	17.6
285	7.8	8.4	6.8	10.4	5.4	1.7	3.29	16.4	53.8
287	0.5	0.6	0.5	0.8	4.5	3.7	1.21	2.2	2.6
289	1.2	1.4	1.2	1.7	5.0	7.0	0.71	5.0	3.6
297	1.6	1.6	1.4	1.6	4.3	7.1	0.61	6.9	4.2
299	0.8	0.8	0.7	0.8	4.8	3.4	1.41	2.0	2.8
300	5.8	6.3	5.5	6.5	5.2	2.9	1.82	17.6	31.9
301	6.2	6.3	5.1	7.1	5.9	1.7	3.49	13.1	45.6
306	7.4	7.8	6.1	7.8	5.0	3.3	1.50	27.7	41.5
309	3.7	3.7	3.3	3.7	4.4	5.2	0.84	11.8	9.8
311	0.3	0.3	0.2	0.3	4.2	10.1	0.42	3.2	1.3
312	1.2	1.2	1.2	1.2	1.2	6.4	0.19	12.4	2.3
313	0.5	0.5	0.5	0.5	1.9	10.2	0.18	26.8	4.9
315	0.0	0.0	0.0	0.0	0.4	7.7	0.05	1.2	0.1
317	0.1	0.1	0.1	0.1	0.0		0.00	0.0	0.0
320	0.2	0.2	0.2	0.2	2.8	11.3	0.25	3.1	0.8
322	0.4	0.4	0.4	0.4	4.4	7.0	0.62	1.5	0.9
324	1.8	1.9	1.6	2.1	4.1	4.3	0.97	4.4	4.3
326	3.4	3.6	3.0	3.8	4.2	2.2	1.97	10.9	21.5
327	7.9	8.1	7.6	9.7	4.6	1.6	2.88	9.0	25.9
328	12.4	12.5	12.0	16.2	8.0	2.4	3.31	23.9	79.2
329	11.3	12.2	10.9	16.2	5.3	1.0	5.62	15.6	87.9
331	10.2	11.3	9.8	13.8	6.0	1.8	3.40	29.0	98.8
332	4.4	4.6	4.0	5.2	4.7	1.8	2.68	9.4	25.1

					Wet Test Meter Data				
Run #	Residual Ozone Dose$_{aq,ss}$ (mg/L)	Residual Ozone Dose$_{aq}$ (mg/L)	Residual Ozone Dose$_{inj}$ (mg/L)	Applied Ozone Dose (mg/L)	Wet Test Total Volume (L)	Time of Wet Test Volume (min)	$Q_{G,ss/Ldys}$ (L/min)	$C_{G,ss/Ldys}$ (mg/L)	Unused Applied Ozone Gaseous Mass Rate (mg/min)
335	0.6	0.7	0.6	0.7	4.3	3.2	1.35	1.0	1.4
337	12.5	15.6	11.5	17.1	5.7	1.2	4.87	26.0	126.5
338	14.5	17.4	12.8	21.2	7.9	1.4	5.62	12.1	67.9
339	0.4	0.5	0.4	0.5	4.4	4.2	1.06	3.3	3.5
342	0.7	0.7	0.7	0.9	1.8	8.4	0.21	13.3	2.8
345	0.7	0.8	0.7	0.8	1.5	9.6	0.16	0.8	0.1
347	2.8	2.8	2.7	2.8	4.5	6.4	0.71	12.8	9.0
350	2.2	2.3	2.1	2.4	5.7	4.9	1.16	8.0	9.3
351	5.3	5.0	4.9	5.6	4.9	2.7	1.83	10.5	19.2
352	1.1	1.1	0.9	1.2	7.7	2.5	3.09	1.7	5.3
355	10.5	11.2	9.0	11.4	4.2	1.1	3.98	17.7	70.3
356	4.2	4.2	4.2	4.2	4.7	4.0	1.17	18.9	22.1
362	4.3	4.3	3.9	4.3	5.0	2.4	2.03	9.6	19.4
432	0.4	0.5	0.4	0.6	5.0	5.8	0.87	3.7	3.2
437	11.1	13.6	11.0	18.3	4.5	1.1	4.07	31.5	128.5
501	5.6	6.3	5.0	7.2	5.0	1.5	3.42	12.6	43.2
565	5.0	5.6	4.9	5.7	4.4	1.4	3.06	12.3	37.7